MICROTOPOGRAPHY-DOMINATED DISCONTINUOUS OVERLAND FLOW MODELING AND HYDROLOGIC CONNECTIVITY ANALYSIS

A Dissertation
Submitted to the Graduate Faculty
of the
North Dakota State University
of Agriculture and Applied Science

By

Jun Yang

In Partial Fulfillment of the Requirements
for the Degree of
DOCTOR OF PHILOSOPHY

Major Department:
Civil and Environmental Engineering

March 2014

Fargo, North Dakota

North Dakota State University
Graduate School

Title

MICROTOPOGRAPHY-DOMINATED DISCONTINUOUS OVERLAND FLOW MODELING AND HYDROLOGIC CONNECTIVITY ANALYSIS

By

Jun Yang

The Supervisory Committee certifies that this ***disquisition*** complies with North Dakota State University's regulations and meets the accepted standards for the degree of

DOCTOR OF PHILOSOPHY

SUPERVISORY COMMITTEE:

Xuefeng Chu
Chair

G. Padmanabhan

Zhulu Lin

Peter G. Oduor

Approved:

4/14/2014	Dinesh Katti
Date	Department Chair

ABSTRACT

Surface microtopography affects a series of complex and dynamic hydrologic and environmental processes that are associated with both surface and subsurface systems, such as overland flow generation, infiltration, soil erosion, and sediment transport. Due to the influence of surface depressions, overland flow essentially features a series of progressive puddle-to-puddle (P2P) filling, spilling, merging, and splitting processes; and hydrologic systems often exhibit threshold behaviors in hydrologic connectivity and the associated overland flow generation process. It is inherently difficult to realistically simulate the discontinuous overland flow on irregular topographic surfaces and quantify the spatio-temporal variations in dynamic behaviors of topography-dominated hydrologic systems. This dissertation research aims to develop a hydrologic model to simulate the discontinuous, dynamic P2P overland flow processes under the control of surface microtopography for various rainfall and soil conditions, and propose new approaches to quantify hydrologic connectivity.

In the developed P2P overland flow model, the depressions of a topographic surface are explicitly incorporated into a well-delineated, cascaded P2P drainage system as individual objects to facilitate the simulation of their dynamic behaviors and interactions. Overland flow is simulated by using diffusion wave equations for a DEM-derived flow drainage network for each puddle-dominated area. In addition, a P2P hydrologic connectivity concept is proposed to characterize runoff generation processes and the related spatio-temporal dynamics. Two modified hydrologic connectivity indices, time-varying connectivity function and connectivity length of the connected areas and ponded areas, are proposed to quantitatively describe the intrinsic spatio-temporal variations in hydrologic connectivity associated with overland flow

generation. In addition, the effects of DEM resolution, surface topography, rainfall distribution, and surface slope on hydrologic connectivity are also evaluated in this dissertation research.

The developed model can be applied to examine the spatio-temporally varying P2P dynamics for hydrologic systems. This model provides a means to investigate the effects of the spatial organization/heterogeneity of surface microtopography, rainfall, and soil on overland flow generation and infiltration processes. In addition, the two proposed hydrologic connectivity indices are able to bridge the gap between the structural and functional hydrologic connectivity and effectively reveal the variability and the threshold behaviors of overland flow generation.

ACKNOWLEDGMENTS

I would like to express my sincere gratitude and appreciation to my advisor, Dr. Xuefeng Chu, for his invaluable guidance, continuous support, and encouragement during my study at NDSU. This dissertation work could never have been completed without his endless advice. What I learned from him in these years is not only knowledge in hydrology, but also the essence of seriousness and honesty.

My sincere appreciation is extended to other committee members, Dr. G. Padmanabhan, Dr. Zhulu Lin, and Dr. Peter Oduor, for their time, inspiration, and suggestions throughout my dissertation research.

I would like to acknowledge the help from my colleagues, Jianli Zhang, Yaping Chi, Leif Sande, Daniel Bogart, Shravan Avadhuta, Noah Habtezion, Yang Liu, and Yingjie Yang for their contributions to the related modeling and experimental work. They made my time in lab joyful and fruitful. I would also like to thank all my friends whose support during these years helped me through the good and tough times.

I gratefully thank the primarily financial support for this research from the National Science Foundation under Grant No. EAR-0907588, Department of Civil and Environmental Engineering, North Dakota State University, and North Dakota Water Resources Research Institute.

I am most thankful to my parents, parents-in-law, and sisters for their unconditional love, support, trust, and encouragement throughout my study. I am, also, indebted to my lovely wife Yaping Chi. She has always been there with me when I was frustrated in the research and lost confidence in myself. Thank her sacrifice and understanding in these years. I would like to thank my daughter Evelyn for the joy and love she brought to me.

TABLE OF CONTENTS

LIST OF TABLES

LIST OF FIGURES

LIST OF ABBREVIATIONS/NOTATIONS

AC .....Connected area

CA .....Contributing area

CL .....Correlation length

CP.....Cumulative rainfall

CV .....Coefficient of variation

$C_{AC}(h, t)$.....Connectivity function of ACs for separation h at time t

DEM.....Digital elevation model

DX.....Grid size of a DEM

FHC.....Functional hydrologic connectivity

h .....lag distance

h.....Separation distance between the centers of cells (DEM grids)

h_k .....Separation distance for separation bin k

HPA.....Average of the mean puddle depths

HPM.....Mean puddle depth

HPMA.....Average of the maximum puddle depths

$ID_{AC}(i, t)$.....ID number of AC for cell i at time t

$L_{AC}(t)$ .....Connectivity length of ACs at time t

MDS.....Maximum depression storage

MPA.....Maximum ponding area

n.....Total number of data points

N (**h**).....Number of pairs spaced at **h**

NB .....Total number of separation bins

NCA .....Number of connected areas

NP .....Number of puddles

NPL .....Number of puddle levels

$N_{cp}(h_k, t)$ .....Number of connected pairs for separation distance h_k at time t

$N_{tp}(h_k, t)$.....Number of total pairs for separation distance h_k at time t

P .....Probability of cell i to connect to cell j

P2P .....Puddle to puddle

PA .....Ponded area

PCA.....Percentage of average connected areas

PD .....Puddle delineation

pdf .....probability density function

R^2.....Coefficient of determination

$r_{CP\text{-}MDS}$.....Normalized cumulative rainfall by MDS

$r_{Q\text{-}P}$.....Ratio of discharge to rainfall input

RR .....Random roughness

S.....Space domain that includes all cells

s.....location

SHC.....Structural hydrologic connectivity

T .....Time domain

X.....State variable

Z .....surface elevation

Δh_k.....Size of separation bin k

$\leftrightarrow$ .....Indicator of connection between cells

γ(h).....Semivariogram

λ_L.....Ratio of grid size (DX) to correlation length (CL) (i.e., DX/CL)

λ_R.....Ratio of random roughness (RR) to correlation length (CL) (i.e., RR/CL)

σ^2 .....variance

CHAPTER 1. INTRODUCTION

A hydrologic system often exhibits spatio-temporal dynamics and complexity due to spatially varying topographic characteristics, soil properties, climatic variables, vegetation, etc. In recent decades, the importance of surface topography on hydrologic processes, e.g., overland flow generation, has increasingly been emphasized (Dunne et al., 1991; Helming et al., 1998; Govers et al., 2000; Darboux and Huang, 2005; Thompson et al., 2010; Chu et al., 2013b).

The spatial variability of surface topography influences overland flow generation (Martin et al., 2008; Chi et al., 2012), delays the initiation of surface runoff (Darboux and Huang, 2005), controls spatial-temporal variations of overland flow depth and velocity (Zhang and Cundy, 1989; Huang and Bradford, 1990; Mwendera and Feyen, 1992; Esteves et al., 2000), affects the flow drainage pattern (Govers et al., 2000; Chu, 2011; Yang et al., 2010; Chi et al., 2012; Chu et al., 2013b), governs the dynamic behaviors of the depressions and hydrologic connectivity of topography-dominated overland flow systems (Darboux et al., 2001; Antoine et al., 2009; Chu et al., 2013b; Yang and Chu, 2012; Yang and Chu, 2013a; Yang and Chu, 2013b), and influences the infiltration (Mwendera and Feyen, 1992; Darboux et al., 2001; Darboux and Huang, 2005; Rossi and Ares, 2012) and water flow in the vadose zone (Sande and Chu, 2012; Liu et al., 2013). In addition to overland flow and infiltration, surface topography also affects soil erosion, sediment movement, and pollutant transport due to the change of local flow depth and velocity (Cogo et al., 1983; Tayfur et al., 1993; Hansen et al., 1999; Chu et al., 2013a).

Depressions on topographic surfaces dominate localized and isolated areas with unique hydrologic properties and mass balance (Chu et al., 2013b). Water levels in depressions show dynamic fluctuation, e.g., rising and falling, due to gaining water or losing water associated with different hydrologic processes. Depressions may interact with each other when they are fully

filled with water, and they may spill water to their adjacent downstream depressions. Depressions may merge with others to form depressions with higher outflow thresholds; or they may split into embedded puddles as the water level falls. Gradually, more and more "localized areas" become connected, and such dynamic behaviors of depressions and the associated hydrologic connectivity result in a stepwise, intermittent changing pattern of outflow hydrograph (Hansen, 2000; Chu, 2011; Yang and Chu, 2012; Chu et al., 2013b; Yang and Chu, 2013b). Therefore, the variability and complexity of the hydrologic behaviors of these depressions (i.e., puddle filling, spilling, merging, and splitting processes) directly influence hydraulic dynamics and spatial variations of overland flow generation process.

The above discussion raises some interesting research questions: How do the depressions on topographic surfaces affect the rainfall partitioning and influence the runoff generation? How do the depressions interact with other depressions when they are fully filled? How does the water stored in depressions change spatially? How to quantify depression-induced dynamic behaviors of the rainfall-runoff system?

Limited knowledge of these research questions significantly hampers the understanding of the associated hydrologic processes. This study specifically focuses on the investigation of these research questions by developing a hydrologic model to simulate hydrologic processes associated with the topography-dominated rainfall-runoff system and proposing indices to quantify the spatio-temporal complexity and dynamics of the rainfall-runoff system. The following literature review focuses on current research conditions in the related research fields, research gaps and the limitations of current studies, and the essential originality and importance of this dissertation research.

1.1. Surface Microtopography-dominated Overland Flow Modeling

In the past decades, a great amount of hydrologic and water quality models were developed for various purposes, e.g., overland flow, flood forecasting, and point source pollution control. Hydrologic modeling has become an effective and useful way to investigate the hydrologic processes. Considerable efforts have been devoted to develop the hydrologic models that account for the influences of topography surfaces (Tayfur et al., 1993; Beven, 1997; Wang and Hjelmfelt, 1998; Jain and Singh, 2005; Tatard et al., 2008; Frei et al., 2010; Antoine et al., 2011; Chu et al., 2013). These hydrologic models can be primarily divided into two categories: empirical model and physically-based model.

The first category is empirical hydrologic models, which incorporate the surface topographic characteristics into certain hydrologic parameters and apply empirical equations to generate a hydrograph. For instance, U.S. Soil Conservation Service infiltration model (SCS, 1972) has been developed based on soil type, land cover, and basin topography to estimate water loss and compute hydrograph. Another typical example is TOPMODEL (Beven, 1997), which is a semi-distributed, quasi-physical model to investigate the effects of catchment heterogeneity and topography on the dynamic hydrological responses. In this model, a topographic index is utilized to represent propensity of a point in watershed by taking into account the slope and contributing area. Due to the intrinsic limitations, empirical models cannot realistically and physically simulate the hydrologic processes in hydrologic systems and be applied to investigate factors individually (e.g., surface depressions) that control the hydrologic processes, e.g., overland flow generation.

In recent decades, the spatio-temporal dynamics of hydrologic processes are increasingly being discussed and spatial data acquisition devices also have been tremendously improved. The

modeling development gradually shifted the focus toward the second type of model: physically-based, process-oriented hydrologic model. This type of model is based on physical laws and takes account of spatial distributed properties of hydrologic system, e.g., topography, soil, vegetation, and rainfall. Over the past several decades, a large amount of numerical models with varying complexity have been developed to simulate overland flow under various conditions.

Although the advancement in numerical modeling of overland flow has been increasingly achieved, it is still a challenge to realistically simulate overland flow over irregular topographic surfaces. The most commonly used equations for overland flow routing are Saint-Venant equations and their approximation forms (e.g., diffusion wave and kinematic wave equations). However, applying these equations for realistic simulation of overland flow over irregular topographic surfaces may suffer from modeling instability and convergence problems, which can be primarily attributed to the highly non-linear nature of these equations and abrupt slopes caused by topographic variations (Woolhiser and Liggett, 1967; Smith, 1985; Gottardi and Venutelli, 1993; Tayfur et al., 1993). Tayfur et al. (1993) found that the numerical solution obtained from overland flow equations over irregular surfaces with significant slope became unstable and convergence could not be reached. In addition, the numerical models are computationally intensive and time consuming; Frei et al. (2010) and Antoine et al. (2011) reported that overland flow simulations over rough surface plots with relatively high DEM resolutions took a couple of months.

Rainfall-runoff models usually route excess rainfall for a two-dimensional spatial domain or a delineated one-dimensional flow drainage network. Surface representation and related topographic flow characteristics (i.e., watersheds and flow drainage network) are mostly acquired from the digital elevation model (DEM). However, the existence of depressions on

topographic surfaces may cause disconnected drainage network and localized sub-watersheds in surface delineation results. To avoid this problem, a commonly used approach is to remove surface depressions to define watershed structures and fully connected drainage networks of topographic surfaces at the very first step of modeling or hydrologic analysis (Tayfur et al., 1993; Garbrecht and Martz, 2000; Jain and Singh, 2005; Tatard et al., 2008). This approach had been applied to the majority of the hydrologic models as a standard procedure. Various algorithms have been proposed in the past three decades to detect and fill the depressions (Marks et al., 1984; Jenson and Domingue, 1988; Planchon and Darboux, 2001; Wang and Liu, 2006). The consequence of using this approach for hydrologic modeling is that the effects of depression on overland flow generation are neglected, and developed numerical models are incapable of specifically accounting for the depressions and their storage and simulating the dynamic behaviors of these depressions (e.g., Esteves et al., 2000; Fiedler and Ramirez, 2000; Tatard et al., 2008). This results in inaccurate prediction of the hydrograph, spatio-temporal varying water depth distributions, and other hydrologic processes (e.g., infiltration and erosion).

In the recent decade, efforts have been devoted to develop process-oriented conceptual models that specifically account for the dynamic depression filling-spilling processes in rainfall-runoff processes (Darboux et al., 2001; Antoine et al., 2009; Appels et al., 2011; Chu et al., 2013). Darboux et al. (2001) used a conditioned-walker method to simulate depression filling and examine runoff triggering for randomly-distributed water input without consideration of infiltration, and further analyzed flow-path connectivity. Antoine et al. (2009) also developed a filling algorithm similar to the one of Darboux et al. (2001) to account for the depression filling process and generate simplified hydrographs. Appels et al. (2011) coupled a ponding and redistribution model with the Philip's infiltration model to simulate filling, merging, and

connecting of depressions over permeable soil surfaces, and further quantified the development of hydrologic connectivity. Shaw et al. (2012) recently developed a conceptual model, SPILL, for the fill-spill of prairie potholes to identify and quantify runoff contributing area for impervious surfaces and uniformly distributed water input. Chu et al. (2010) proposed a new surface delineation approach to characterize surface topography with a focus on delineating puddles, and the developed puddle delineation (PD) software has been applied to delineate puddles at different levels, determine their hierarchical relationships, and deal with special topographic conditions. Furthermore, a novel structure for modeling P2P dynamic processes has been proposed based on the PD software to realistically simulate puddle filling-spilling-merging-splitting processes (Chu et al., 2013).

Different from either the empirical models or physically-based models, this type of process-oriented conceptual models (Darboux et al., 2001; Antoine et al., 2009; Appels et al., 2011; Shaw et al., 2012) center on analyzing the dynamic behaviors of depressions and investigating hydrologic connectivity by simulating dynamic depression filling, spilling, and merging processes. In addition, these models have some major assumptions or limitations such as: (1) instantaneous water transfer on land surfaces, and (2) hypothetical or steady uniformly-distributed rainfall and no net water loss (i.e., no loss or rainfall is greater than infiltration and other losses). In reality, however, rainfall varies spatially and temporally, which alters the dynamic filling-spilling processes of individual puddles and their hierarchical relationships associated with puddle merging and connecting, and further affects the development of dynamic contributing areas and hydrologic connectivity (Chu et al., 2013). Most importantly, if water losses (e.g., infiltration and evaporation) are simulated and rainfall is smaller than the total loss, water levels in puddles may decrease. As a result, a higher-level merged puddle may split into a

number of lower-level puddles. However, none of the existing models simulate puddle splitting, one of the essential processes related to real P2P dynamics, or account for the realistic P2P dynamics under real complex rainfall and infiltration conditions (Chu et al., 2013).

From the above discussion, it has become apparent that both physically-based numerical models and process-oriented conceptual models have their unique merits in the simulation of topography-dominated rainfall-runoff processes, however, they both suffer from various limitations or problems. This leads to an interesting question: is it possible to propose a new modeling structure/approach that combines the conceptual models with the traditional numerical models to overcome some of their limitations and extend the modeling capabilities in dynamic discontinuous overland flow processes over infiltrating surfaces?

1.2. Surface Topography-dominated Hydrologic Connectivity

In recent years, the importance of threshold behaviors in hydrologic, environmental, and ecological systems has been studied by many researchers (e.g., McDonnell, 2003; Lehmann et al., 2007; Zehe and Sivapalan, 2009). Leibowitz and Vining (2003) described the spilling process of prairie pothole wetlands and the associated biological effects. Dynamic storage in wetlands showed significant influences on stream runoff response, and hydrologically connected storages had a strong "hysteretic relationship" with stream flow (Spence, 2006; Spence et al., 2010). Spence et al. (2007) successfully applied a transfer function and storage threshold to predict the efficiency of runoff production.

To reveal the variability and complexity of hydrologic systems, hydrologic connectivity has been frequently examined in the recent decade (e.g., Darboux et al., 2001; Brierley et al., 2006; Bracken and Croke, 2007; Antoine et al., 2009). Hydrologic connectivity, as a unique hydrologic behavior or response of hydrologic systems, indicates spatio-temporal conveyance

passage to transfer water and the related mass over a land surface (Pringle et al., 2003; Bracken and Croke, 2007; Tetzlaff et al., 2007).

The dynamic development of hydrologic connectivity serves as a driving mechanism to alter spatio-temporal variations of a series of hydrologic, geomorphologic, and environmental processes, such as overland flow trigging, infiltration, and solute transport processes. Therefore, it is of particular importance to examine the topography-affected hydrologic connectivity and the related dynamic overland generation process, which are the foundations of understanding other hydrologic processes. Lehmann et al. (2007) used a percolation theory to quantify the threshold processes and the relationship of rainfall input and outflow discharge. Runoff response of wetland basins increased with hydrologic connectivity of the stream network (Phillips et al., 2011). Smith et al. (2010) emphasized the importance of analyzing antecedent moisture, temporal structure of rainfall conditions, and flow resistance to quantify the spatial and temporal variations in hydrologic connectivity. In addition, a series of studies have been conducted to investigate hydrologic connectivity of topographic surfaces and to characterize the dynamic behaviors of overland flow generation (Darboux et al., 2001; Antoine et al., 2009; Antoine et al., 2011; Appels et al., 2011). These studies applied the conceptual models and hydrologic connectivity indicators (e.g., simplified hydrograph and relative surface connection function) to characterize the connectivity properties of topography-dominated hydrologic systems and describe their hydrologic behaviors.

However, these two hydrologic connectivity indicators (i.e., simplified hydrograph and relative surface connection function) (Antoine et al., 2009; Antoine et al., 2011) may not necessarily account for the spatio-temporal variations in the generation and evolution processes of overland flow within a topography-dominated hydrologic system. Simplified hydrograph and

the relative surface connection function only represent the response of topographic surfaces that have been connected with and contributed water to the system outlets. It is thus in great need to propose new hydrologic connectivity indices and reveal the spatio-temporal changes in hydrologic connectivity affected by surface topography within hydrologic systems.

As described earlier, tremendous progress in the development of distributed hydrologic models has been achieved in recent years, which largely relies on the advancement of acquisition methods for distributed data, e.g., surface DEM. Surface DEMs with high resolutions are becoming available, such as 30m, 10m, 3m, and even 1 m for a large variety of locations. A critical question faced by many hydrologists is: how does the DEM resolution or grid size affect the characterization of surface microtopographic properties (e.g., slope, curvature, etc), delineation of surface topographic features (e.g., depressions and channels), as well as hydrologic modeling results?

A great number of studies have been conducted to examine the effects of DEM resolution on fundamental topographic parameters including slope, curvatures, and drainage length (Kuo et al., 1999; Molnár and Julien, 2000; Dutta and Herath, 2001; Thompson et al., 2001; Moglen and Hartman, 2001). Due to the importance of the surface depressions on hydrologic processes, research efforts were also devoted to quantify the influences of DEM resolution on depression geometric properties (maximum depression storage, maximum ponding area, mean puddle depth, and contributing area) (Huang and Bradford, 1990; Kamphorst et al., 2000; Abedini et al., 2006). These studies analyzed the relationships of the delineated depression properties and DEM resolution, a parameter associated with specific field or watershed scale. However, varied, even contrary conclusions have been obtained in these studies. In addition, little research has been done to investigate the DEM resolution effects on the quantification of the complexity and

dynamics of the hydrologic behaviors (e.g., hydrologic connectivity). Therefore, research is needed to systematically evaluate the DEM resolution effects on depression properties and associated hydrologic connectivity for the topography-dominated rainfall-runoff system.

1.3. Dissertation Objectives

This dissertation research focuses on improving the understanding of the dynamic and complex behaviors of topography-dominated rainfall-runoff system. Specific objectives of this study are:

(1) to develop a physically-based, distributed model that is able to simulate microtopography-dominated overland flow and infiltration with the conjunction of threshold-controlled, dynamic puddle filling-merging-spilling-splitting processes under various topographic, soil, and rainfall conditions;

(2) to improve the understanding of microtopography-controlled hydrologic connectivity and its relation to the dynamic overland flow generation processes; and

(3) to investigate the DEM resolution effects on the hydrotopographic properties of depressions and intrinsic spatio-temporal variations in hydrologic connectivity associated with overland flow generation.

1.4. Organization of the Dissertation

This dissertation is structured as follows. It begins with a general introduction and the objectives of this dissertation research. The general introduction is then followed by Chapter 2 through Chapter 4, which present the major findings of this dissertation research. Chapter 2 presents a new modeling approach to improve the simulation of microtopography-dominated discontinuous overland flow processes over infiltrating surfaces, which is based on a paper under preparation. Chapter 3 focuses on the quantification of the spatio-temporal variations in

hydrologic connectivity of small-scale topographic surfaces under various rainfall conditions; it is based on a paper published in the Journal of Hydrology (Yang and Chu, 2013b). Chapter 4 is an investigation of the effects of DEM resolution on surface depression properties and hydrologic connectivity, which has been published in the Journal of Hydrologic Engineering (Yang and Chu, 2013a). The dissertation ends with a conclusion chapter, which summarizes the major findings from this dissertation research.

1.5. References

Antoine, M., Javaux, M., and Bielders, C., 2009. What indicators can capture runoff-relevant connectivity properties of the micro-topography at the plot scale? Adv. Water Resour., 32(8), 1297-1310.

Antoine, M., Javaux, M., and Bielders, C., 2011. Integrating subgrid connectivity properties of the micro-topography in distributed runoff models, at the interrill scale. J. Hydrol., 403, 213-223.

Appels, W. M., Bogaart, P. W., and van der Zee, S. E. A. T. M., 2011. Influence of spatial variations of microtopography and infiltration on surface runoff and field scale hydrological connectivity. Adv. Water Resour., 34(2), 303-313.

Beven, K. J., 1997. TOPMODEL: a critique. Hydrol. Process., 11, 1069-1085.

Bracken, L. J., and Croke, J., 2007. The concept of hydrological connectivity and its contribution to understanding runoff-dominated geomorphic systems. Hydrol. Process., 21, 1749-1763.

Brierley, G., Fryirs, K., and Jain, V., 2006. Landscape connectivity: the geographic basis of geomorphic applications. Area, 38(2), 165-174.

Chi, Y., Yang, J., Bogart, D., and Chu. X., 2012. Fractal analysis of surface microtopography and its application in understanding hydrologic processes. Transactions of the ASABE. 55(5):1781-1792.

Chu, X., 2011. Characterization of Microtopography and its Hydrologic Significance. P1-14, In: Modeling Hydrologic Effects of Microtopographic Features, edited by X. Wang, Nova Science Publishers, Inc.

Chu, X., Nelis, J., and Rediske, R., 2013a. Preliminary study on the effects of surface microtopography on tracer transport in a coupled overland and unsaturated flow system. J. Hydrol. Eng., 18(10), 1241-1249.

Chu, X., Yang, J., Chi, Y., and Zhang, J., 2013b. Dynamic puddle delineation and modeling of puddle-to-puddle filling-spilling-merging-splitting overland flow processes. Water Resour. Res., 49(6), 3825-3829.

Chu, X., Zhang, J., Chi, Y., and Yang, J., 2010. An improved method for watershed delineation and computation of surface depression storage. P1113-1122, In: Watershed Management 2010: Innovations in Watershed Management under Land Use and Climate Change, Proceedings of the 2010 Watershed Management Conference, edited by K. W. Potter and D. K. Frevert. American Society of Civil Engineers, Reston, VA.

Cogo, N. P., Moldenhauer, W. C., and Foster, G. R., 1983. Effect of crop residue, tillage-induced roughness, and runoff velocity on size distribution of eroded soil aggregates, Soil Sci. Soc. America J., 47(5), 1005-1008.

Darboux, F., Davy, P., Gascuel-Odoux, C., and Huang, C., 2002. Evolution of soil surface roughness and flowpath connectivity in overland flow experiments. Catena, 46(2-3), 125-139.

Darboux, F., and Huang, C., 2005. Does soil roughness increase or decrease water and particle transfer? Soil Sci. Soc. America J., 69(3), 748-756.

Dunne, T., Zhang, W., and Aubry, B. F., 1991. Effects of rainfall, vegetation, and microtopography on infiltration and runoff. Water Resour. Res., 27(9), 2271-2285.

Dutta, D., and Herath, S., 2001. Effect of DEM accuracy in flood inundation simulation using distributed hydrological models. Seisan Kenkyu, 53(11), 602-605.

Esteves, M., Faucher, X., Galle, S., and Vauclin, M., 2000. Overland flow and infiltration modelling for small plots during unsteady rain: numerical results versus observed values. J. Hydrol., 228(3-4), 265-282.

Fiedler, F. R., and Ramirez, J. A., 2000. A numerical method for simulating discontinuous shallow flow over an infiltrating surface. Int. J. Numer. Meth. Fl., 32(2), 219-239.

Frei, S. G., Lischeid, G., and Fleckenstein, J.H., 2010. Effects of micro-topography on surface–subsurface exchange and runoff generation in a virtual riparian wetland – a modeling study. Adv. Water Resour., 33 (11), 14. doi:10.1016/j.advwatres.2010.07.006.

Garbrecht, J., and Martz, L. W., 2000. TOPAZ: An Automated Digital Landscape Analysis Tool for Topographic Evaluation, Drainage Identification, Watershed Segmentation and Subcatchment Parameterization: TOPAZ User Manual. Grazinglands Research Laboratory, USDA Agricultural Research Services, El Reno, OK.

Gottardi, G., and Venutelli, M., 1993. A control-volume finite element model for two-dimensional overland flow. Adv. Water Resour., 16, 227-284.

Govers, G., Takken, I., and Helming, K., 2000. Soil roughness and overland flow. Agronomie, 20(2), 131-146.

Hansen, B., 2000. Estimation of surface runoff and water-covered area during filling of surface microrelief depressions, Hydrol. Process., 14(7), 1235-1243.

Hansen, B., Schjønning, P., and Sibbesen, E., 1999. Roughness indices for estimation of depression storage capacity of tilled soil surfaces. Soil Till. Res., 52(1-2), 103-111.

Hayashi, M., van der Kamp, G., and Schmidt, R., 2003. Focused infiltration of snowmelt water in partially frozen soil under small depressions. J. Hydrol., 270(3-4), 214-229.

Helming, K., Römkens, M. J. M., and Prasad, S. N., 1998. Surface roughness related processes of runoff and soil loss: a flume study. Soil Sci. Soc. America J., 62, 243-250.

Huang, C., and Bradford, J. M., 1990. Depressional storage for Markov – Gaussian surfaces. Water Resour. Res., 26(9), 2235-2242.

Jain, M. K., and Singh, V. P., 2005. DEM-based modeling of surface runoff using diffusion wave equation. J. Hydrol., 302, 107-126.

Jenson, S. K., and Domingue, J. O., 1988. Extracting topographic structure from digital elevation for geographic information system analysis. Photogramm. Eng. Rem. S., 54(1), 1593-1600.

Kamphorst, E. C., Jetten, V., Guerif, J., Pitkanen, J., Iversen, B. V., Douglas, J. T., and Paz, A., 2000. Predicting depressional storage from soil surface roughness. Soil Sci. Soc. Am. J., 64(5), 1749-1758.

Kuo, W., Steenhuis, T. S., McCulloch, C. E., Mohler, C. L., Weinstein, D. A., DeGloria, S. D., and Swaney, D. P., 1999. Effect of grid size on runoff and soil moisture for a variable-source-area hydrology model. Water Resour. Res., 35(11), 3419-3428.

Lehmann, P., Hinz, C., McGrath, G., Tromp-van Meerveld, H. J., and McDonnell, J. J., 2007. Rainfall threshold for hillslope outflow: an emergent property of flow pathway connectivity. Hydrol. Earth Syst. Sci., 11, 1047-1063.

Leibowitz, S. G., and Vining, K. C., 2003. Temporal connectivity in a prairie pothole complex, Wetlands, *23*(1), 13-25.

Liu, Y., Yang, J., Chu, X., 2003. Infiltration and unsaturated flow under the influence of surface microtopography - model simulations and experimental observations, p468-475. In: Showcasing the Future, Proceedings of the 2013 ASCE World Environmental and Water Resources Congress, edited by C. L. Patterson, S. D. Struck, and D. J. Murray. American Society of Civil Engineers.

Marks, D., Dozier, J.**,** and Frew**,** J.**,** 1984**.** Automated basin delineation from digital elevation data**.** Geo-Processing, 2, 299-311.

Martin, Y., Valeo, C., and Tait, M., 2008. Centimetre-scale digital representations of terrain and impacts on depression storage and runoff. Catena, 75, 223-233.

McDonnell, J. J., 2003. Where does water go when it rains? Moving beyond the variable source area concept of rainfall-runoff response. Hydrol. Process., 17,1869-1875.

Moglen, G. E., and Hartman, G. L., 2001. Resolution effects on hydrologic modeling parameters and peak discharge. J. Hydrol. Eng., 6(6), 490-497.

Molnár, D. K., and Julien, P. Y., 2000. Grid-size effects on surface runoff modeling. J. Hydrol. Eng., 5(1), 8-16.

Mwendera, E. J., and Feyen, J., 1992. Estimation of depression storage and Manning's resistance coefficient from random roughness measurements. *Geoderma*, 52(3-4), 235-250.

Phillips, R. W., Spence, C., and Pomeroy, J. W., 2011. Connectivity and runoff dynamics in heterogeneous basins. Hydrol. Process., *25*(19), 3061-3075.

Planchon, O., and Darboux, F., 2002. A fast, simple and versatile algorithm to fill the depressions of digital elevation models. Catena, 46, 159-176.

Pringle, C., 2003. What is hydrologic connectivity and why is it ecologically important? Hydrol. Process., 17(13), 2685-2689.

Rossi, M. J., and Ares, J. O., 2012. Depression storage and infiltration effects on overland flow depth-velocity-friction at desert conditions: field plot results and model. Hydrol. Earth Syst. Sci., 16, 3293-3307.

Sande, L., and Chu. X., 2012. Laboratory experiments on the effect of microtopography on soil-water movement: Spatial variability in wetting front movement. Applied and Environmental Soil Science. Volume 2012, Article ID 679210, 8 pages, doi:10.1155/2012/679210.

Shaw, D. A., Pietroniro, A., and Martz, L. W., 2012. Topographic analysis for the prairie pothole region of Western Canada. Hydrol. Process., doi:10.1002/hyp.9409.

Smith, G. D., 1985. Numerical solution of partial differential equations: finite difference methods. Oxford, Clarendon press.

Smith, M. W., Bracken, L. J., and Cox, N. J., 2010. Toward a dynamic representation of hydrological connectivity at the hillslope scale in semiarid areas. Water Resour. Res., 46, W12540, doi:10.1029/2009WR008496.

Spence, C., 2006. Hydrological processes and streamflow in a lake dominated water course. Hydrol. Process., 20(17), 3665-3681.

Spence, C., 2007. On the relation between dynamic storage and runoff: A discussion on thresholds, efficiency, and function. Water Resour. Res., 43(12), doi:10.1029/2006WR005645.

Spence, C., Guan, X. J., Phillips, R., Hedstrom, N., Granger, R., and Beid, B., 2010. Storage dynamics and streamflow in a catchment with a variable contributing area. Hydrol. Processes, 24(16), 2209-2221.

Tatard, L., Planchon, O., Wainwright, J., Nord, G., Favis-Mortlock, D., Silvera, N., Ribolzi, O., Esteves, M., and Huang, C., 2008. Measurement and modelling of highresolution flow-velocity data under simulated rainfall on a low-slope sandy soil. J. Hydrol., 348(1-2), 1-12.

Tayfur, G., Kavvas, M. L., Govindaraju, R. S., and Storm, D. E., 1993. Application of St. Venant equations for two-dimensional overland flows over rough infiltrating surfaces. J. Hydraul. Eng., 119 (1), 51-63.

Tetzlaff, D., Soulsby, C., Bacon, P. J., Youngson, A. F., Gibbins, C., and Malcolm, I. A., 2007. Connectivity between landscapes and riverscapes – a unifying theme in integrating hydrology and ecology in catchment science? Hydrol. Process., 21(10), 1385-1389.

Thompson, J. A., Bell, J. C., and Butler, C. A., 2001. Digital elevation model resolution: effects on terrain attribute and quantitative soil-landscape modeling. Geoderma, 100(1-2), 67-89.

Thompson, S. E., Katul, G. G., and Porporato, A., 2010. Role of microtopography in rainfall–runoff partitioning: an analysis using idealized geometry. Water Resour. Res., 46, W07520, doi:10.1029/2009WR008835.

U. S. Soil Conservation Service (SCS), 1972. SCS National engineering handbook, Sec. 4, Hydrology, USDA. Last accessed online (August, 2013): ftp://ftp.wcc.nrcs.usda.gov/wntsc/H&H/NEHhydrology/ch21.pdf

Wang, L., and Liu, H., 2006. An efficient method for identifying and filling surface depressions in digital elevation models for hydrologic analysis and modelling. Int. J. Geogr. Inf. Sci., 20(3), 193-213.

Wang, M., and Hjelmfelt, A. T., 1998. DEM based overland flow routing Model. J. Hydrol. Eng., 3(1), 1-8.

Winter, T. C., and LaBaugh, J. W., 2003. Hydrologic considerations in defining isolated wetlands. Wetlands, 23(3), 532-540.

Woolhiser, D. A., and Liggett, J. A., 1967. Unsteady 1-dimensional flow over a plane - rising hydrograph. Water Resour. Res., 3(3), 753-771.

Yang, J., and Chu, X., 2012. Effects of surface microtopography on hydrologic connectivity. p339-348. In: Crossing Boundaries, Proceedings of the 2012 ASCE World Environmental and Water Resources Congress, Edited by E. D. Loucks. American Society of Civil Engineers.

Yang, J., and Chu, X., 2013a. Effects of DEM resolution on Surface Depression Properties and Hydrologic Connectivity. J. Hydrol. Eng., 18(9), 1157-1169.

Yang, J., and Chu, X., 2013b. Quantification of the spatio-temporal variations in hydrologic connectivity of small-scale topographic surfaces under various rainfall conditions. J. Hydrol., In press. doi: http://dx.doi.org/10.1016/j.jhydrol.2013.09.013

Yang, J., Chu, X., Chi, Y., and Sande, L., 2010. Effects of rough surface slopes on surface depression storage, p4427-4436. In: Challenges of Change, Proceedings of the 2010 World Environmental and Water Resources Congress, edited by R. N. Palmer. American Society of Civil Engineers.

Zhang, W., and Cundy, T. W., 1989. Modeling of two-dimensional overland flow. Water Resour. Res., 25(9), 2019-2035.

Zehe, E., and Sivapalan**,** M**.,** 2009**.** Threshold behaviour in hydrological systems as (human) geo-ecosystems: manifestations, controls, implications**.** Hydrol. Earth Syst. Sci., 13, 1273-1297.

CHAPTER 2. A NEW MODELING APPROACH TO IMPROVE THE SIMULATION OF MICROTOPOGRAPHY-DOMINATED DISCONTINUOUS OVERLAND FLOW PROCESSES OVER INFILTRATING SURFACES

2.1. Abstract

Realistic modeling of discontinuous overland flow on irregular topographic surfaces has been proven to be a challenge. This study aims to develop a modeling approach to simulate the discontinuous puddle-to-puddle (P2P) overland flow dynamics for infiltrating surfaces with various microtopographic characteristics. In the P2P model, puddles were integrated in a well-delineated, cascaded drainage system to facilitate explicit simulation of their dynamic behaviors and interactions. Overland flow and infiltration were respectively simulated by using the diffusion wave model and a modified Green-Ampt model for the DEM-derived flow drainage network that consisted of a series of puddle-based units. The new P2P model was tested by using a series of data from laboratory overland flow experiments for various microtopographic, soil, and rainfall conditions. The numerical simulation results highlighted the good performances of the new proposed model in examining the effects of varying spatial organization/heterogeneity in the factors that control overland flow generation and infiltration processes.

2.2. Introduction

The importance of surface microtopography in surface runoff, infiltration, and other hydrologic processes has been emphasized (Dunne et al., 1991; Hairsine et al., 1992; Helming et al., 1998; Govers et al., 2000; Darboux and Huang, 2005; Chu et al., 2010; Thompson et al., 2010; Chu et al., 2013). The spatial variability of surface microtopography influences overland flow generation (Martin et al., 2008), delays the initiation of surface runoff (Darboux and Huang, 2005), enhances the retention of runoff water (Abedini et al., 2006), controls spatial and temporal

variations of overland flow depth and velocity (Zhang and Cundy, 1989; Huang and Bradford, 1990; Esteves et al., 2000; Fiedler and Ramirez, 2000), and influences the infiltration rate (Darboux et al., 2001; Köhne et al., 2009; Rossi and Ares, 2012) and unsaturated flow (Liu et al., 2013). A series of modeling studies have demonstrated the importance of quantifying the actual surface topography and the related hydraulic effects in hydrologic models (Zhang and Cundy, 1989; Tayfur et al., 1993; Esteves et al., 2000). Due to the existence of depressions on topographic surfaces, overland flow often features with discontinuous characteristic and threshold-controlled puddle filling and spilling behaviors (Chu et al., 2013). Such a topography-dominated, threshold-driven overland flow process varies spatially and temporally and is referred to as puddle-to-puddle (P2P) dynamics (Chu et al., 2013). While the impacts of surface topography on runoff and infiltration processes have been well understood, limited effort has been made to quantitatively characterize such impacts (Helming et al., 1998; Govers et al., 2000; Darboux and Huang, 2005).

In the recent decade, research efforts have been made to conceptually model the hydrologic role of surface microtopography and quantify hydrologic connectivity and the associated dynamic variability in contributing areas. Darboux et al. (2001) developed a conditional-walker method to simulate depression filling and water redistribution on rough surfaces, and further evaluate the influence of surface microtopography on discharge. Antoine et al. (2009) applied a model similar to the one developed by Darboux et al. (2001) and further proposed a functional connectivity indicator (relative surface connection function) that linked surface connection to the filling of surface depression storage. Shaw et al. (2012) developed a conceptual model SPILL for the fill-spill of depressions and applied it to quantify runoff

contributing areas of the wetlands in the Prairie Pothole Region with assumptions of impervious surfaces and uniformly-distributed water input.

The aforementioned conceptual models did not take into account the spatio-temporally varying rainfall and infiltration processes. Instead, a steady and uniform rainfall distribution was assumed. In addition, instantaneous water transfer over a microtopographic surface was commonly assumed in such conceptual models (e.g., Darboux et al., 2001; Darboux et al., 2002; Antoine et al., 2009; Appels et al., 2011; Shaw et al., 2012), which may not be valid for large-scale hydrologic system. To consider the runoff water transferring time and depression storage, Antoine et al. (2011) integrated the connectivity information of subgrids (relative surface connectivity function) into the hydrograph by implementing two corrective procedures, one of which involved use of the continuity equation. However, a uniform slope and a 1D sheet flow were assumed in their modeling.

Various physically-based distributed models have been widely used to simulate overland flow processes. In such models, the Saint-Venant equations or the simplified forms (diffusion wave and kinematic wave equations) were numerically solved. However, these models are often limited to modeling of continuous overland flow. Particularly, they may suffer from modeling instability and convergence problems due to the high non-linear nature of the governing equations and abrupt slopes caused by topographic variations (Woolhiser and Liggett, 1967; Smith, 1985; Gottardi and Venutelli, 1993; Tayfur et al., 1993). To avoid the numerical oscillations, many hydrologic models relies smoothing DEMs and removing depressions (Tayfur et al., 1993; Jain and Singh, 2005; Tatard et al., 2008). In addition, numerical models are computationally intensive and time consuming. For instance, Antoine et al. (2011) found that the computation time of a diffusion wave model for a small plot (1×1 m^2 and 2-mm DEM

resolution) was three orders of magnitude slower (100 days) than that of their simplified conceptual model (10 min). Importantly, those numerical models (e.g., Esteves et al., 2000; Fiedler and Ramirez, 2000; Tatard et al., 2008) do not explicitly account for surface depressions and their storage, and simulate the dynamic behaviors of the depressions.

Therefore, both simplified conceptual models and physically-based distributed models have some critical limitations. This study aims to develop a new modeling approach that combines the capabilities of the conceptual models and the traditional numerical models to mitigate their limitations and improve the modeling applicability for complex topographic conditions. This is the first attempt to develop a physically-based distributed model that is able to simulate topography-dominated, discontinuous overland flow and infiltration in conjunction with the modeling of threshold-controlled, dynamic P2P filling-spilling-merging-splitting processes under various microtopographic, soil, and rainfall conditions.

2.3. Development of the P2P Overland Flow Model

Chu et al. (2013) developed a P2P modeling framework for simulating the microtopography-controlled P2P filling-spilling-merging-splitting overland flow dynamics and detailed the conceptual version of the P2P model. The P2P modeling included both cell-to-cell (C2C) and P2P flow routing for a set of puddle-based units (PBUs) in a well-delineated, cascaded drainage system. The P2P conceptual model focused on characterization of surface microtopography and modeling of the dynamic P2P filling, spilling, merging, and splitting processes, and accounted for unsteady, nonuniform rainfall and water losses (e.g., infiltration and evaporation). Instantaneous C2C and P2P water transfer was assumed in the conceptual model. This study is an extension of the modeling work of Chu et al. (2013). Based on the P2P conceptual model, this full version of the P2P model incorporates a quasi-3D numerical model,

which consists of a diffusion wave model for simulating overland flow and a modified Green-Ampt model (Chu and Marino, 2005) for simulating infiltration and unsaturated flow.

2.3.1. Overview of the P2P overland flow modeling framework

The flowchart of the full version of the P2P overland flow model is shown in Fig. 2.1. The model input data include basic simulation parameters, surface DEM, soil hydraulic property parameters, meteorologic data, and puddle delineation results from the PD program (Chu et al. 2010). In the P2P model, a series of nested loops are implemented for water routing, including time loop, basin loop, PBU loop, C2C loop, and P2P loop.

A topographic surface may consist of a number of basins, depending on the surface microtopographic characteristics and the number of outlets at the boundaries of the surface. Within a time step, water routing is performed for all basins (Fig. 2.1). Overland flow in a basin is essentially controlled by a cascaded P2P drainage system (Fig. 2.2). This system consists of a series of PBUs due to the existence of surface depressions, which break the continuity and connectivity of the topographic surface (Fig. 2.2). The PBUs often have relatively independent hydrologic characteristics and exhibit strong spatial and temporal variability (Fig. 2.2). Based on the puddle delineation results from the PD program (Chu et al. 2010), the P2P model tracks the PBUs of each basin and detects their upstream-downstream relationships. PBU is a basic simulation unit within a basin routing loop (Fig. 2.1). A PBU further consists of a number of contributing cells (DEM grids) and a highest-level puddle, which may include a group of lower-level embedded puddles (Chu et al., 2013) (Fig. 2.2). The threshold of the highest-level puddle connects this PBU to its downstream PBU (Fig. 2.2). Overland flow is routed for all PBUs by following their sequences in the well-delineated, cascaded P2P flow drainage system (Chu et al., 2013) (Fig. 2.1). Two routing procedures (i.e., C2C and P2P) are implemented for all PBUs (Figs.

2.1 and 2.2) (Chu et al., 2013). The C2C water routing transfers water from upstream to downstream cells, eventually to the water-ponded cells (i.e., puddle cells), while the P2P water routing simulates the dynamic filling and depleting of puddles and their interactions (i.e., spilling, merging, and splitting) (Fig. 2.2). The simulation for a basin ends when flow routing is completed for all PBUs in the basin, and the modeling continues until all basins are simulated (Fig. 2.1).

In the P2P model, the water sources of any overland cell include lateral inflow from its upstream cell(s) and rainfall input while the sink terms consist of lateral outflow to its downstream cell, infiltration, and evaporation (Fig. 2.2). Non-uniform and unsteady rainfall and evaporation are simulated in the P2P model by specifying a number of rainfall and evaporation zones.

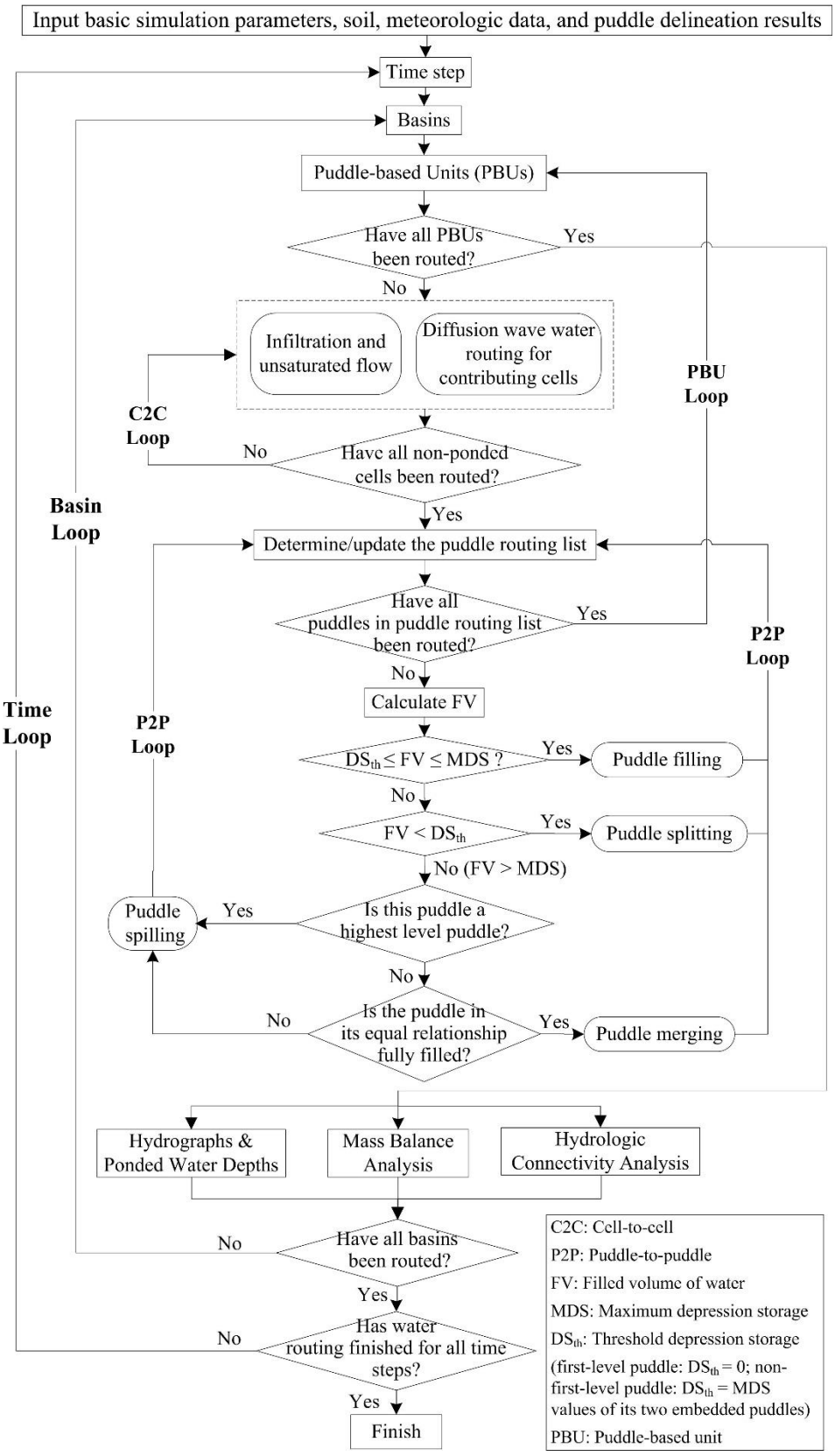

Fig. 2.1. Flowchart of P2P overland flow model

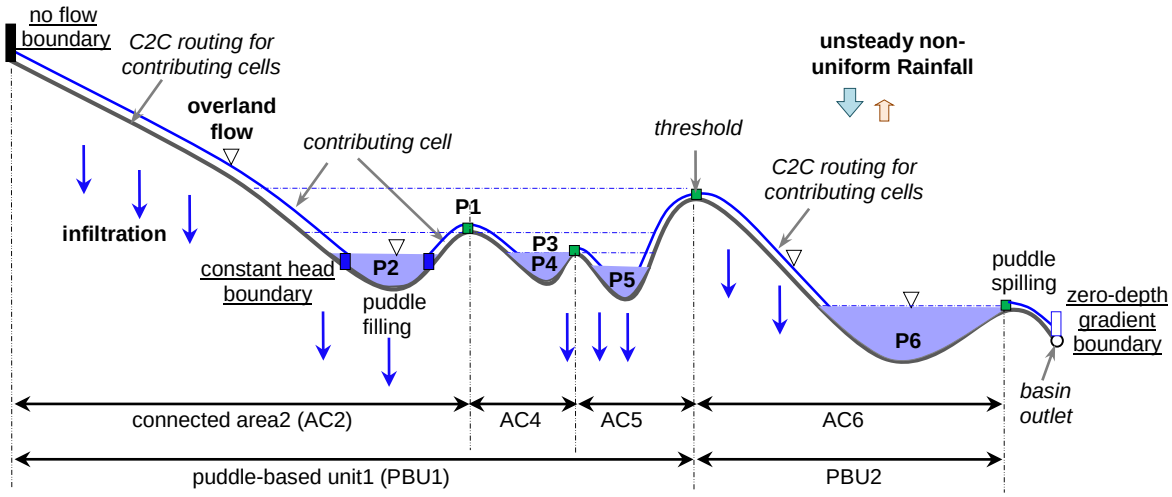

Fig. 2.2. Topography-dominated overland flow dynamics, cell-to-cell (C2C) and puddle-to-puddle (P2P) water routing procedures, and boundary conditions [note: P1 and P3 are higher-level merged puddles (e.g., P3 includes P4 and P5); connected area (AC) corresponds to a non-fully-filled puddle (e.g., P4 and AC4)]

2.3.2. C2C overland flow routing

The PBUs on a topographic surface may have varying sizes and irregular geometric shapes. To facilitate the flow routing on such irregular spatial domains, a DEM-based drainage network is identified for each PBU based on the D8 method (O'Callaghan and Mark, 1984) (Fig. 2.3). The drainage network of a PBU is determined by tracking all contributing cells using their flow directions backward from the puddle center or outlet of the PBU. The sequence of the cells in the derived flow drainage network essentially records the contributing relationships from one cell to another cell, or from multiple cells to one cell (Fig. 2.3). By taking advantage of these contributing relationships of cells in the flow drainage network, the C2C overland flow routing is conducted by simulating water movement from the most upstream cells to water-covered cells in the puddle(s) of the PBU (Fig. 2.3). Note that the water-ponded puddle cells are excluded in the C2C routing, and that the C2C simulation domain may change with the rising/falling in the

ponded water levels of the puddles as more/fewer cells covered by water (Fig. 2.3). The P2P routing initiates for a PBU after the C2C routing is completed (Fig. 2.1).

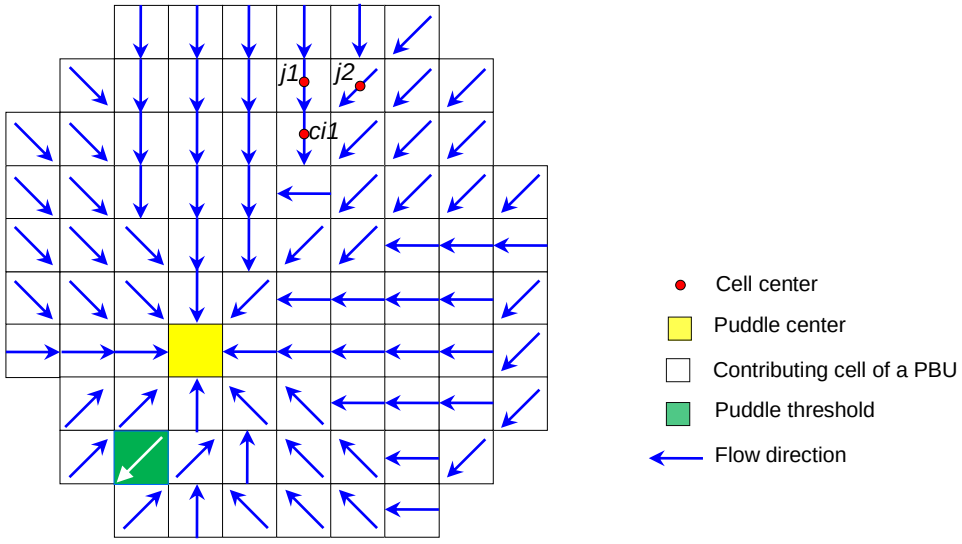

Fig. 2.3. Spatial discretization of D8 flow drainage network of a puddle-based unit (PBU)

Studies have demonstrated that the diffusion wave model is sufficiently accurate for modeling overland flow and adequate for a variety of practical applications (Woolhiser and Liggett, 1967; Morris and Woolhiser, 1980; Gonwa and Kavvas, 1986; Zhang and Cundy, 1989; Tayfur et al., 1993; Wang and Hjelmfelt, 1998; Jain and Singh, 2005). In the P2P model, a 1D diffusion wave model is used for C2C overland flow modeling for a time-varying spatial domain of each PBU. The continuity and momentum equations of the 1D diffusion wave overland flow model can be respectively expressed as:

$$a\frac{\partial h(x,t)}{\partial t}+\frac{\partial [Q(x,t)]}{\partial x}=a[q_{s,in}(x,t)-q_{s,out}(x,t)] \tag{2.1}$$

and

$$\frac{\partial h(x,t)}{\partial x}=S_0(x)-S_f(x,t) \tag{2.2}$$

where h = water depth [L]; x = distance along the flow direction [L]; a = channel width [L]; t = time [T]; $Q(x,t)$ = flow rate [L^3/T]; $q_{s,in}(x, t)$ = recharge rate of source terms [L/T]; $q_{s,out}(x, t)$ = discharge rate of sink terms [L/T]; S_0 = surface slope; and S_f = friction slope. The Manning's equation is applied to calculate flow velocity and account for flow resistance.

Rainfall is the only water source in the P2P model while the sink terms include infiltration and evaporation of the ponded water. In addition, the cells that directly connect to the thresholds of an upstream puddle (or PBU) may also receive spilled water when the upstream puddle is fully filled (Fig. 2.2).Thus, the recharge or discharge rates from source and sink terms are respectively given by:

$$q_{s,in}(x,t) = r(x,t) + hsp(x,t) \tag{2.3}$$

and

$$q_{s,out}(x,t) = e(x,t) + f(x,t) \tag{2.4}$$

where r = rainfall intensity [L/T]; e = evaporation rate [L/T]; f = infiltration rate [L/T]; and hsp = flow rate of spilled water from the upstream puddle or PBU [L/T].

Fig. 2.4 shows the discretization of the temporal and spatial simulation domains. h represents the water depth at the end of each time step; and the source and sink terms (i.e., $q_{s,in}$ and $q_{s,out}$) are constant within a time step (Fig. 2.4a). Fig. 2.4b displays the discretization of the spatial domain for the one-dimensional channel. Cells in Fig. 2.4b represents DEM grids, each cell has a center, at which it is assumed that the water depth and other state variables are constant across the entire cell.

The MacCormack method (MacCormack, 1969) is used to solve the diffusion wave equations [Eqs. (2.1) and (2.2)]. Specifically, the predictor procedure is implemented to calculate the predicted water depth $\overline{h(i,k+1)}$ by using the forward finite difference approximations for

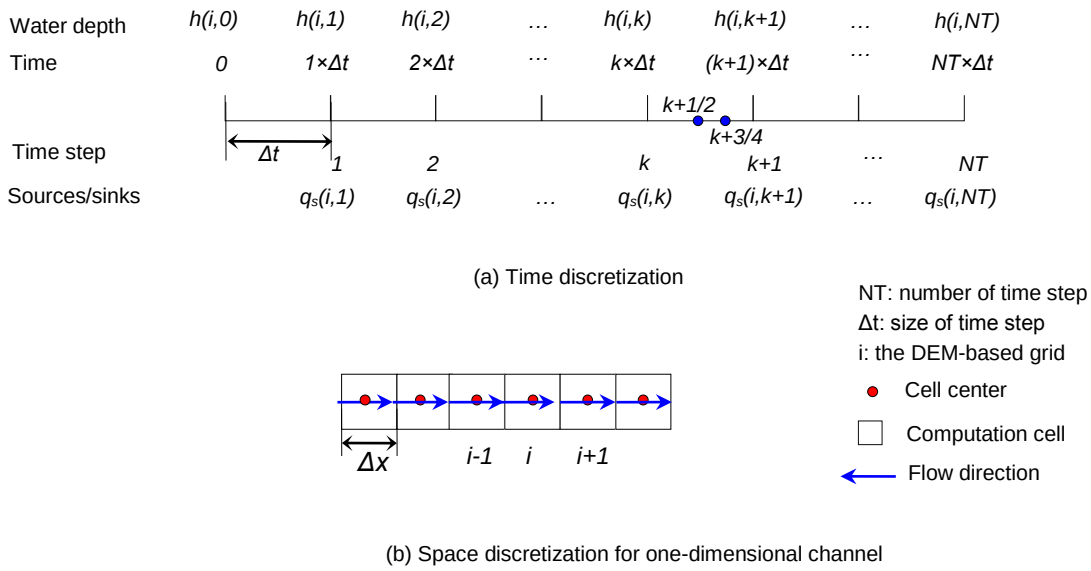

Fig. 2.4. Time and spatial discretization of the simulation domains

both time and space. Following the MacCormack method, the predictor finite difference form of Eq. (2.1) can be expressed as:

$$\Delta x \frac{\overline{h(i,k+1)} - h(i,k)}{\Delta t} = -\frac{Q(i+1,k) - Q(i,k)}{\Delta x} + \Delta x[q_{s,in}(i,k+\frac{1}{2}) - q_{s,out}(i,k+\frac{1}{2})] \qquad (2.5)$$

where Δx = cell size [L]; k = time step; i = cell number; and $q_{s,in}(i,k+\frac{1}{2})$ and $q_{s,out}(i,k+\frac{1}{2})$ = recharge and discharge (inflow and outflow) rates of source and sink terms for cell i at time $k+1/2$, respectively. Solving Eq. (2.5) yields the predicted water depth $\overline{h(i,k+1)}$:

$$\overline{h(i,k+1)} = h(i,k) - \frac{\Delta t[Q(i+1,k) - Q(i,k)]}{\Delta x^2} + \Delta t[q_{s,in}(i,k+\frac{1}{2}) - q_{s,out}(i,k+\frac{1}{2})] \qquad (2.6)$$

$Q(x,t)$ is calculated by using the Manning's equation:

$$Q(x,t) = \frac{\Delta x}{n(x)}[h(x,t)]^{\frac{5}{3}}[S_f(x,t)]^{\frac{1}{2}} \qquad (2.7)$$

where $n(x)$ = Manning's roughness coefficient. The friction slope S_f is calculated using the momentum equation:

$$S_f(x,t) = S_0(x) - \frac{\partial h(x,t)}{\partial x} \tag{2.8}$$

Q(i,k) and *Q(i+1,k)* in Eq. (2.6) are given by incorporating the backward finite difference form of the momentum equation [Eq. (2.2)] into Eq. (2.7):

$$Q(i,k) = \frac{\Delta x}{n(i)}[h(i,k)]^{\frac{5}{3}}[S_0(i) - \frac{h(i,k) - h(i-1,k)}{\Delta L_{i,i-1}}]^{\frac{1}{2}} = Q_{up-in}(i,k) \tag{2.9}$$

$$Q(i+1,k) = \frac{\Delta x}{n(i+1)}[h(i+1,k)]^{\frac{5}{3}}[S_0(i+1) - \frac{h(i+1,k) - h(i,k)}{\Delta L_{i,i+1}}]^{\frac{1}{2}} = Q_{out}(i,k) \tag{2.10}$$

where ΔL= distance between the centers of two cells [L], which is equal to Δx if flow is along x or y direction or $\sqrt{2}\Delta x$ if flow is along a diagonal direction (Fig. 2.3); $Q_{up\text{-}in}(i,k)$ = upstream inflow of cell *i* at time step *k* [L^3/T]; and $Q_{out}(i,k)$ = outflow of cell *i* at time step *k* [L^3/T]. Substituting Eqs. (2.9) and (2.10) into Eq. (2.6) gives:

$$\overline{h(i,k+1)} = h(i,k) + \frac{\Delta t[Q_{up-in}(i,k) - Q_{out}(i,k)]}{\Delta x^2} + \Delta t[q_{s,in}(i,k+\frac{1}{2}) - q_{s,out}(i,k+\frac{1}{2})] \tag{2.11}$$

According to the DEM-based D8 flow drainage network, cell *i* may receive water from a number of upstream cells (Fig. 2.3). The total inflow of cell *i*, $Q_{in}(i,k)$, can be calculated as the summation of the outflow Q_{out} from its upstream contributing cells as follows:

$$Q_{in}(i,k) = \sum_{j=1}^{nncc_i} Q_{out}(j,k) \tag{2.12}$$

where $nncc_i$ = number of upstream cells that contribute water to cell *i*. Thus, based on the D8 flow drainage network, Eq. (2.11) can be further expressed as:

$$\overline{h(i,k+1)} = h(i,k) + \frac{\Delta t[Q_{in}(i,k) - Q_{out}(i,k)]}{\Delta x^2} + \Delta t[q_{s,in}(i,k+\frac{1}{2}) - q_{s,out}(i,k+\frac{1}{2})] \tag{2.13}$$

For the corrector procedure, backward finite difference method is implemented for both time and space. As shown below, the time increment used in the corrector procedure is $\Delta t/2$.

$$\Delta x \frac{h(i,k+1)-h(i,k+\frac{1}{2})}{\Delta t/2} = -\frac{\overline{Q(i,k+1)}-\overline{Q(i-1,k+1)}}{\Delta x} + \Delta x[q_{s,in}(i,k+\frac{3}{4}) - q_{s,out}(i,k+\frac{3}{4})] \quad (2.14)$$

$$h(i,k+1) = h(i,k+\frac{1}{2}) - \frac{\Delta t}{2}\frac{\overline{Q(i,k+1)}-\overline{Q(i-1,k+1)}}{\Delta x^2} + \frac{\Delta t}{2}[q_{s,in}(i,k+\frac{3}{4}) - q_{s,out}(i,k+\frac{3}{4})] \quad (2.15)$$

in which $q_{s,in}(i,k+\frac{3}{4})$ and $q_{s,out}(i,k+\frac{3}{4})$ are the source and sink terms at time point *k +3/4*, respectively. $\overline{Q(i,k+1)}$ and $\overline{Q(i-1,k+1)}$ are calculated by incorporating forward finite difference approximation of the momentum equation [Eq. (2.2)].

$$\overline{Q(i,k+1)} = \frac{\Delta x}{n(i)}[\overline{h(i,k+1)}]^{\frac{5}{3}}[S_0(i) - \frac{\overline{h(i+1,k+1)}-\overline{h(i,k+1)}}{\Delta L_{i,i+1}}]^{\frac{1}{2}} = \overline{Q_{out}(i,k+1)} \quad (2.16)$$

$$\overline{Q(i-1,k+1)} = \frac{\Delta x}{n(i-1)}[\overline{h(i-1,k+1)}]^{\frac{5}{3}}[S_0(i-1) - \frac{\overline{h(i,k+1)}-\overline{h(i-1,k+1)}}{\Delta L_{i,i-1}}]^{\frac{1}{2}} = \overline{Q_{up-in}(i,k+1)} \quad (2.17)$$

Thus, Eq. (2.15) can be rewritten as:

$$h(i,k+1) = h(i,k+\frac{1}{2}) - \frac{\Delta t}{2}\frac{\overline{Q_{out}(i,k+1)}-Q_{up-in}(i,k+1)}{\Delta x^2} + \frac{\Delta t}{2}[q_{s,in}(i,k+\frac{3}{4}) - q_{s,out}(i,k+\frac{3}{4})] \quad (2.18)$$

Similar to the predictor procedure, the total inflow of a cell can be calculated based on the D8 flow drainage network (Fig. 2.3):

$$\overline{Q_{in}(i,k+1)} = \sum_{j=1}^{nncc} \overline{Q_{out}(j,k+1)} \quad (2.19)$$

$h(i,k+\frac{1}{2})$ is given by:

$$h(i,k+\frac{1}{2}) = \frac{1}{2}[h(i,k) + \overline{h(i,k+1)}] \quad (2.20)$$

Hence, the final expression for the water depth at time step *k+1* for the corrector procedure is given by:

$$h(i,k+1)=\frac{1}{2}\left\{h(i,k)+\overline{h(i,k+1)}+\Delta t\,\frac{\overline{Q_{in}(i,k+1)}-\overline{Q_{out}(i,k+1)}}{\Delta x^2}+\Delta t[q_{s,in}(i,k+\frac{3}{4})-q_{s,out}(i,k+\frac{3}{4})]\right\} \quad (2.21)$$

The procedures to conduct the computation of each of the predictor and corrector numerical schemes can be detailed in the following three steps. Firstly, the outflow values for all contributing cells are calculated (i.e., Eqs. 2.10 and 2.16) following the order of their sequences outlined in the DEM-based drainage network. Secondly, the inflow values for all contributing cells are calculated by accounting for the outflow values (calculated in step 1) from their upstream contributing neighboring cells (Fig. 2.3) (i.e., Eqs. 2.12 and 2.19). Thirdly, the water depths of time step *k+1* for predictor and corrector steps are calculated (i.e., Eqs. 2.13 and 2.21).

2.3.2.1. Initial condition

In the C2C modeling, all contributing cells in PBUs are assumed to be dry initially:

$$h(x,t)\big|_{t=0}=0 \qquad x\in\Omega_{cc} \quad (2.22)$$

For a base point *i* at time *0*:

$$h(i,0)=0 \qquad i\in\Omega_{cc} \quad (2.23)$$

where Ω_{cc} = contributing cells (i.e., spatial domain for the diffusion wave routing) (Figs. 2.2 and 2.5).

The water depth *h* at time step *1* can be calculated using the initial water depth values (i.e., time step *0*). The predictor approximation of the water depth at time step *1* can be derived using Eq. (2.13) by substituting time steps from *k*, *k+1* for *0*, and *1*, respectively:

$$\overline{h(i,1)}=h(i,0)-\frac{\Delta t[Q(i+1,0)-Q(i,0)]}{\Delta x^2}+\Delta t[q_{s,in}(i,\frac{1}{2})-q_{s,out}(i,\frac{1}{2})] \quad (2.24)$$

Since the water depth *h* at time step *0* is equal to zero for all contributing cells, *Q(i+1,0)* and *Q(i,0)* are equal to zero. Therefore, the above equation can be rewritten as follows:

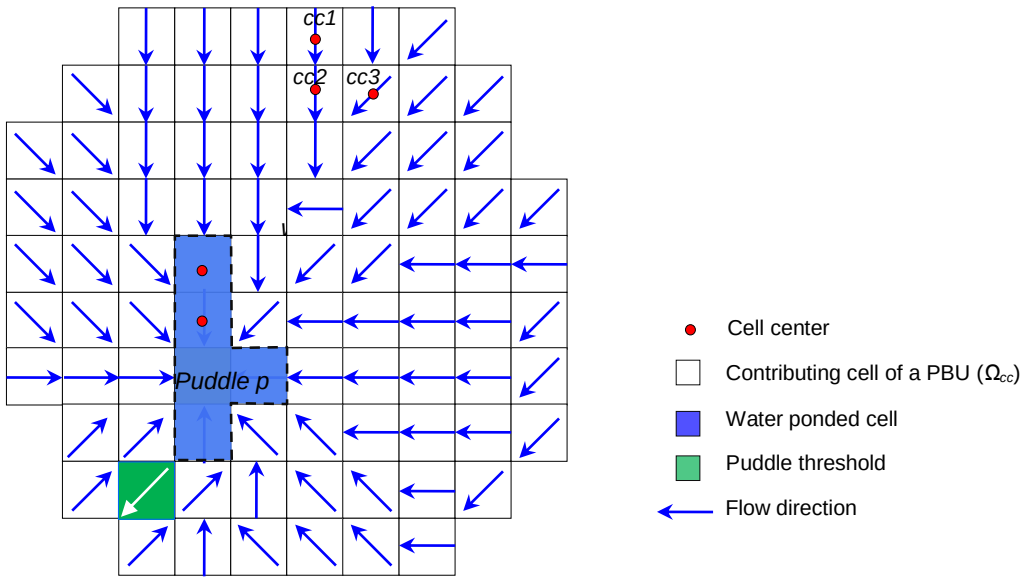

Fig. 2.5. Initial ponding condition of a puddle-based unit (PBU) for t = 0 (note: at t = 0, puddle p is not fully filled (e.g., with maximum depression storage)

$$\overline{h(i,1)} = \Delta t[q_{s,in}(i,\frac{1}{2}) - q_{s,out}(i,\frac{1}{2})] \tag{2.25}$$

Based on Eq. (2.21), the corrector approximation of the water depth at time step *1* can be derived as follows:

$$h(i,1) = \frac{1}{2}\left\{\overline{h(i,1)} + \Delta t\frac{\overline{Q_{in}(i,1)} - \overline{Q_{out}(i,1)}}{\Delta x^2} + \Delta t[q_{s,in}(i,\frac{3}{4}) - q_{s,out}(i,\frac{3}{4})]\right\} \tag{2.26}$$

2.3.2.2. Boundary conditions

Three types of boundary conditions are considered in the P2P overland flow model to handle the interactions between the C2C modeling domain and the outside surroundings, including the water-covered puddle cells. These boundary conditions include: (1) no flow boundary for the most upstream cells of PBUs (Figs. 2.2 and 2.6), (2) constant head boundary for the C2C routing cells that directly connected to the water-ponded puddle cells (Figs. 2.2 and 2.6), and (3) zero-depth gradient boundary for the outlet cells (Figs. 2.2).

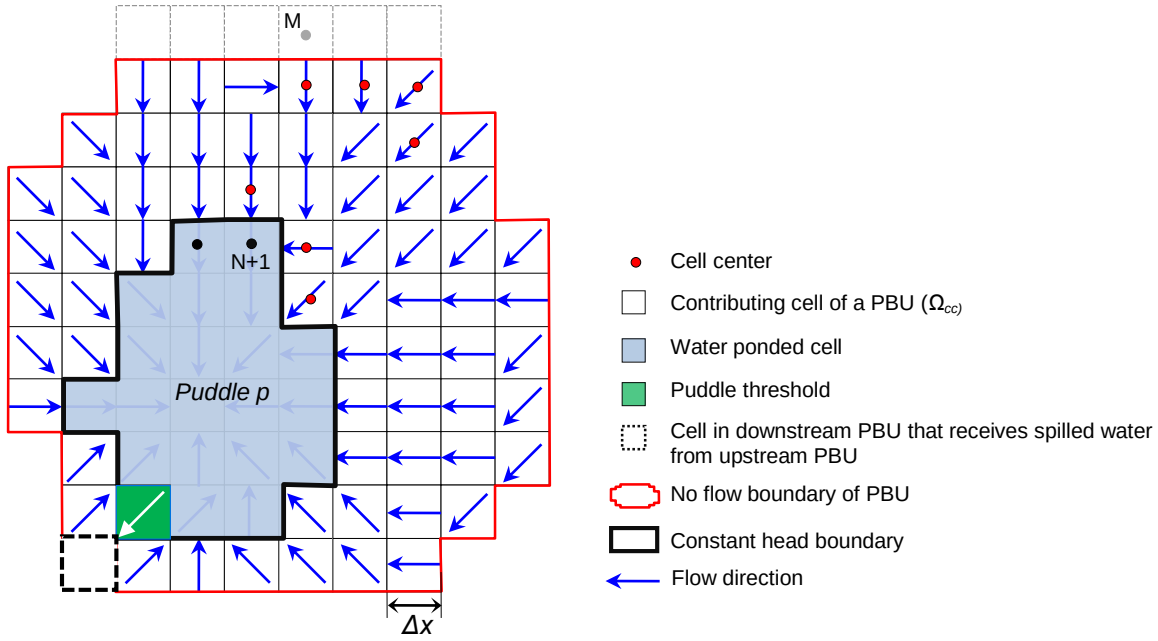

Fig. 2.6. Flow drainage network, contributing cells, water ponded cells, no flow boundary, and constant head boundary of a puddle-based unit (PBU)

(1) No flow boundary

The most upstream boundary cells of the drainage network of a PBU have a closed boundary (Figs. 2.2 and 2.6). The inflow of the boundary cells from the outside surrounding is zero:

$$Q\ (x,t) = 0 \qquad\qquad x \in \Omega_{NFB} \tag{2.27}$$

where Ω_{NFB} = no flow boundary domain (Fig. 2.6). Eq. (2.27) implies that a boundary cell N receives zero flow from its upstream outside cell M (i.e., outflow of dummy cell M) at time step k:

$$Q_{out}(M,k) = 0 \qquad\qquad M \in \Omega_{NFB} \tag{2.28}$$

The predictor approximation of the water depth for the cell N (Fig. 2.6) can be calculated using water depth at the time step k based on the Eq. (2.13), which can be expressed as:

$$\overline{h(N,k+1)} = h(N,k) - \Delta t \frac{Q_{in}(N,k) - Q_{out}(N,k)}{\Delta x^2} + \Delta t[q_{s,in}(N,k+\frac{1}{2}) - q_{s,out}(N,k+\frac{1}{2})] \tag{2.29}$$

in which, $Q_{in}(N,k)$ is calculated as:

$$Q_{in}(N,k) = \sum_{j=1}^{nncc_N} Q_{out}(j,k) + Q_{out}(M,k) = \sum_{j=1}^{nncc_N} Q_{out}(j,k) \quad (2.30)$$

where $nncc_N$= the number of neighboring boundary cells that contribute water to the boundary cell *N*. Following the Eq. (2.21), the water depth *h* for the corrector procedure at time step *k* for the cell *N* can be expressed as:

$$h(N,k+1) = \frac{1}{2}\left\{ h(N,k) + \overline{h(N,k+1)} - \Delta t \frac{\overline{Q_{in}(N,k+1)} - \overline{Q_{out}(N,k+1)}}{\Delta x^2} + \Delta t[q_{s,in}(N,k+\frac{3}{4}) - q_{s,out}(N,k+\frac{3}{4})] \right\} \quad (2.31)$$

(2) Constant head boundary

The constant head boundary is applied to transfer water between the C2C contributing cells and the water-ponded puddle cells (Fig. 2.6). A constant head boundary cell (cell *N*) is linked to its downstream puddle cell (cell *N*+1). The water elevation of the puddle cell (*N*+1) is equal to the uniform water level of its corresponding puddle, which is assumed constant within a time step.

$$h(x,t) + z(x) = zhp(p,t) \qquad x \in \Omega_{CHB}(p,t) \quad (2.32)$$

$$h(N+1,k) + z(N+1) = zhp(p,k) \qquad N+1 \in \Omega_{CHB}(p,k) \quad (2.33)$$

where z*hp(t)* = water elevation of puddle *p* at time *t* [L]; *z(x)* = elevation at *x* [L]; $\Omega_{CHB}(p, k)$ = constant head boundary domain at time step *k* for puddle *p; h(N+1,k)* = water depth of cell *N+1* at time step *k* [L]; and $\Omega_{CHB}(p,k)$ = constant head boundary domain at time step *k* for puddle *p*. Note that the water level of a puddle or its water-ponded cells is assumed constant within one time step in the C2C water routing procedure, but it may change over time due to the dynamic P2P process.

The water depth of the predictor step for a cell *N* (e.g., N_1 Fig. 2.6) that directly links to the water ponded cell *N+1* can be calculated as:

$$\overline{h(N,k+1)} = h(N,k) + \frac{\Delta t[Q_{in}(N,k) - Q_{out}(N,k)]}{\Delta x^2} + \Delta t[q_{s,in}(N,k+\frac{1}{2}) - q_{s,out}(N,k+\frac{1}{2})] \quad (2.34)$$

in which, $Q_{out}(N,k)$ can be calculated as:

$$Q_{out}(N,k) = \frac{\Delta x}{n(N+1)}[h(N+1,k)]^{\frac{5}{3}}[S_0(N+1) - \frac{zhp(p,k) - z(N+1,k) - h(N,k)}{dx_{N,N+1}}]^{\frac{1}{2}} \quad (2.35)$$

Similarly, the water depth for the corrector procedure for the cell N can be calculated as:

$$h(N,k+1) = \frac{1}{2}\left\{h(N,k) + \overline{h(N,k+1)} + \Delta t \frac{\overline{Q_{in}(N,k+1)} - \overline{Q_{out}(N,k+1)}}{\Delta x^2} + \Delta t[q_{s,in}(N,k+\frac{3}{4}) - q_{s,out}(N,k+\frac{3}{4})]\right\} \quad (2.36)$$

The outflow discharge $Q'_{out}(N,k+1)$ from the cell N to the constant head boundary cell $N+1$ of puddle p at time $k+1$ (Fig. 2.6) can be calculated as the average of the outflow of the cell N from the predictor and corrector steps:

$$Q'_{out}(N,k+1) = \frac{1}{2}[Q_{out}(N,k) + \overline{Q_{out}(N,k+1)}] \quad (2.37)$$

Cell $N+1$ may receive inflow from several its neighboring C2C routing cells (i.e., N_1 and N_2, Fig. 2.6) based on the D8 flow drainage network. The total inflow from the neighboring contributing cells N to the cell $N+1$, $Q'_{in}(N+1,k+1)$ can be calculated as the summation of the outflow discharges of upstream neighboring C2C routing cells.

$$Q'_{in}(N+1,k+1) = \sum_{N=1}^{nncc_{N+1}} \overline{Q'_{out}(N,k+1)} \qquad N+1 \in \Omega_{CHB}(p,k) \quad (2.38)$$

where $nncc_{N+1}$ = the number of the upstream neighboring C2C routing cells N that contribute water to the constant head boundary cell $N+1$.

Thus, the total inflow of the puddle p, $Q''_{in}(p,k+1)$, from its constant head boundary cells can be calculated as:

$$Q''_{in}(p,k+1) = \sum_{N+1=1}^{nchb_p} Q'_{in}(N+1,k+1) \qquad N+1 \in \Omega_{CHB}(p,k) \quad (2.39)$$

where $nchb_p$ = the number of cells in the constant head boundary domain $\Omega_{CHB}(p,k)$ of the puddle p. The calculated inflow discharge to the puddle p is used for the simulation of the P2P routing procedure. Note that the water level of a puddle or its water-ponded cells is assumed constant within one time step in the C2C water routing procedure, but it may change over time due to the dynamic P2P process.

(3) Zero-depth gradient boundary

The outflow boundaries (a set of outlet cells delineated by the PD program) are located at the most downstream ends of the entire drainage network. The zero-depth gradient boundary is applied to these outlet cells:

$$\frac{\partial h}{\partial x} = 0 \qquad x \in \Omega_{ZDGB} \tag{2.40}$$

$$h(N+1,k) = h(N,k) \qquad N \in \Omega_{ZDGB} \tag{2.41}$$

where Ω_{ZDGB} = zero-depth gradient boundary domain; N = outlet boundary cell; and $N+1$ = outside dummy cell (Fig. 2.7).

Based on the Eq. (2.13), the water depth for the predictor step of an outlet boundary cell N (Fig. 2.7) can be calculated as:

$$\overline{h(N,k+1)} = h(N,k) + \frac{\Delta t[Q_{in}(N,k) - Q_{out}(N,k)]}{\Delta x^2} + \Delta t[q_{s,in}(N,k+\frac{1}{2}) - q_{s,out}(N,k+\frac{1}{2})] \tag{2.42}$$

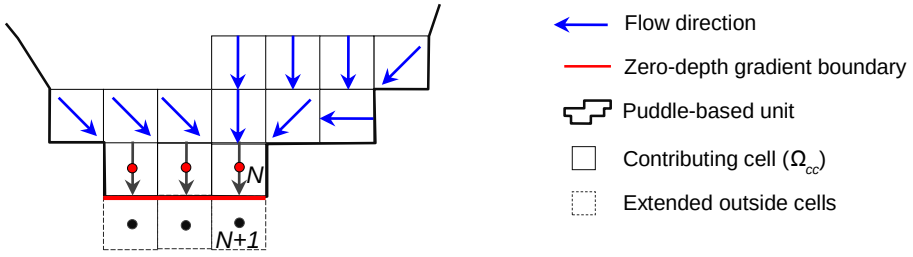

Fig. 2.7. Zero-depth gradient boundary condition

Similarly, the corrector procedure water depth for the cell *N* can be calculated based on the Eq. (2.21):

$$h(N,k+1)=\frac{1}{2}\left\{h(N,k)+\overline{h(N,k+1)}+\Delta t\frac{\overline{Q_{in}(N,k+1)}-\overline{Q_{out}(N,k+1)}}{\Delta x^2}+\Delta t[q_{s,in}(N,k+\frac{3}{4})-q_{s,out}(N,k+\frac{3}{4})]\right\} \quad (2.43)$$

The outflow discharge $Q'_{out}(N,k+1)$ from the cell *N* (Fig. 2.7) at time $k+1$ can be calculated as the average of the outflow discharge from the cell *N* of the predictor and corrector steps:

$$Q'_{out}(N,k+1)=\frac{1}{2}[Q_{out}(N,k)+\overline{Q_{out}(N,k+1)}] \quad (2.44)$$

The total outflow $Q''_{out}(k+1)$ from a surface can be calculated as the summation of outflow discharges from all outflow boundary cells:

$$Q''_{out}(k+1)=\sum_{n=1}^{nczg} Q'_{out}(N,k+1) \quad (2.45)$$

where *nczg* = the number of outlet cells.

The aforementioned finite difference numerical scheme for solving the diffusion wave equations is stable if the Courant-Friedrichs-Lewy criterion is satisfied (Huang and Song, 1985; Jain and Singh, 2005).

$$\max\left\{\frac{\Delta t[u(i,k)+\sqrt{gh(i,k)}]}{\Delta x}\right\}\le 1 \qquad i\in\Omega_{cc} \quad (2.46)$$

where *g*=acceleration due to gravity [L/T^2].

2.3.3. P2P overland flow routing

The P2P water routing links to the C2C modeling through the constant head boundaries and involves simulation of the puddle filling, spilling, merging, and splitting processes after water routing from contributing cells to the water-covered puddle cells of a PBU (Figs. 2.1 and

2.2). A PBU may include one first-level puddle (e.g., puddle P6 in PBU2, Fig. 2.2) or a group of embedded puddles at multiple levels (e.g., puddles P1-P5 in PBU1, Fig. 2.2). The P2P water routing consists of two major steps: (1) creating/updating a puddle routing list and (2) conducting the P2P water routing for each puddle in the puddle routing list.

The dynamic P2P routing for a time step may not involve all puddles of a PBU. In the P2P model, the puddle routing list for a time step is utilized to regulate the puddles that are "active" in the P2P processes. Whether or not a puddle is involved in the P2P routing at a time step depends on its filling condition and the relationships with its neighboring puddles. For instance, if a PBU has a single-level puddle (e.g., puddle P6 in PBU2, Fig. 2.2), this puddle is added to the puddle routing list. For a group of multi-level puddles, whether or not the highest-level puddle (e.g., puddle P1, Fig. 2.2) and its embedded puddles (e.g., puddles P2-P5 of PBU1, Fig. 2.2) are included in the puddle routing list depends on their filling status indicated by a puddle ponding index. Three puddle ponding index values (0, 1, and 100) are used to represent the unfilled (e.g., puddle P1, Fig. 2.2), partially-filled (e.g., puddle P2, Fig. 2.2), and fully-filled conditions (e.g., puddle P6, Fig. 2.2), respectively. The P2P routing involves a sequence of puddle filling, spilling, merging, and splitting for all puddles on the puddle routing list. The puddle routing list is a dynamic one, which is updated by adding or removing puddles to/from the list after completing water routing due to any of the spilling, merging, and splitting processes for a puddle (Fig. 2.1).

The P2P routing for a puddle on the puddle routing list depends on the amount of available water in this puddle and the relationships with its neighboring puddles. First, the total volume of water available to fill the puddle (Fig. 2.1) is calculated based on: (1) the water ponded in the puddle at the beginning of current time step, (2) the water loss or gain from the

source and sink terms, and (3) inflow from the upstream contributing cells simulated by the C2C water routing. Based on this calculated total water volume and the stage-area-volume relationship of the puddle, P2P modeling is performed for the following three conditions (Fig. 2.1):

Condition 1: If the total available water volume of the puddle being routed is greater than zero and smaller than its maximum depression storage, a puddle filling process occurs (Fig. 2.1, puddle P2 in Fig. 2.2). Based on the stage-area-volume relationship of the puddle, the inundation area and the corresponding water-ponded puddle cells are identified and the level of ponded water of this puddle and the associated cells is determined. It is assumed that all water-ponded puddle cells have a uniform water level (e.g., puddle P2 in Fig. 2.2).

Condition 2: Due to infiltration and evaporation of the ponded water, an individual puddle can be dry. In this case, a higher-level puddle that consists of a number of lower-level embedded puddles will split into its lower-level puddles (puddle splitting process) if the net volume of available water is negative (Fig. 2.1). In the P2P model, the ponding index of this higher-level puddle shifts to 0 (i.e., unfilled condition). The lower-level embedded puddles are added to the puddle routing list, and corresponding changes also are made to their ponding index values. For example, due to water losses, a splitting process is trigged for puddle P3 (Fig. 2.2), forming two lower-level embedded puddles P4 and P5 (Fig. 2.2). The puddle splitting process occurs only when the water level of a merged puddle drops below the threshold of its embedded puddles (e.g., the threshold point A of puddles P4 and P5 in Fig. 2.2).

Condition 3: If the volume of water available for the puddle being routed is greater than its maximum depression storage, three cases that may involve both spilling and merging processes occur (Fig. 2.1): (1) if the puddle being routed is a single level puddle or a puddle at

the highest level, the excess water spills through its threshold(s) to the downstream cell(s) (Fig. 2.1) (e.g., puddle P6 in Fig. 2.2); (2) if the puddle being routed (e.g., puddle P4 in Fig. 2.2) shares a common threshold with another puddle that is not fully filled (e.g., P5, Fig. 2.2), the excess water spills to that puddle; and (3) if the puddle being routed shares a common threshold with another puddle that is already fully filled, the two puddles merge and form a higher-level puddle. This merged puddle is then added to the puddle routing list and its ponding index is changed accordingly.

After each puddle in the puddle routing list completes its water routing, the puddle routing list is updated until all puddles in the list are routed (Fig. 2.1). Within one time step, the water level in a puddle may rise or drop dramatically, and the water routing process generally involves puddles at different levels. If the highest level puddle in a PBU reaches the fully-filled condition (e.g., P1, Fig. 2.2), the excess water spills to its downstream PBU (PBU2, Fig. 2.2), and then water routing for next PBU initiates (Fig. 2.1). Following the cascaded overland flow drainage pattern, such a modeling procedure is performed for all PBUs. The simulation for a basin ends when all of the PBUs in the basin complete their flow routing (Fig. 2.1). Then, the modeling continues for next basin until all basins complete their P2P water routing (Fig. 2.1). The total discharge from the entire surface is calculated as the summation of the discharges from all basins.

A surface may have some special topographic features (e.g., flats and multi-threshold puddles). In addition to water routing for regular puddles, special schemes also are developed and incorporated in the P2P model to cope with the water routing for these special topographic features. In the case of a multi-threshold puddle, the filling process is similar to that for regular puddles. However, after this puddle is fully-filled, the excess water is evenly distributed to all the

thresholds of the puddle and spills to their downstream cells or puddles. A flat is treated as a "flat puddle" that is able to transfer runoff water, but has zero depression storage (i.e., it cannot store any water) (Chu et al. 2013). The P2P model provides modeling details on the dynamic C2C and P2P processes, puddle filling status, ponded water distributions, discharges at basin outlets, and mass balance analyses for all time steps.

2.3.4. Modified Green-Ampt equations for infiltration and unsaturated flow simulation

Infiltration and unsaturated flow are simulated for all cells in a PBU by using the modified Green-Ampt model (Chu and Marino, 2005) (Fig. 2.1). The modified Green-Ampt model incorporated in the P2P model simulates infiltration into layered soils of arbitrary initial soil moisture distributions and rainfall excess under complex rainfall patterns. Two distinct periods, pre-ponding and post-ponding, are taken into account in the infiltration modeling. The model tracks the movement of wetting front along each soil profile, checks the ponding status, and handles the shift between ponding and non-ponding conditions. In addition, the model simulates soil water drainage and redistribution for dry time periods between rainfall events (Chu and Marino, 2006).

2.3.5. Modeling of time-varying hydrologically-connected areas

Depressions break the connectivity of a topographic surface and generate a number of hydrologically localized areas, which are referred to as "connected areas" (ACs) (Fig. 2.2). At the initial stage of the rainfall-runoff process, all cells within an AC drain runoff water to the corresponding puddle (e.g., AC2 in Fig. 2.2). After the puddle is fully filled, it spills the excess water to its downstream cell(s) or puddle(s), which develops the connection between the two ACs, inducing expansion or evolution of ACs. Any hydrologic connection of an AC to the outlet of the surface may result in a stepwise increase in the outlet discharge. Note that an AC is

different from a PBU in two aspects: (1) PBUs are a series of "static" topographic domains serving as basic units in the P2P overland flow routing, while ACs are time-varying contributing areas associated with unfilled or partially-filled depressions and basin outlets; and (2) PBUs include a highest-level puddle and probably a set of embedded puddles (e.g., puddles P1-P5 for PBU1 in Fig. 2.2), while each AC relates to one unfilled or partially-filled puddle regardless of the level of the puddle.

In the P2P model, identification of initial ACs ($t = 0$) starts from the basin outlet(s) and the centers of all first-level puddles based on the flow directions determined by the PD program (Chu et al., 2010). These DEM-determined ACs may change over time, depending on the surface topographic characteristics and water sources and sinks of the system. For any time steps, such time-varying ACs are determined starting from the basin outlets and unfilled or partially-filled puddles by adding: (1) their contributing cells and (2) any upstream ACs that are fully filled and have connected to the AC being identified. These time-varying ACs are utilized to analyze hydrologic connectivity and the related threshold behaviors.

2.3.6. Testing of the P2P overland flow model

The conceptual version of the P2P model has been tested using experimental data for imperious surfaces to demonstrate its capability in simulating the P2P dynamics (Chu et al., 2013) and quantifying the related hydrologic conductivity (Yang and Chu, 2013). In this study, the P2P model was compared against the analytical solution to a kinematic wave overland flow model (Woolhiser, 1975) for a smooth hillslope surface. The area of the smooth hillslope surface was 60.0×30.0 m^2 and its slope was 5.0%. A steady and uniform rainfall with an intensity of 7.62 cm/hr and a duration of 30 min was applied in the modeling.

Few existing studies combined overland flow experiments with modeling of the P2P overland flow dynamics for infiltrating soil surfaces of various depressions. In this study, three laboratory overland flow experiments were used to verify the capability of the P2P model in simulating the dynamic P2P filling-spilling-merging-splitting processes for microtopography-influenced, infiltrating soil surfaces under various rainfall conditions (Bogart, 2014). Table 2.1 shows the basic information on the three laboratory overland flow experiments. Experiments 1 and 2 were conducted using two soil surfaces with distinct microtopographic characteristics (rough and smooth, Figs. 2.8a and 2.8b) under the same soil and initial moisture conditions. Similar unsteady rainfall events with the same duration (Table 2.1) were applied for these two experiments. A much larger soil surface (Fig. 2.8c), different soil type and initial soil moisture content, and a steady rainfall event (Table 2.1) were applied for Experiment 3.

Table 2.1. Descriptions of three laboratory overland flow experiments

Experiment	Surface	Surface Size (m^2)	Duration (min)	Rainfall Intensity (cm/hr)	Initial Water Content	Soil Type
1	S1	1.0×0.6	92	Unsteady nonuniform: 5.90 (25 min) - 1.15 (42.5 min) - 3.56 (16.5 min) - 5.90 (8 min)	0.213	silty clay
2	S2	1.0×0.6	92	Unsteady nonuniform: 6.00 (25 min) -1.17 (42.5 min) - 3.52 (16.5 min) - 6.00 (8 min)	0.213	silty clay
3	S3	3.0×1.2	80	Steady nonuniform: 3.23 (60 min)	0.145	silty clay loam

Surfaces S1-S3 were scanned by using an instantaneous-profile laser scanner and their high-resolution DEMs were acquired. A four-head Norton-style rainfall simulator was utilized to generate rainfall for the three experiments. The data collected from the experiments included: outlet discharges, wetting front depths, and a set of critical times (e.g., ponding time, and puddle

spilling and merging times). The experiments continued until the outlet discharge approached to a steady state. P2P modeling was then performed by using the same experimental data (e.g., DEMs, soil properties, and meteorologic data). The simulation results were then compared with the observed data from the experiments.

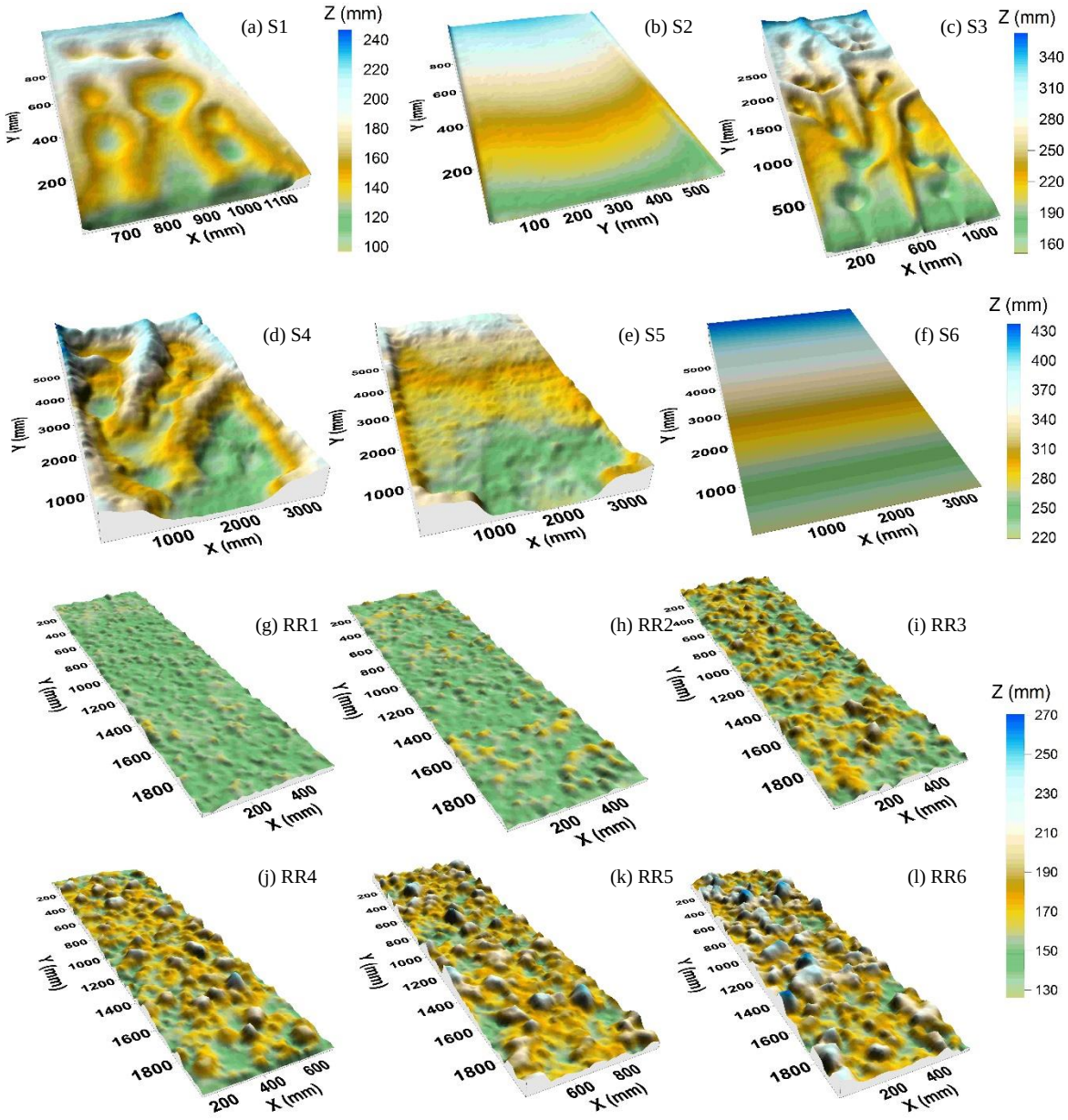

Fig. 2.8. DEMs of twelve topographic surfaces used for P2P overland flow modeling

2.3.7. Analyses of overland flow dynamics and infiltration for various microtopographic and rainfall conditions

To better understand the combined effects of surface microtopography and rainfall characteristics on the dynamic P2P overland flow processes under the influence of infiltration, the P2P model was applied to nine selected surfaces that had different microtopographic characteristics and various rainfall conditions were simulated. The surfaces included: (1) two field plots (S4 and S5) with an area of 3.5×6.0 m^2 and an overall slope of 2.5% (Figs. 2.8d and 2.8e); (2) a smooth hillslope surface (S6, Fig. 2.8f), which had the same area and slope as those of surfaces S4 and S5; and (3) six random roughness surfaces (RR1 - RR6) with an area of 0.6×2.0 m^2 (Figs. 2.8g and 2.8l). The random roughness values for the six RR surfaces increased from 0.34 cm for RR1 to 1.5 cm for RR6. Surfaces S4-S5 and RR1-RR6 were scanned by using the instantaneous-profile laser scanner to obtain their high-resolution DEMs. The statistical descriptions of the six random roughness surfaces were detailed by Chu et al. (2012) and Chi et al. (2012).

In the P2P modeling, a steady uniform rainfall event with an intensity of 2.2 cm/hr (Rain 1, Fig. 2.9) was firstly applied to surfaces S4-S6 and RR1-RR6 to examine the effects of surface microtopography on the P2P overland flow processes. Then, three unsteady rainfall events (Rain 2-4, Fig. 2.9) were applied to surfaces S4-S6 to discuss the influences of temporal variability in rainfall on the P2P dynamics (Table 2.2). Note that the three unsteady rainfall events (Rain 2-4) had the same cumulative rainfall as that of the steady rainfall event (Rain 1). Clay loam soil with an initial moisture content of 0.32 was used in these simulations (Table 2.2). The Manning's roughness coefficient *n* values were 0.025 for surfaces S4-S6 and 0.030 for surfaces RR1-RR6. The rainfall duration was 60 min for all the simulations (Table 2.2).

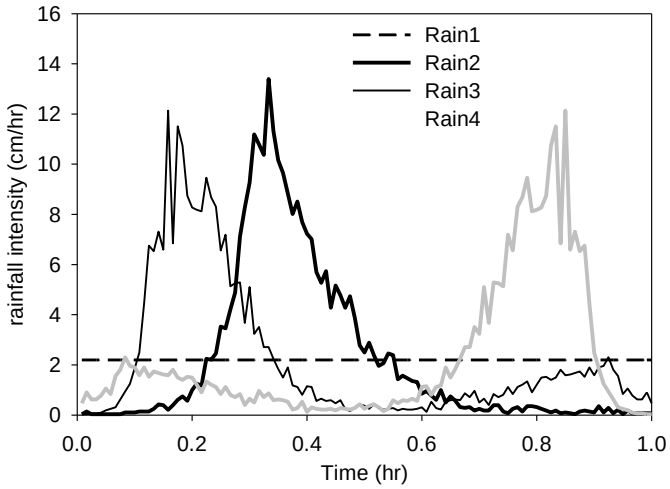

Fig. 2.9. Four rainfall events used for P2P overland flow modeling (Rain 1: steady rain with an intensity of 2.2 cm/hr; Rain 2-4: unsteady rain with the same cumulative rain as Rain 1)

Table 2.2. Modeling data for field surfaces S4-S6 and random roughness surfaces RR1-RR6 under Rainfall 1-4 (Rain 1: steady rainfall with an intensity of 2.2 cm/hr; Rain 2-4: unsteady rainfall with the same cumulative rainfall as that of Rain 1)

Surface	Surface Area (m^2)	Duration (min)	Rainfall	Initial Water Content	Soil Type
S4-S6	6.0×3.5	60	Rain 1-4	0.32	Clay loam
RR1-RR6	2.0×0.6		Rain 1		

2.4. Results and Discussion

2.4.1. P2P model vs. analytical kinematic wave model

Fig. 2.10 shows the comparison of the hydrographs simulated by the analytical kinematic wave model (Woolhiser, 1975) and the P2P model for the impervious hillslope surface. Good agreement has been achieved. As shown in Fig. 2.10, both hydrographs display a significant increase initially (rising limb) and reach an equilibrium state with a constant discharge of 137.15 m^3/hr (equilibrium stage), which equals the rate of the rainfall input. As rainfall ceases at t = 30 min, the discharge decreases dramatically and approaches to zero (falling limb). The comparison results indicate that the P2P model is able to accurately simulate overland flow for contributing cells (i.e., C2C water routing). Fig. 2.10 also shows the comparison of the hydrographs from the

P2P overland flow model for impervious and infiltrating surfaces. Due to the infiltration process, a delayed initiation of surface runoff (rising limb), a lower steady outlet discharge, and a steeper falling limb can be observed.

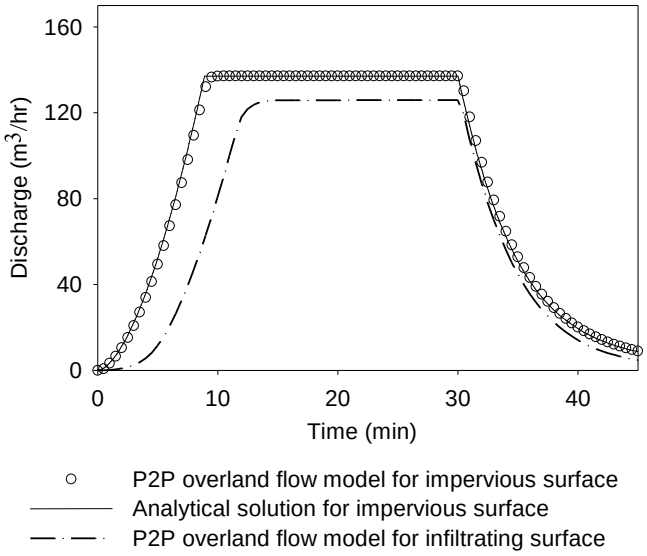

Fig. 2.10. Comparisons of the hydrographs simulated by the P2P overland flow model and an analytical kinematic wave model for both impervious and infiltrating conditions

2.4.2. P2P modeling vs. laboratory overland flow experiments

Fig. 2.11 shows the comparison between the observed and simulated hydrographs for experiments 1-3 (Table 2.1). To evaluate the goodness of fit, the Nash–Sutcliffe modeling efficiency coefficient (Nash and Sutcliffe, 1970) was calculated for each pair of the observed and simulated data. The modeling efficiency values were 0.95, 0.89, and 0.99 for experiments 1-3, respectively. Four stages can be identified for the hydrographs of surfaces S1 and S2 (Figs. 2.11a and 2.11b) corresponding to the changes in rainfall intensity. Initially (stage 1), there was no ponded water on the surfaces, and all rainwater infiltrated into soil. Gradually, the rainfall intensity (5.90 cm/hr for S1) exceeded the infiltration capacity; and surface ponding occurred and outlet discharge initiated (Fig. 2.11a). The discharge dropped to zero due to the significant decrease in rainfall intensity (from 5.90 to 1.15 cm/hr for S1) (stage 2, Fig. 2.11a), and the

connections between puddles for surface S1 were broken as the water levels in puddles dropped below their thresholds due to infiltration. The hydrograph of experiment 1 started to rise again when the rainfall intensity changed to 3.56 cm/hr for S1 (stage 3, Fig. 2.11a). The discharge showed a remarkable stepwise increase when the rainfall intensity increased to 5.90 cm/hr for S1 (stage 4, Fig. 2.11a). A similar changing pattern and the four stages can be observed for the hydrograph for experiment 2 (Fig. 2.11b).

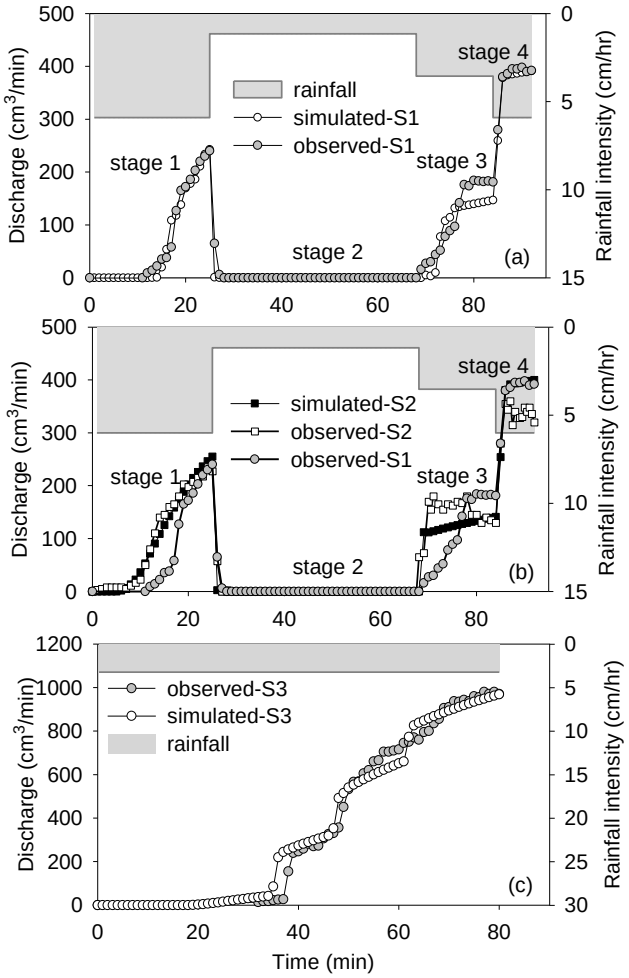

Fig. 2.11. Comparison of the observed and simulated hydrographs for surfaces S1-S3

The comparisons of the hydrographs for surfaces S1 and S2 indicate that the smooth surface (S2, Fig. 2.8) for experiment 2 had a faster increase in hydrograph and yielded more surface runoff during the initial period of stages 1 and 3 (Figs. 2.11a and 2.11b). This also has

been observed in several previous laboratory and field experimental studies (e.g., Zobeck and Onstad, 1987; Moore and Singer, 1990; Hairsine and Rose, 1992; Gómez and Nearing, 2005). The difference in runoff generation for the smooth and rough surfaces diminished gradually with persistent rainfall (i.e., later period of stages 1 and 3, Fig. 2.11b), which was consistent with the findings from Moore and Singer (1990) and Gómez and Nearing (2005). The final observed and simulated discharges at stage 4 were significantly higher than those at stage 1 for both surfaces (S1 and S2, Figs. 2.11a and 2.11b) although two stages had the same rainfall intensity (5.90 cm/hr). This can be attributed to the decrease in soil infiltrability at the later stage as more soil was fully saturated and wetting front moved to deeper soil. From Fig. 2.11b, it also can be observed that surface S1 had "steeper" increases in the hydrographs at stages 1 and 3 than surface S2 due to the threshold behaviors (spilling process) of several major puddles (Fig. 2.8a).

The observed and simulated hydrographs for surface S3 exhibit a strong stepwise increasing pattern (Fig. 2.10c), which can be attributed to its unique microtopographic characteristics (e.g., distribution and organization of puddles and their geometric properties) (Fig. 2.8c) and the threshold flow associated with the puddle filling-spilling-merging dynamics. When all puddles were fully filled, the entire surface contributed runoff water to the outlet through the well-connected drainage system, which led to a significant increase in the hydrograph (Fig. 2.11c). These modeling details and the comparisons against the observed data demonstrate the ability of the P2P model to accurately simulate the timing and magnitude of the response of the system to various rainfall inputs and capture the microtopography-influenced P2P dynamics and overland flow generation processes.

Fig. 2.12 shows the simulated and observed ponding, spilling, and re-spilling times (i.e., critical P2P times) for the major puddles on surfaces S1 and S3 during experiments 1 and 3.

These puddles showed dissimilar behaviors in the P2P processes due to a number of controlling factors. Basically, the simulated critical times match the observed ones for both experiments (Fig. 2.12). The mass balance analyses for the three experiments and the corresponding simulations are summarized in Table 2.3. The average relative errors of the cumulative surface runoff (outlet discharge), cumulative infiltration, and depression storage for the three experiments were 3.85%, 1.06%, and 0.00%, respectively (Table 2.3). Infiltration was the dominant process, accounting for 76.87%, 74.89%, and 76.01% of the total rainfall input for experiments 1-3, respectively (based on the simulated values, Table 2.3). The mass balance analyses also confirmed that the smooth surface S2 generated more surface runoff (24.95% of the total rainfall) than the rough surface S1 (20.58% of the total rainfall). The difference between the simulated cumulative outlet discharges for surfaces S1 and S2 (1.40×10^3 cm^3) was much greater than the storage loss from surface S1 (i.e., 0.75×10^3 cm^3), indicating that the rough surface S1 with depressions strengthened the infiltration process. The simulated runoff water retained on the contributing area was not significant for the three experiments (Table 2.3). The average simulated overland flow depths of the contributing cells by the end of the simulation period were 0.031, 0.070, and 0.031 mm for surfaces S1-S3 (experiments 1-3), respectively; and the average ponded water depths in depressions for surfaces S1 and S3 were 7.82 and 13.05 mm, respectively. The simulated flow velocities were 2.26, 2.17, and 1.59 cm/s for surfaces S1-S3 (experiments 1-3), respectively.

Experiments 1-3 and the associated modeling applications demonstrated the capability of the P2P model in simulating the P2P dynamics, outlet hydrographs, infiltration, and other hydrologic processes under the influence of surface microtopography for unsteady rainfall. The simulated critical times revealed the threshold behaviors of microtopography-controlled overland

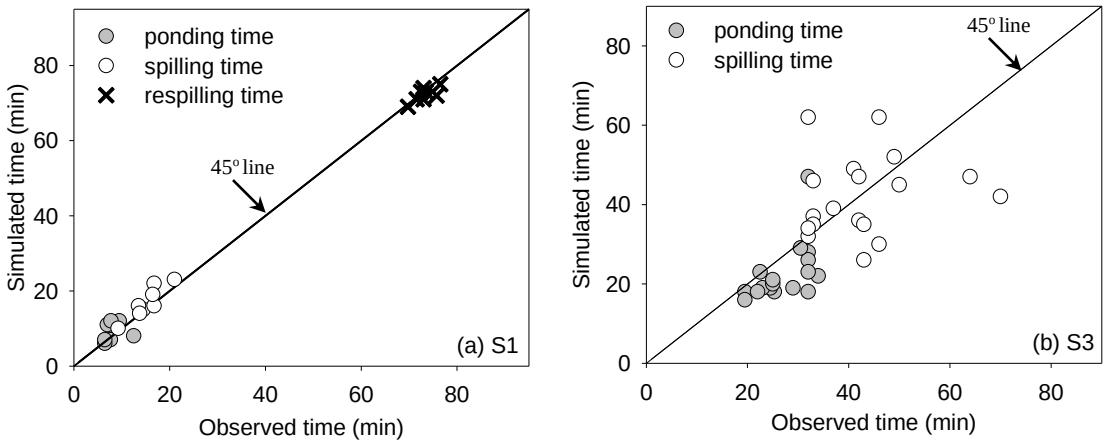

Fig. 2.12. Comparison of the observed and simulated critical times (i.e., puddle ponding, spilling, and respilling times) for all major puddles of surfaces S1 and S3

flow. These tests also highlighted the unique features of the P2P model: (1) it explicitly incorporated surface depressions and their contributing areas (PBUs) into the well-delineated, cascaded P2P drainage system; and (2) within each of the PBUs, it implemented two-domain modeling: C2C modeling for the contributing cells and P2P modeling for all puddle cells. Such unique features of the P2P model (1) facilitated the joint modeling of the P2P overland flow dynamics and the microtopography-dominated infiltration process; (2) reduced the simulation time since the number of iterations for each PBU within a time step was determined by a limited number of contributing cells; and (3) enhanced the numerical stability since the ponded cells in puddles were excluded in the C2C numerical modeling. It is the puddle cells that generally have much deeper ponded water and are subject to strong variations. The modeling for these cells is prone to numerical difficulties (e.g., stability and convergence problems).

Table 2.3. Mass balance analyses for experiments 1-3 and comparison with the simulations

Experiment	Mass Balance Terms	Observed ($\times 10^3$ cm^3)	Simulated ($\times 10^3$ cm^3)	Relative Error (%)
1 (S1)	Cumulative rainfall	30.13	30.13	0.00
	Cumulative runoff	6.64	6.20	6.63
	Cumulative infiltration	22.73	23.16	1.89
	Depression storage	0.75	0.75	0.00
	Water on contributing area	-	0.02	-
2 (S2)	Cumulative rainfall	30.46	30.46	0.00
	Cumulative runoff	7.78	7.60	2.31
	Cumulative infiltration	22.68	22.81	0.57
	Depression storage	0.00	0.00	0.00
	Water on contributing area	-	0.04	-
3 (S3)	Cumulative rainfall	154.90	154.90	0.00
	Cumulative runoff	28.36	29.10	2.61
	Cumulative infiltration	118.58	117.74	0.71
	Depression storage	7.96	7.96	0.00
	Water on contributing area	-	0.09	-

2.4.3. Combined effects of rainfall and surface microtopography on rainfall partition and unsaturated flow

Fig. 2.13 shows the spatial distributions of the simulated overland flow depths at t = 1.0 hr for surfaces S4, S5, and RR4 under Rain 1. The simulated overland flow depths for surface S4 exhibited a strong non-uniform distribution. Runoff water was mainly stored in the large depressions (Fig. 2.13a). Following the cascaded drainage system determined by surface microtopography, runoff water drained from upstream to downstream puddles (Fig. 2.13a). The delineation results for the field plot surface S5 (Fig. 2.8e) and the slopping surface S6 (Fig. 2.8f) indicated distinct cascaded P2P and C2C drainage systems. Surface S5 was featured with many well-connected small depressions, forming a series of micro-rills (Fig. 2.13b) while surface S6

was characterized by relatively uniform sheet flow along the surface slope. The simulated overland flow depths for surface RR4 had a scattered and random distribution (Fig. 2.13c).

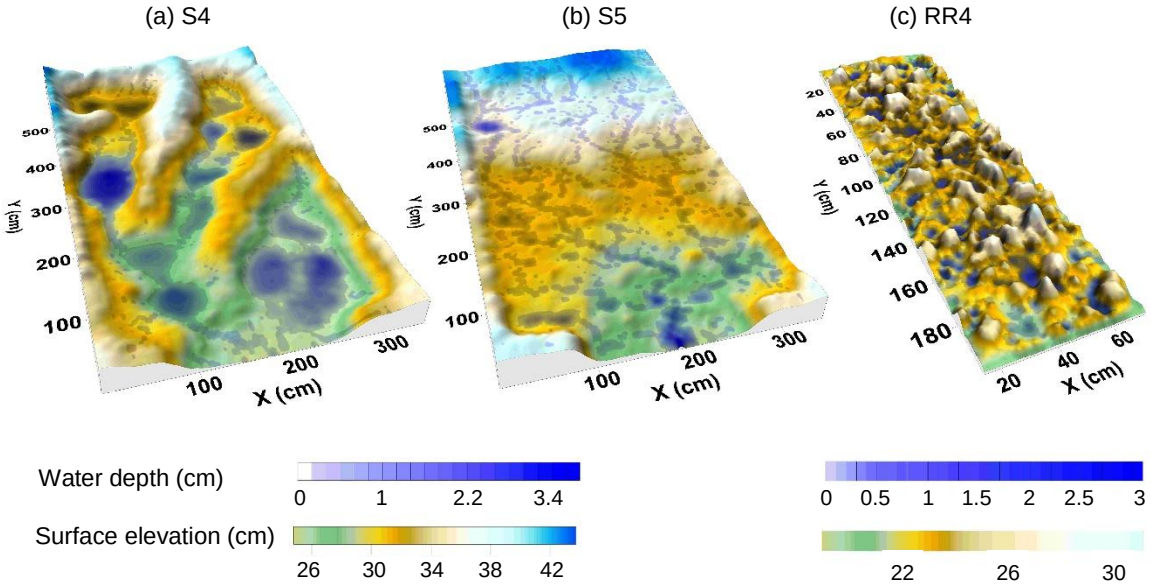

Fig. 2.13. Spatial distributions of the simulated flow depths (h) for surfaces S4, S5, and RR4

Fig. 2.14 shows the simulated hydrographs for surfaces S4-S6 and RR1-RR6 under Rain 1. Although surfaces S5 and S6 had distinct drainage patterns and water distributions of overland flow depths (Fig. 2.13b), their hydrographs were very similar. Their cumulative runoff values were 23.51% and 23.29% of the total rainfall input, respectively (Table 2.4). However, the rough field plot surface S4 generated much less surface runoff, 14.90% of the total rainfall due to its large depression storage (43.79×10^3 cm^3, 9.48% of the total rainfall input, Table 2.4). The hydrographs of surfaces S5 and S6 (Figs. 2.8e and 2.8f) exhibited a smooth increasing pattern while the rough surface S4 (Fig. 2.8d) showed a strong stepwise increasing pattern because of the dynamic P2P processes and the associated threshold behaviors (Fig. 2.14a). The hydrographs of the six random roughness surfaces RR1-RR6 displayed variable increasing patterns (Fig. 2.14b), which can be attributed to the differences in their microtopographic characteristics (e.g., sizes of soil aggregations and maximum depression storage). The changing patterns of the

simulated hydrographs for these nine surfaces (S4-S6 and RR1-RR6) confirmed that overland flow generation was strongly affected by the microtopography-dominated, threshold-controlled, dynamic expansion of the areas that connected and contributed runoff water to the outlet(s).

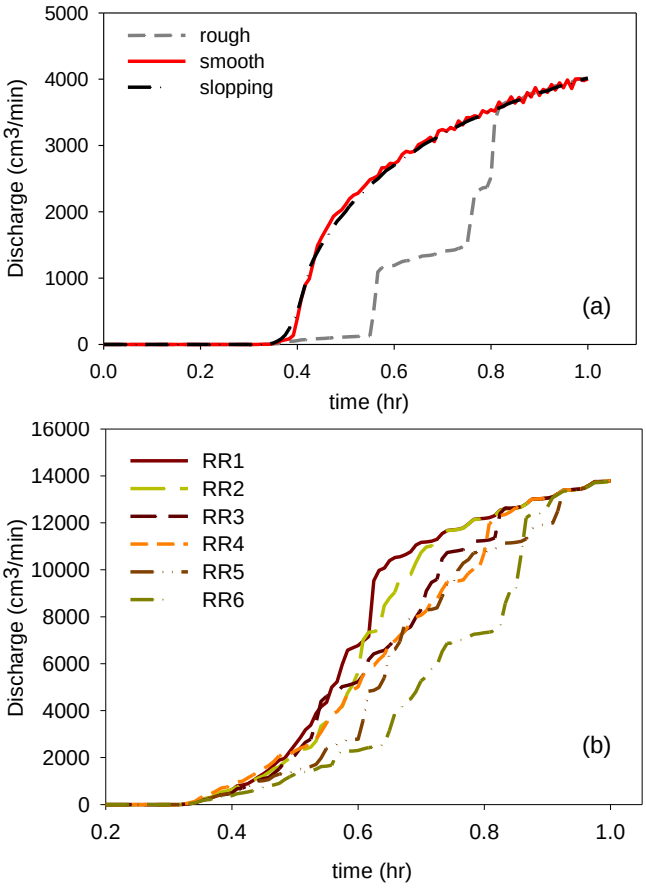

Fig. 2.14. Simulated hydrographs for surfaces S4-S6 and RR1-RR6 under Rain 1 (steady uniform rainfall with an intensity of 2.2 cm/hr)

Fig. 2.15 shows the relationships of random roughness with maximum depression storage and cumulative runoff for surfaces RR1-RR6. As expected, a rougher surface with a higher random roughness index had greater maximum depression storage, and consequently generated less surface runoff at the earlier stage (Fig. 2.14). The changing pattern of a hydrograph largely depended on puddles, their organizations or relationships, and their microtopographic properties (e.g., maximum depression storage).

Table 2.4. Summarized simulation results for surfaces S4-S6 and rain1-4*

Surface	Mass Balance Terms	Rain 1	Rain 2	Rain 3	Rain 4
S4	Cumulative rainfall ($\times 10^3$ cm^3)	462.00	462.00	462.00	462.00
	Depression storage ($\times 10^3$ cm^3)	43.79	27.98	40.07	39.58
	Water on contributing area ($\times 10^3$ cm^3)	0.95	0.00	0.00	0.00
	Cumulative infiltration ($\times 10^3$ cm^3)	348.42	254.95	301.08	235.35
	Cumulative runoff ($\times 10^3$ cm^3)	68.84	179.07	120.85	187.07
	Mean depth of wetting front (cm)	7.26	5.34	6.28	4.85
	Coefficient of variation of wetting front depths	0.01	0.13	0.09	0.04
S5	Cumulative rainfall ($\times 10^3$ cm^3)	462.00	462.00	462.00	462.00
	Depression storage ($\times 10^3$ cm^3)	2.89	0.23	2.56	1.61
	Water on contributing area ($\times 10^3$ cm^3)	2.45	0.00	0.00	0.00
	Cumulative infiltration ($\times 10^3$ cm^3)	348.04	241.44	290.58	232.34
	Cumulative runoff ($\times 10^3$ cm^3)	108.62	220.33	168.85	228.05
	Mean depth of wetting front (cm)	7.25	5.05	6.06	4.78
	Coefficient of variation of wetting front depths	0.00	0.05	0.04	0.02
S6	Cumulative rainfall ($\times 10^3$ cm^3)	462.00	462.00	462.00	462.00
	Depression storage ($\times 10^3$ cm^3)	0.00	0.00	0.00	0.00
	Water on contributing area ($\times 10^3$ cm^3)	6.37	0.00	0.00	0.00
	Cumulative infiltration ($\times 10^3$ cm^3)	348.05	240.48	291.53	233.58
	Cumulative runoff ($\times 10^3$ cm^3)	107.58	221.52	170.47	228.42
	Mean depth of wetting front (cm)	7.25	5.00	6.00	4.75
	Coefficient of variation of wetting front depths	0.00	0.00	0.01	0.01

Note: * Rain 1: steady rainfall with an intensity of 2.2 cm/hr; Rain 2-4: unsteady rainfall with the same cumulative rain as that of Rain 1.

To examine the effects of unsteady rainfall on the P2P overland flow processes and unsaturated flow (e.g., wetting front movement), a series of simulations were conducted for surfaces S4-S6 (Fig. 2.8) by applying Rain 2-4 (Fig. 2.9). The simulated hydrographs are shown

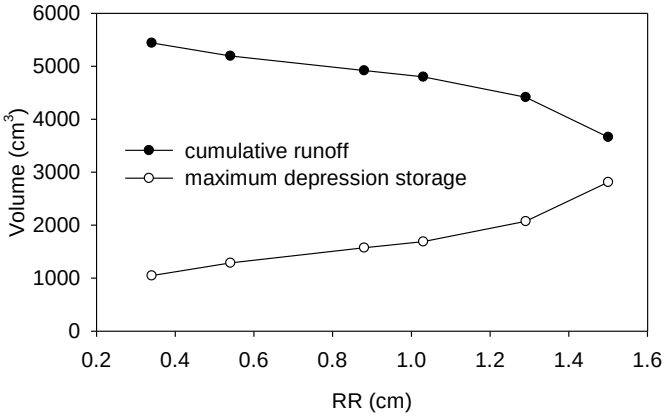

Fig. 2.15. Relationships between the simulated cumulative runoff or maximum depression storage and random roughness (RR) for surfaces RR1-RR6

in Fig. 2.16 and the simulation results are summarized in Table 2.4. It can be observed from Fig. 2.16 that the hydrographs of different surfaces were significantly affected by the temporal variations of rainfall although they had the same cumulative rainfall by t = 1.0 h (Table 2.4). The peaks of Rain 2-4 ranged from 12.13 to 13.39 cm/hr (Fig. 2.9). These unsteady rain events (Rain 2-4) generated more surface runoff during the high rainfall intensity periods (Fig. 2.16) and yielded higher cumulative runoff than the steady rain event (Rain 1) (Table 2.4). The rainfall event with a peak occurring at the later stage (e.g., Rain 4) produced a higher peak flow rate (e.g., 32,118 cm^3/min for surface S5, Fig. 2.16), and resulted in greater cumulative runoff and smaller cumulative infiltration than the rain events with an earlier peak (e.g., Rain 2 and 3) (Table 2.4). This can be attributed to the combined influence of the higher rainfall intensity and the decreased soil infiltrability at the later stage.

For the unsteady rainfall (Rain 2-4), surface microtopography also had clear influences on the simulated hydrographs. The rough field plot surface S4 had a delayed rising limb in the hydrograph, but reached a peak flow rate similar to that of surfaces S5 and S6 (Fig. 2.16). More importantly, surface S4 had a greater final mean depth of wetting front than surfaces S5 and S6

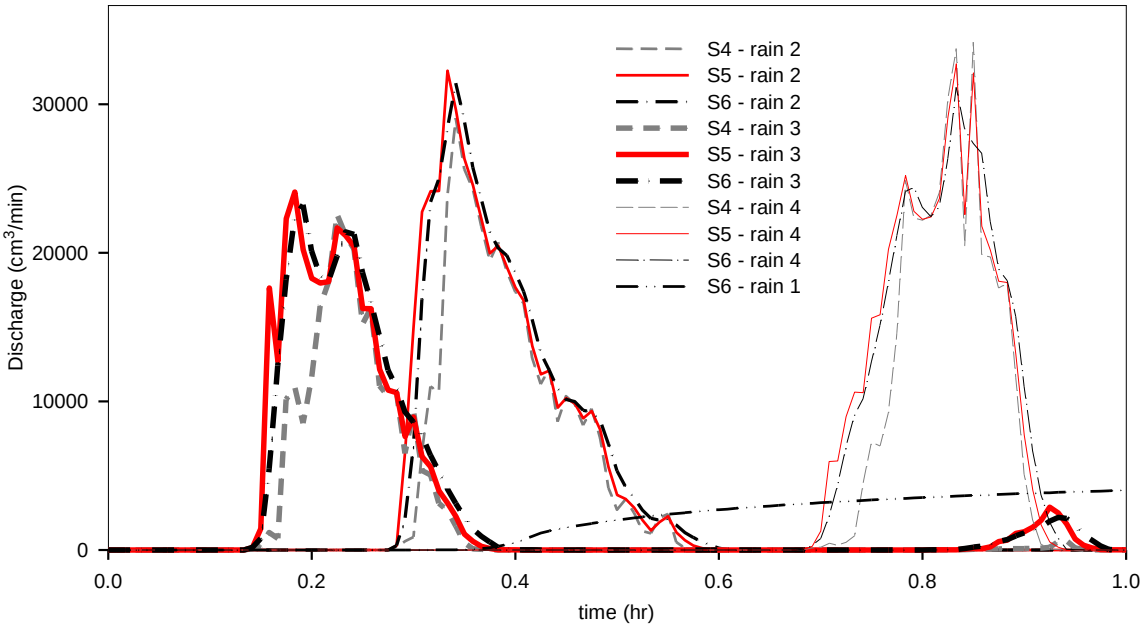

Fig. 2.16. Simulated hydrographs for field surfaces S4 - S6 for four rainfall events (Rain 1: steady rain with an intensity of 2.2 cm/hr; Rain 2-4: unsteady rain with the same cumulative rainfall as Rain 1)

for Rain 2-4 (Table 2.4). The differences in the final mean wetting front depths of the rough and smooth field plot surfaces (i.e., surfaces S4 and S5) narrowed down as the peak of rain was delayed from Rain 3 to Rain 2 and Rain 4 (Table 2.4). In addition, as indicated by the coefficient of variation of wetting front depths (Table 2.4), the spatial variations in the wetting front depths decreased for the rain events with a later discharge peak for surfaces S4 and S5.

The cumulative infiltration was affected by surface microtopography and rainfall characteristics. Surface depressions were critical to the rainfall partition process. Not only did they function as water storage, but also served as a persistent water source that enhanced infiltration. Surface microtopography also influenced unsaturated flow and controlled the spatial variations in wetting front depths. Thus, it can be concluded that the combined influence of rainfall characteristics and surface microtopography altered the rainfall partition, outlet peak flow, cumulative runoff, surface depression storage, cumulative infiltration, and the spatial

variations in wetting front. The findings from this study emphasized the importance of surface microtopography and rainfall features in the dynamic P2P overland flow, infiltration, and unsaturated flow processes.

2.5. Conclusions

It has been a challenge to physically simulate the spatially and temporally varied, discontinuous overland flow and infiltration under the influence of complex surface microtopography. The unique features of the developed P2P model include: (1) a unique two-domain (C2C and P2P), hierarchical modeling structure, which improved the model performance in the simulation of overland flow under complex microtopographic conditions, (2) physically simulated overland flow routing for contributing cells in conjunction with the P2P dynamics modelling by accounting for the threshold behaviors and interactions of puddles (i.e., filling, spilling, merging, and splitting), and (3) simulated infiltration and unsaturated flow of a microtopography-dominated surface-subsurface system for spatially and temporally varied rainfall, heterogeneous soil, and arbitrary initial soil moisture and surface ponded water distributions. The applicability of the P2P model was verified by comparing with the experimental data. The model provided essential details on overland flow, infiltration, surface ponding, unsaturated flow, and the dynamic variability in hydrologic connectivity under various rainfall, microtopography, and soil conditions.

The developed model can be applied to analyze depression storage/runoff/infiltration relationships and investigate the complexity of overland flow and infiltration processes. In addition, the developed model is also useful to examine the spatio--temporally varying P2P dynamics, which can be further applied for the characterization of threshold behaviors and analysis of hydrologic connectivity.

2.6. References

Abedini, M. J., Dickinson, W. T., and Rudra, R. P., 2006. On depressional storages: the effect of DEM spatial resolution. J. Hydrol., 318, 138–50.

Appels, W. M., Bogaart, P. W., and van der Zee, S., 2011. Influence of spatial variations of microtopography and infiltration on surface runoff and field scale hydrological connectivity. Adv. Water Resour., 34(2), 303–13.

Antoine, M., Javaux, M., and Bielders, C., 2011. Integrating subgrid connectivity properties of the micro-topography in distributed runoff models, at the interrill scale. J. Hydrol., 403, 213-223, doi 10.1016/j.jhydrol.2011.03.027.

Antoine, M., Javaux, M., and Bielders, C., 2009. What indicators can capture runoff-relevant connectivity properties of the micro-topography at the plot scale? Adv. Water Resour., 32(8), 1297–310, doi:10.1016/j.advwatres.2009.05.006.

Bogart, D., 2014. Hydrologic experiments and analysis – the effect of microtopography on runoff generation. Master Thesis. North Dakota Stage University, USA.

Chi, Y., Yang, J., Bogart, D., and Chu, X., 2012. Fractal analysis of surface microtopography and its application in understanding hydrologic processes. Trans. ASABE, 55(5), 1781-792.

Chu, X., and Marino, M. A., 2005. Determination of ponding condition and infiltration into layered soils under unsteady conditions. J. Hydrol., 313, 195– 207.

Chu, X., and Marino, M. A., 2006. Simulation of infiltration and surface runoff - A Windows-based hydrologic modeling system HYDROL-INF, P1-8. In: Examining the Confluence of Environmental and Water Concerns, Proceedings of the 2006 World Environmental and Water Resources Congress, edited by Randall Graham. American Society of Civil Engineers. doi: 10.1061/40856(200)429.

Chu, X., Yang, J., and Chi, Y., 2012. Quantification of soil random roughness and surface depression storage: Methods, applicability, and limitations. Trans. ASABE, 55(5), 1699-710.

Chu, X., Yang, J., Chi, Y., and Zhang, J., 2013. Dynamic puddle delineation and modeling of puddle-to-puddle filling-spilling-merging-splitting overland flow processes. Water Resour. Res., 49(6), 3825-3829.

Chu, X., Zhang, J., Chi, Y., and Yang, J., 2010. An improved method for watershed delineation and computation of surface depression storage. P1113-1122, In: Watershed Management 2010: Innovations in Watershed Management under Land Use and Climate Change, Proceedings of the 2010 Watershed Management Conference, edited by K.W. Potter and D.K. Frevert. American Society of Civil Engineers. doi:10.1061/41143(394)100.

Darboux, F., Davy, P., and Gascuel-Odoux, C., 2002. Effect of depression storage capacity on overland-flow generation for rough horizontal surfaces: water transfer distance and scaling. Earth Surf. Proc. Land, 27(2), 177–91.

Darboux, F., Davy, P., Gascuel-Odoux, C., and Huang, C., 2001. Evolution of soil surface roughness and flowpath connectivity in overland flow experiments. Catena, 46(2–3), 125–39.

Darboux, F., and Huang, C., 2005. Does soil roughness increase or decrease water and particle transfer? SSSAJ, 69(3), 748–56.

Dunne, T., Zhang, W., and Aubry, B. F., 1991. Effects of rainfall, vegetation, and microtopography on infiltration and runoff. Water Resour. Res., 27(9),2271–85.

Esteves, M., Faucher, X., Galle, S., and Vauclin, M., 2000. Overland flow and infiltration modelling for small plots during unsteady rain: numerical results versus observed values. J. Hydrol., 228(3–4), 265–82.

Fiedler, F. R., and Ramirez, J. A., 2000. A numerical method for simulating discontinuous shallow flow over an infiltrating surface. Int. J. Numer. Methods Fluids, 32(2), 219–39.

Gomez, J. A., and Nearing, M. A., 2005. Runoff and sediment losses from rough and smooth soil surfaces in a laboratory experiment. Catena, 59, 253–66.

Gonwa, W. S., and Kavvas, M. L., 1986. A modified diffusion wave equation for flood propagation in trapezoidal channels. J. Hydrol., 83, 119-36.

Gottardi, G., and Venutelli, M., 1993. A control-volume finite element model for two-dimensional overland flow. Adv. Water Resour., 16, 227–84.

Govers, G., Takken, I., and Helming, K., 2000. Soil roughness and overland flow. Agronomie, 20(2), 131–46.

Hairsine, P. B., Moran, C. J., and Rose, C. W., 1992. Recent developments regarding the influence of soil surface characteristics on overland flow and erosion. Aust. J. Soil Res., 30, 249–64.

Helming, K., Römkens, M. J. M., and Prasad, S. N., 1998. Surface roughness related processes of runoff and soil loss: a flume study. SSSAJ, 62, 243–50.

Huang, C., and Bradford, J. M., 1990. Depressional storage for Markov – Gaussian surfaces. Water Resour. Res., 26(9), 2235–242.

Huang, J., and Song, C. C. S., 1985. Stability of dynamic flood routing schemes. J. Hydraul. Eng., 111(12), 1497-505.

Jain, M. K., and Singh, V. P., 2005. DEM-based modeling of surface runoff using diffusion wave equation. J. Hydrol., 302, 107–26. doi:10.1016/j.hydrol.2004.06.04.

Köhne, J. M., Köhne, S., and Simunek, J., 2009. A review of model applications for structured soils: a) water flow and tracer transport. J. Contam. Hydrol., 104, 4–35.

Liu, Y., Yang, J., and Chu, X., 2013. Infiltration and unsaturated flow under the influence of surface microtopography - model simulations and experimental observations, p468-475. In: Showcasing the Future, Proceedings of the 2013 ASCE World Environmental and Water Resources Congress, edited by C. L. Patterson, S. D. Struck, and D. J. Murray. American Society of Civil Engineers.

MacCormack, R. W. 1969. The effect of viscosity in hypervelocity impact cratering. AIAA Paper 69-354, Ohio: Cinicinnati.

Martin, Y., Valeo, C., and Tait, M., 2008. Centimetre-scale digital representations of terrain and impacts on depression storage and runoff. Catena, 75, 223–33.

Moore, D. C., and Singer, M. J., 1990. Crust formation effects on soil erosion processes. SSSAJ, 54, 1117-123.

Morris, E. M., and Woolhiser, D. A., 1980. Unsteady one-dimensional flow over a plane: partial equilibrium and recession hydrographs. Water Resour. Res., 16(2), 355–60.

Nash, J. E., and Sutcliffe, J. V., 1970. River flow forecasting through conceptual models. Part I-A discussion of principles. J. Hydrol., 10(3), 282-290.

O'Callaghan, J. F., and Mark, D. M., 1984. The extraction of drainage networks from digital elevation data. Comput. Vision Graphics Image Proc., 28, 323–44.

Rossi, M. J., and Ares, J. O., 2012. Depression storage and infiltration effects on overland flow depth-velocity-friction at desert conditions: field plot results and model. Hydrol. Earth Syst. Sci., 16, 3293–307

Shaw, D. A., Pietroniro, A., and Martz, L. W., 2012. Topographic analysis for the prairie pothole region of Western Canada. Hydrol. Process., 27(22). doi:10.1002/hyp.9409

Smith, G. D., 1985. Numerical solution of partial differential equations: finite difference methods. Oxford: Clarendon press.

Tatard, L., Planchon, O., Wainwright, G., Nord, J., Favis-Mortlock, D., Silvera, N., et al., 2008. Measurement and modelling of highresolution flow-velocity data under simulated rainfall on a low-slope sandy soil. J. Hydrol., 348, 1–12.

Tayfur, G., Kavvas, M. L., Govindaraju, R. S., and Storm, D. E., 1993. Application of St. Venant equations for two-dimensional overland flows over rough infiltrating surfaces. J. Hydraul. Eng., 119, 51-63.

Thompson, S. E., Katul, G. G., and Porporato, A., 2010. Role of microtopography in rainfall–runoff partitioning: an analysis using idealized geometry. Water Resour. Res., 46(W07520). doi:10.1029/2009WR008835.

Wang, M., and Hjelmfelt, A. T., 1998. DEM based overland flow routing Model. J. Hydrol. Eng., 3(1), 1-8.

Woolhiser, D. A., and Liggett, J. A., 1967. Unsteady 1-dimensional flow over a plane—rising hydrograph. Water Resour. Res., 3(3), 753–71.

Woolhiser, D. A., 1975. Simulation of unsteady overland flow. Unsteady flow in open channels, K. Mahmood and V. Yevjevich, eds., Vol. II, Water Resources Publications, Fort Collins, Colorado, 485-508.

Yang, J., and Chu, X., 2013. Quantification of the spatio-temporal variations in hydrologic connectivity of small-scale topographic surfaces under various rainfall conditions. J. Hydrol., 505, 65-77.

Zhang, W., and Cundy, T. W., 1989. Modeling of two-dimensional overland flow. Water Resour. Res., 25(9), 2019–35.

Zobeck, T. M., and Onstad, C. A., 1987. Tillage and rainfall effects on random roughness: a review. Soil Till. Res., 9, 1–20.

CHAPTER 3. QUANTIFICATION OF THE SPATIO-TEMPORAL VARIATIONS IN HYDROLOGIC CONNECTIVITY OF SMALL-SCALE TOPOGRAPHIC SURFACES

3.1. Abstract

Land surfaces are generally not smooth and show certain irregularity. Overland flow on such surfaces is essentially discontinuous and exhibits strong variability and complexity. Modeling of the spatio-temporal variability and heterogeneity of overland flow and the hydrotopographic effects has been proven to be a challenge. The objective of this study was to quantitatively describe the intrinsic spatio-temporal variations in hydrologic connectivity associated with overland flow generation. Firstly, a puddle-to-puddle (P2P) hydrologic connectivity concept was proposed to characterize runoff generation processes and the related spatio-temporal dynamics. Secondly, a laboratory overland flow experiment was conducted to characterize the dynamic puddle filling and spilling processes, hydrologic connectivity, and outlet discharge. Thirdly, a conceptual P2P model was applied to simulate the P2P overland flow dynamics, calculate flow discharge, and track the evolution of hydrologically connected areas. Particularly, two modified hydrologic connectivity indices, time-varying connectivity function and connectivity length, were proposed to characterize the properties and dynamic changes in hydrologic connectivity. Furthermore, the influences of surface topography, rainfall, and surface slope on hydrologic connectivity were evaluated. The proposed hydrologic connectivity indices effectively revealed the variability and the threshold behavior of overland flow generation. It was demonstrated that the dynamic P2P processes governed hydrologic connectivity, controlled surface runoff generation, and altered the flow drainage patterns. Temporal variations of rainfall intensity changed the occurrence timing of the P2P dynamics and evolution of connected areas, while spatial variations of rainfall intensity directly influenced the overall development of

hydrologic connectivity of a hydrologic system. Surface slope showed considerable influences on hydrologic connectivity. The results suggested that critical slope(s) could exist, at which a sharp change in flow drainage area and hydrologic connectivity occurred.

3.2. Introduction

Hydrologic connectivity has been studied in many disciplines in recent years (Darboux et al., 2001; Brierley et al., 2006; Bracken and Croke, 2007; Antoine et al., 2009). However, there is no widely accepted definition of hydrologic connectivity in the field of surface hydrology (Bracken and Croke, 2007; Antoine et al., 2009). Hydrologic connectivity has been used to represent the spatio-temporal conveyance passage to transfer water and the related mass over a land surface (Pringle et al., 2003; Bracken and Croke, 2007; Tetzlaff et al., 2007). Due to the irregularity of surface topography, surface depressions often break hydrologic connectivity of topographic elements, which leads to spatially varying and independent localized hydrologic units across the surface. During a rainfall event, depressions on the surface may be filled gradually, which results in dynamic formation/evolution of the areas that are hydrologically connected. The dynamic development of hydrologic connectivity serves as a driving mechanism to alter spatio-temporal variations of a series of hydrologic, geomorphologic, and environmental processes, such as overland flow trigging, infiltration, and solute transport processes. Therefore, it is of particular importance to examine the microtopography-affected hydrologic connectivity and the related dynamic overland runoff generation process. Several studies have been conducted to investigate hydrologic connectivity of topographic surfaces and to characterize the dynamic behaviors of overland flow generation (Darboux et al., 2001; Antoine et al., 2009; Antoine, 2010; Antoine et al., 2011; Appels et al., 2011).

Indicators can be utilized to characterize the connectivity properties of a hydrologic system and describe the related hydrologic behaviors. Structural hydrologic connectivity has been used to describe hydrologic connectivity of topographic surfaces without considering dynamic hydrologic processes (Antoine et al., 2009; Lexartza-Artza and Wainwright, 2009). Antoine et al. (2009) compared six structural connectivity indicators including semivariogram, relative bivariate entropy, *n*-point rectilinear connectivity, connectivity function integral scale, Euler number, and percolation thresholds. They concluded that the first three indicators were not able to discriminate the spatial connectivity patterns. For the last three indicators, it was difficult to relate them to hydrologic behaviors.

In contrast, functional hydrologic connectivity characterizes the system responses to dynamic inputs and the complex system structure (Bracken and Croke, 2007). Functional hydrologic connectivity is a function of structural hydrologic connectivity, and functional hydrologic connectivity in turn may change structural hydrologic connectivity through certain hydrologic and geomorphologic processes (e.g., soil erosion). Some models have been developed to quantify functional hydrologic connectivity (e.g., Darboux et al., 2001; Antoine et al., 2009; Appels et al., 2011) and different indicators have been proposed to describe the functional hydrologic connectivity properties of topographic surfaces. Simplified hydrograph is widely used to quantify the relationship between normalized discharge and cumulative rainfall (Darboux et al., 2001; Antoine et al., 2009; Antoine, 2010; Appels et al., 2011). Antoine et al. (2009) proposed a relative surface connection function that linked hydrologic connections to the depression storage filling. Based on the relative surface connection function, Antoine et al. (2011) further proposed two corrective procedures to account for the effects of both depression storage and surface detention dynamics and improve the hydrograph prediction.

Previous studies on functional hydrologic connectivity focused mainly on analyzing simplified outlet hydrographs (Darboux et al., 2001; Antoine et al., 2009; Antoine, 2010; Antoine et al., 2011; Appels et al., 2011) and relative surface connection function (Antoine et al., 2009; Antoine, 2010; Antoine et al., 2011). Bracken and Croke (2007) emphasized the importance of combined structural and functional hydrologic connectivity studies and described the needs for new approaches and metrics to discover the intrinsic factors that controlled runoff generation, instead of solely examining hydrographs for functional hydrologic connectivity analysis. Darboux et al. (2002) also pointed out that hydrographs did not necessarily account for the spatio-temporal variations in the generation and evolution processes of overland flow within a surface. Simplified hydrograph and the relative surface connection function represent the response of the surface areas that have connected and contributed runoff water to the outlet(s) of the drainage system, even for small spatial and temporal scales. Few efforts have been made to reveal the spatio-temporal changes in hydrologic connectivity affected by surface microtopography within an overland flow system. Different from the previous work, this study intends to quantify such spatial and temporal variations in hydrologic connectivity and seek the linkage that bridges the gaps between structural and functional hydrologic connectivity properties. In addition, rainfall, as one of the major system inputs, influences hydrologic connectivity and the related hydrologic and geomorphologic processes. However, to the best of our knowledge, little research has been conducted to evaluate the rainfall effects on hydrologic connectivity. Therefore, the objectives of this study are: (1) to improve the understanding of microtopography-controlled hydrologic connectivity and its relation to the dynamic overland flow generation processes by combined modeling and experimental studies; (2) to introduce two modified hydrologic connectivity indices to quantitatively describe the spatio-temporal

variations in hydrologic connectivity; and (3) to evaluate the effects of surface topography, rainfall distribution and surface slope on hydrologic connectivity.

3.3. Materials and Methods

3.3.1. Puddle-to-puddle (P2P) hydrologic connectivity

Overland flow on a rough surface is characterized by discontinuous P2P filling-spilling-merging-splitting dynamics (Chu et al., 2013), which involve a series of hydrologically connected areas (ACs) and individual ponding areas (PAs) under the influence of surface microtopography. This hierarchical connecting process is herein referred to as "P2P hydrologic connectivity." Note that AC represents the area that contributes runoff water to a puddle or an outlet, while PA represents the area covered by ponded water (i.e., puddle area). In this study, two field plot surfaces of distinct topographic features [Plot 1 - rough surface (Figs. 3.1a and 3.1b); Plot 2 - smooth surface (Fig. 3.1c)] are used to illustrate the P2P dynamics and the hierarchical drainage system and demonstrate the concept of P2P hydrologic connectivity.

As shown in Fig. 3.1a, during such an earlier stage, depressions break the connectivity of topographic elements, forming a number of ACs which essentially are the contributing areas for non-fully filled puddles or outlets. Two types of AC can be identified. The first type of AC links directly to the boundaries of the surface drainage system and consists of a number of contributing cells (i.e., DEM grids) and an outlet (e.g., AC1 and Outlet 1 in Fig. 3.1a). Such an AC makes direct contribution of runoff to the outlet. The second type of AC, without direct linkage to the outlet, may include a non-fully filled puddle, a threshold, and a number of contributing cells (e.g., AC6 in Fig. 3.1a). The ACs derived solely from surface topography (DEM) represent the static properties of hydrologic connectivity (i.e., structural hydrologic connectivity). An AC has the potential to expand and connect to its upstream/downstream areas

at different stages of the overland flow generation processes (Fig. 3.1a). An AC expands when the water level in its puddle reaches the threshold and spills to the downstream area (e.g., AC2 formed by two ACs including two merged puddles, Fig. 3.1a). A puddle and its AC may have multiple thresholds, through which the puddle spills and links to its downstream AC. Such an upstream-downstream relationship is determined by the D8 method (O'Callaghan and Mark 1984). The second type ACs may expand within the system or connect to the first type ACs, through which runoff water discharges to the outlet(s). The outlet hydrograph features a stepwise changing pattern as more areas are connected to the outlet. When all puddles are fully filled, the development of ACs is completed and the entire surface drains runoff water to the outlets (Fig. 3.1b). At this final stage, two large ACs (new AC1 and AC2) discharge through Outlets 1 and 2, respectively (Fig. 3.1b). The evolution/formation of ACs leads to dynamic variations in the related hydrologic and geomorphologic processes across the spatial domain. This study attempts to quantify the spatio-temporal variability in hydrologic connectivity within the P2P hierarchical drainage system.

Surface microtopography and puddle characteristics determine the properties of ACs and maximum depression storage. An AC with a larger contributing area tends to collect more runoff water while an AC with greater maximum depression storage is capable of storing more water, as illustrated in Fig. 3.1a. The ACs of a higher ratio of contributing area to maximum depression storage have a higher potential to be fully filled, developing connections to their downstream areas. Accordingly, a downstream puddle may have higher possibility to be fully filled due to the increased water contribution from the expansion of upstream ACs. The smooth surface (Plot 2) exhibits dissimilar spatial distributions of ACs and PAs (Fig. 3.1c). Plot 2 has smaller and shallower puddles, and smaller ACs than Plot 1 (Fig. 3.1c). Due to the limited depression storage

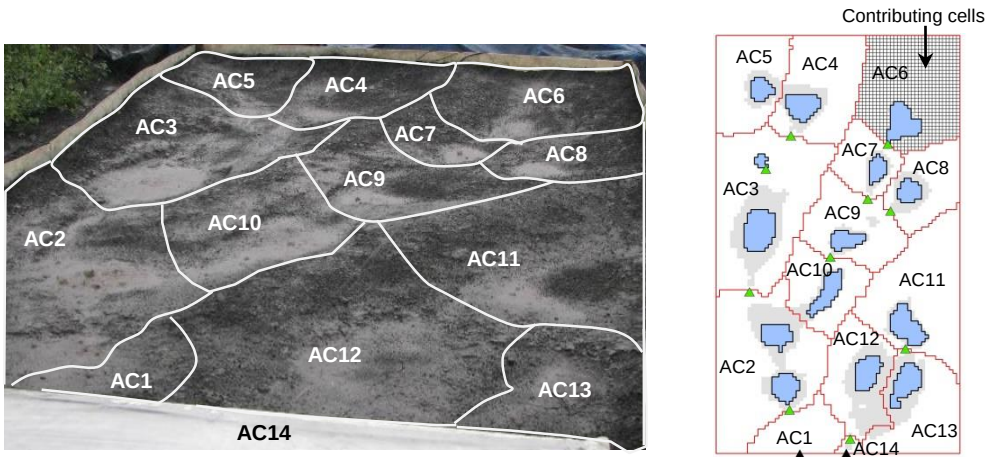

(a) Connected areas (ACs) at an earlier stage of runoff generation for plot 1

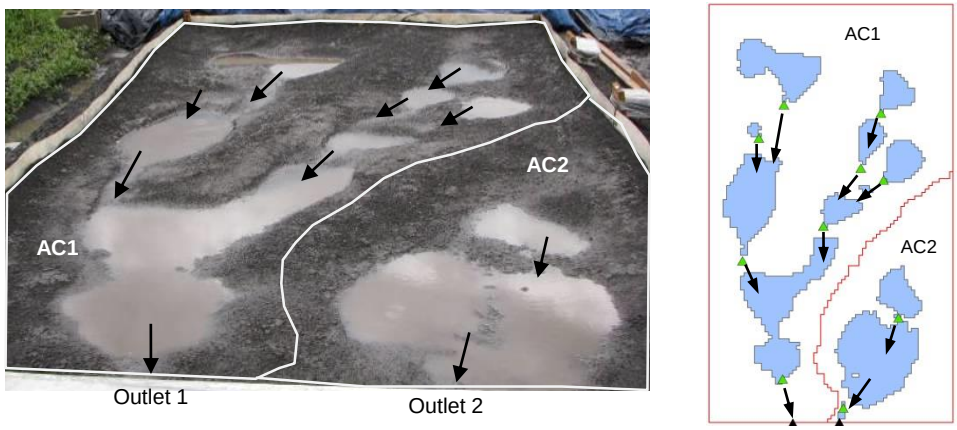

(b) Connected areas (ACs) at the final stage of runoff generation for plot 1

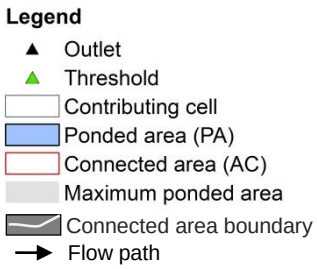

(c) Final stage of runoff generation for plot 2

Fig. 3.1. Dynamic puddle filling-spilling processes and evolution/formation of hydrologically connected areas (ACs) for field plots 1 and 2

on Plot 2, its ACs are more easily connected, which results in faster runoff generation and higher discharge at the earlier stage of overland flow generation (Fig. 3.1c). Thus, it is of importance to

investigate the spatio-temporal variations in ACs and the threshold behaviors associated with the overland flow generation processes. In addition, hydrologic connectivity can be affected by spatial and temporal distributions of rainfall and surface slope. These two factors have been evaluated in this study.

3.3.2. P2P conceptual model

In this study, a P2P conceptual model (Chu et al., 2013) was utilized for simulating the P2P filling-spilling-merging-splitting dynamics and analyzing hydrologic connectivity. The model incorporated a puddle delineation program (Chu et al., 2010) for characterizing surface depressions/puddles and calculating the hydrotopographic parameters. The unique features of the puddle delineation software included its capabilities of delineating puddles for different threshold-controlled levels and determining the hierarchical relationships of puddles based on their geometric structures (e.g., their centers and overflow thresholds) and spatial locations in the DEM-determined flow drainage system (Chu et al., 2013). The P2P concept model facilitated the modeling of overland flow within individual puddles (puddle filling) and the P2P dynamics between puddles (puddle spilling, merging, and splitting) in a cascaded, puddle-oriented drainage system (Chu et al., 2013). The model explicitly simulated the time-varying P2P overland flow processes under unsteady, nonuniform rainfall and water losses (e.g., losses due to infiltration and evaporation). Instantaneous water transfer between cells and puddles was assumed in the P2P conceptual model (Chu et al., 2013). The total discharge from a surface was calculated by summing up the water drained to the DEM-determined outlets of the surface. In the P2P conceptual model, development/evolution of ACs and PAs across a topographic surface was tracked for all time steps. At the beginning ($t = 0$), identification of ACs for the original surface started from the outlet(s) of the surface and the centers of first-level puddles (Chu et al., 2010).

The contributing cells of ACs were identified based on the flow directions and accumulations determined by the puddle delineation program (Chu et al., 2010). The resulting ACs represented the structural hydrologic connectivity properties of the surface. Note that those DEM-determined ACs were subject to changes over time, depending on the surface topographic characteristics and the water sources/sinks of the system. For any time steps, a similar searching process was implemented to determine the time-varying ACs that were used to quantify functional hydrologic connectivity. Specifically, the searching process started from the outlet(s) of the surface and the non-fully filled puddles and continued until all contributing cells and the upstream ACs connected to the current AC were identified. The P2P conceptual model provided: (1) the spatio-temporal distributions of ACs and PAs for structural and functional hydrologic connectivity analyses, and (2) the simplified outlet hydrograph and relative surface connection function (Antoine et al., 2009) for functional hydrologic connectivity analysis.

3.3.3. Time-varying hydrologic connectivity indices

Based on Western et al. (2001), two modified hydrologic connectivity indices, time-varying connectivity function and connectivity length, were proposed in this study to characterize the statistical properties of ACs and the dynamic changes in ACs across a topographic surface during a rainfall-runoff event. Specifically, at each time step, the surface consists of a number of ACs with unique ID numbers identified by the P2P conceptual model. Each AC further includes numerous hydrologically connected cells with the same ID. Note that the ID numbers for all cells may change over time due to the P2P dynamics and the development of ACs.

The procedures for computing connectivity function of ACs can be summarized as follows: (1) determination of pairs and separation bins: each cell *i* can form a number of pairs

with other cells (*j*). The distance *h* between the centers of two cells of each pair is assigned to a separation bin *k*, and the number of pairs for each separation bin *k* is then calculated; (2) determination of connected pairs: each separation bin *k* includes a number of pairs, and within each separation bin, the cells of pairs are considered connected if they have the same ID number. In this way, the number of connected pairs can be determined for each separation bin *k*; and (3) calculation of connectivity function of ACs: the connectivity function of ACs is calculated as the ratio of the number of connected pairs to the total number of pairs in the corresponding separation bin *k* at time *t*. The time-varying connectivity function and connectivity length of ACs can be respectively expressed as:

$$C_{AC}(h,t) = P[i \leftrightarrow j \,|\, ID_{AC}(i,t) = ID_{AC}(j,t);\ i,j \in S;\ t \in T] = \frac{N_{cp}(h_k,t)}{N_{tp}(h_k,t)} \tag{3.1}$$

$$L_{AC}(t) = \int_0^{\infty} C_{AC}(h,t)\,dh = \sum_{k=1}^{NB} C_{AC}(h_k,t)\cdot \Delta h_k \qquad (t \in T) \tag{3.2}$$

where $C_{AC}(h, t)$ = connectivity function of ACs for separation *h* at time *t*; *P* = probability of cell *i* to connect to cell *j*; $ID_{AC}(i, t)$ = ID number of AC for cell *i* at time *t*; *h* = separation distance between cell centers; h_k = separation distance for separation bin *k*; $N_{cp}(h_k, t)$ = number of connected pairs for separation distance h_k at time *t*; $N_{tp}(h_k, t)$ = number of total pairs for separation distance h_k at time *t*; *S* = spatial domain that includes all cells; *T* = time domain; $L_{AC}(t)$ = connectivity length of ACs at time *t*; *NB* = total number of separation bins; Δh_k = size of separation bin *k*.; and $\leftrightarrow$ = indicator of connection between two cells. The connectivity function of ACs represents the lag-dependent and time-varying probability of hydrologic connections between AC-oriented cells across the entire spatial domain. The connectivity length of ACs represents the average AC-oriented, time-varying connectivity length for the entire surface. Furthermore, we proposed maximum connectivity length of ACs, a length where the connectivity

function becomes zero. The two indices are able to reveal the temporal changes in ACs (development/evolution of the P2P-based connectivity), which can be further used to analyze the threshold behavior of overland flow generation.

Similarly, a ponding connectivity index – connectivity function of PAs was proposed to quantify the connections through PAs and characterize spatial and temporal distributions of the PAs. In the P2P conceptual model, PAs represented the water ponded areas of puddles where flow velocity was zero. The procedures for computing the connectivity function of PAs were similar to those for the connectivity function of ACs, but it was assumed that the cells within a PA were connected. In addition, connectivity length of PAs and maximum connectivity length of PAs were calculated to represent the average and maximum sizes of the PAs.

In this study, structural hydrologic connectivity was analyzed by quantifying the "static" connectivity properties of ACs at $t = 0$ (no ponded water), while functional hydrologic connectivity was analyzed by using four indicators: (1) connectivity function and connectivity length of ACs, (2) connectivity function and connectivity length of PAs, (3) simplified hydrograph (Antoine et al., 2009), and (4) relative surface connection function (Antoine et al., 2009). The first two indicators proposed herein for functional hydrologic connectivity characterize the spatio-temporal variations of hydrologic connectivity, while the third and fourth indicators provide valuable information on the overall response of the topographic surface to rainfall inputs at the outlet. Simplified hydrograph denotes the discharge normalized by cumulative rainfall as a function of time, cumulative rainfall, or cumulative rainfall normalized by maximum depression storage (Antoine et al., 2009). The relative surface connection function is expressed as the ratio of surface area connected to the downstream boundary to the total surface area as a function of the water stored in the depressions of the surface (Antoine et al.,

2009). Normalization of these variables enables one to compare hydrologic connectivity for various topographic conditions (e.g., area, slope, roughness, and maximum depression storage) and water sources/sinks (e.g., rainfall).

3.3.4. Creation of surfaces and acquisition of their DEMs

Three laboratory-scale surfaces (S1 – S3) and two field plot surfaces (S4 – S5) were created and used in this study (Fig. 3.2). Specifically, surface S1 was utilized for a combined experimental and modeling study on hydrologic connectivity, and surfaces S2-S5 were used for hydrologic connectivity modeling and analyses only. Surface S1 (Fig. 3.2a) was created using a styrofoam board with an area of 0.40 m^2 and a slope of 1.07%. This surface was characterized with several major puddles of typical P2P relationships (e.g., upstream-downstream relationship). Surfaces S2 and S3 (Figs. 3.2b and 3.2c) were generated by randomly distributing soil aggregates across an area of 1.0 m × 0.8 m, featuring uniform and homogeneous microtopography but dissimilar roughness conditions (the random roughness values for S2 and S3 were 1.30 and 0.41 cm, respectively). The slopes of surfaces S2 and S3 were 5.16% and 4.12%, respectively. The two field plot surfaces S4 and S5 (Figs. 3.2d and 3.2e) had an area of 5.6 m × 3.2 m and represented real complicated, non-uniform, and heterogeneous microtopographic conditions. S4 and S5 had an overall slope of around 3.0% towards their outlets. High-resolution DEMs of these five surfaces were obtained by using an instantaneous-profile laser scanner (Darboux and Huang, 2003; Chu et al., 2010).

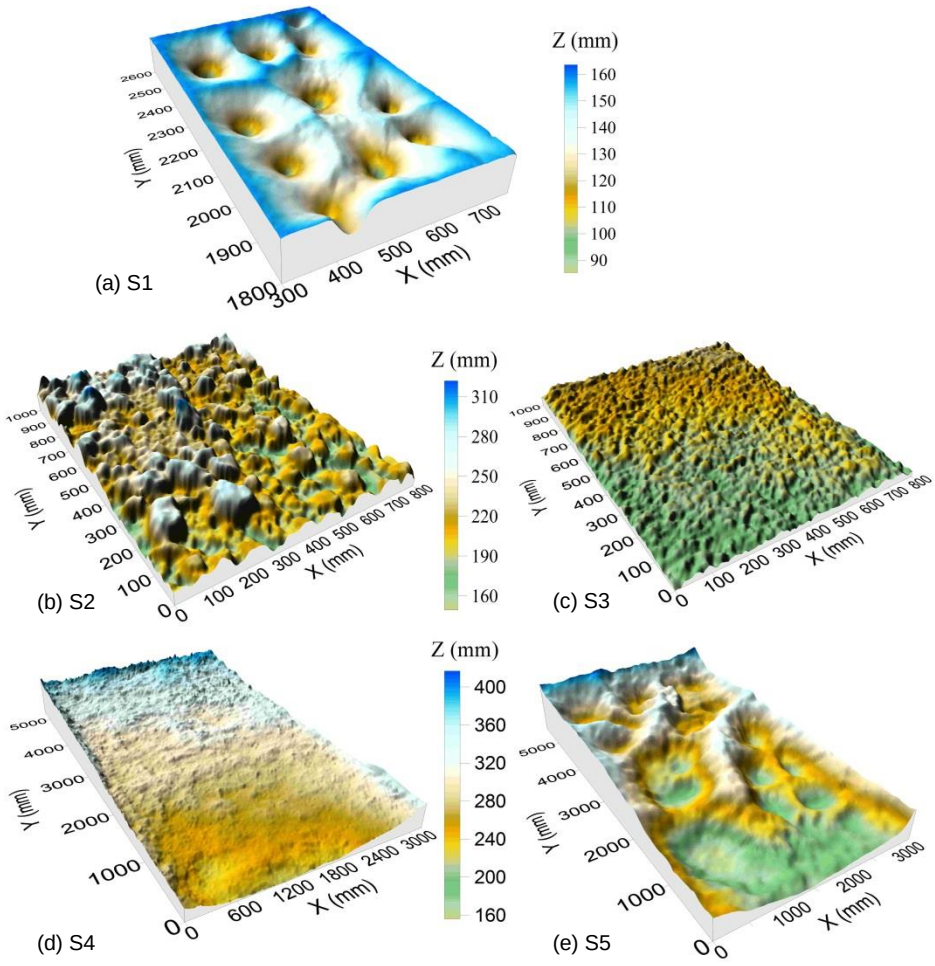

Fig. 3.2. DEMs of topographic surfaces S1 - S5

3.3.5. Combined P2P experimental and modeling study

Surface S1 was selected for this combined experimental and modeling study on hydrologic connectivity. An overland flow experiment was conducted for S1. The rainfall was generated by using a 4-head Norton-style rainfall simulator and the average rainfall intensity was 3.34 cm/hr. There was no infiltration for this impervious surface. Discharge was collected at the outlet and measured with a time interval of 20 sec. During the experiment, observation times were recorded, at which major puddles started spilling through their thresholds. The experiment was stopped when all puddles were fully filled and the flow system approached to a steady state.

Furthermore, the P2P conceptual model was applied to simulate the P2P overland flow process under the same conditions (e.g., rainfall and surface microtopography). The performance of the P2P concept model was evaluated by comparing the simulated simplified hydrograph and critical times (e.g., fully-filled times) against the observed data. The normalized objective function (NOF) (Ibbitt and O'Donnell, 1971) and modeling efficiency (EF) (Nash and Sutcliffe, 1970) were used to quantify the goodness of fit. They can be respectively expressed as:

$$\mathrm{NOF} = \frac{1}{\overline{X_O}} \sqrt{\frac{1}{n} \sum_{i=1}^{n} (X_{O,i} - X_{S,i})^2} \tag{3.3}$$

$$\mathrm{EF} = 1 - \frac{\sum_{i=1}^{n} (X_{O,i} - X_{S,i})^2}{\sum_{i=1}^{n} (X_{O,i} - \overline{X_O})^2} \tag{3.4}$$

where X = state variable (normalized discharge or P2P critical times); $\overline{X}$ = mean of X; n = total number of data points; and subscripts $_O$ and $_S$ denote the observed and simulated data, respectively. Note that if all observed values are the same as the simulated ones, NOF and EF equal 0 and 1, respectively.

3.3.6. P2P modeling for structural and functional hydrologic connectivity analyses

Surfaces S2 – S5 (Figs. 3.2b – 3.2e) were selected and P2P conceptual modeling was conducted to quantify spatio-temporal variations in hydrologic connectivity by using the proposed connectivity function and connectivity length indices and to analyze the effects of surface topographic characteristics on hydrologic connectivity. Different steady, uniform rainfall events were used in these simulations for surfaces S2 – S5. The P2P conceptual modeling for surfaces S2 and S5 was used for both structural and functional hydrologic connectivity analyses. To focus on the new method of microtopography-dominated P2P hydrologic connectivity and to

keep consistent with the existing hydrologic connectivity analysis methods (e.g. Antoine et al., 2009) for comparison purposes, infiltration was not simulated in this study. In the structural hydrologic connectivity analysis, we analyzed: (1) the spatial distributions of ACs, (2) their histograms, and (3) connectivity function and connectivity length of ACs. For functional hydrologic connectivity, we examined: (1) the simulated simplified hydrographs and the relative surface connection functions (e.g. Antoine et al., 2009), (2) the temporal variability in connectivity functions of ACs and PAs, and (3) the relationships between connectivity lengths of ACs or PAs, and time or cumulative rainfall.

3.3.7. Rainfall vs. hydrologic connectivity

Natural rainfall varies in both time and space, which may complicate the development of hydrologic connectivity and overland flow generation processes. To investigate such influences, P2P conceptual modeling was conducted for seven different rainfall events, including three steady uniform rainfall events (R1, R2, and R3), two steady nonuniform rainfall events (R4 and R5), and two unsteady uniform rainfall events (R6 and R7) (Fig. 3.3). The intensities of rainfall events R1, R2, and R3 were 0.58, 0.70, and 0.82 cm/hr, respectively. The rainfall intensity of R4 gradually changed spatially (Fig. 3.3b), while the spatial distribution of rainfall intensity of R5 exhibited much stronger variations (Fig. 3.3c). Events R4 and F5 had the same average rainfall intensity of 0.58 cm/hr, which equaled that of R1. The unsteady rainfall events R6 and R7 had the same cumulative rainfall as the steady rain event R1 (0.48 cm), but their intensities varied in time (Fig. 3.3a). The simulated simplified hydrographs and the variations in connectivity lengths of ACs and PAs were analyzed for different rainfall conditions. Surface S2 (Fig. 3.2b) was used to examine the rainfall effects on functional hydrologic connectivity since the puddles on surface S2 had relatively uniform geometric properties and did not show strong spatial heterogeneity.

For such a surface, discussion of the results would be easier and the conclusions could be further applied to surfaces with more complex topographic conditions.

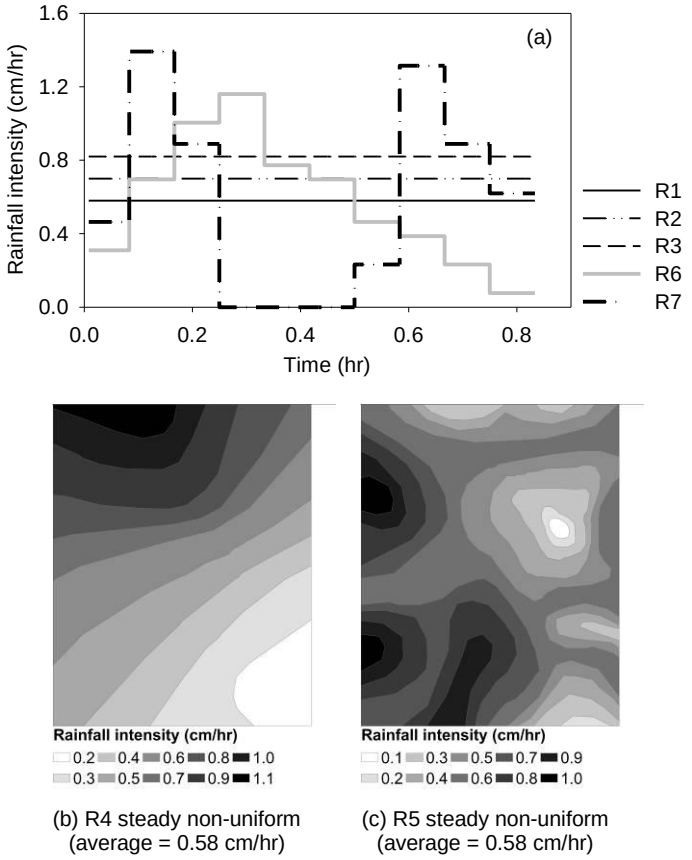

(b) R4 steady non-uniform (average = 0.58 cm/hr)

(c) R5 steady non-uniform (average = 0.58 cm/hr)

Fig. 3.3. Three steady uniform rainfall events (R1-R3), two steady non-uniform rainfall events (R4 and R5), and two unsteady uniform rainfall events (R6 and R7) used in this study

3.3.8. Surface slope vs. hydrologic connectivity

As one of the important factors, surface slope influences the dynamic hierarchical connecting processes of a topography-dominated overland flow system. A preliminary study was conducted to examine the slope effects on hydrologic connectivity. Based on surface S2, four different sloping surfaces were generated by using a coordinate conversion program (Yang et al., 2010). The slopes ranged from 5.16% to 19.81%. The P2P conceptual model was applied to these sloping surfaces for a steady, uniform rainfall event with an intensity of 0.58 cm/hr. The

simulated simplified hydrographs and the computed connectivity lengths for these sloping surfaces were compared and the effects of surface slope on hydrologic connectivity were evaluated.

3.4. Results and Discussion

3.4.1. Combined experimental and modeling study for hydrologic connectivity analysis

Fig. 3.4a shows the observed and simulated simplified hydrographs for surface S1 and the evolution of connectivity lengths of ACs and PAs with time (Fig. 3.4). Interesting variations in hydrologic connectivity can be observed from the special observation and simulation times at which puddles started spilling (Fig. 3.4b). Good agreement can be observed between the observed and simulated simplified hydrographs (Fig. 3.4a) and their normalized objective function and modeling efficiency are 0.11 and 0.96, respectively. The relatively simple relationships of puddles of surface S1 ensured precise measurement of the timing of puddle spilling and observation of the development of ACs and hydrologic connectivity during the experiment. The puddle spilling times from the simulation match the observed ones from the experiment (i.e., the squares are closely distributed along the 45^{o} line) (Fig. 3.4b). The normalized objective function and modeling efficiency for the simulation and observation times are 0.12 and 0.94.

Both observed and simulated simplified hydrographs display immediate increases at the beginning (point O) (Fig. 3.4a). Both hydrographs show a stepwise increasing pattern (Fig. 3.4a), implying dramatic changes in hydrologic connectivity. After a puddle is fully filled and starts spilling, if the corresponding AC directly connects to the outlet of the surface, a step-wise increase in discharge occurs (Fig. 3.4a). Each step-wise increase in the simplified hydrograph can be attributed to a new puddle spilling process and the corresponding evolution of ACs, as

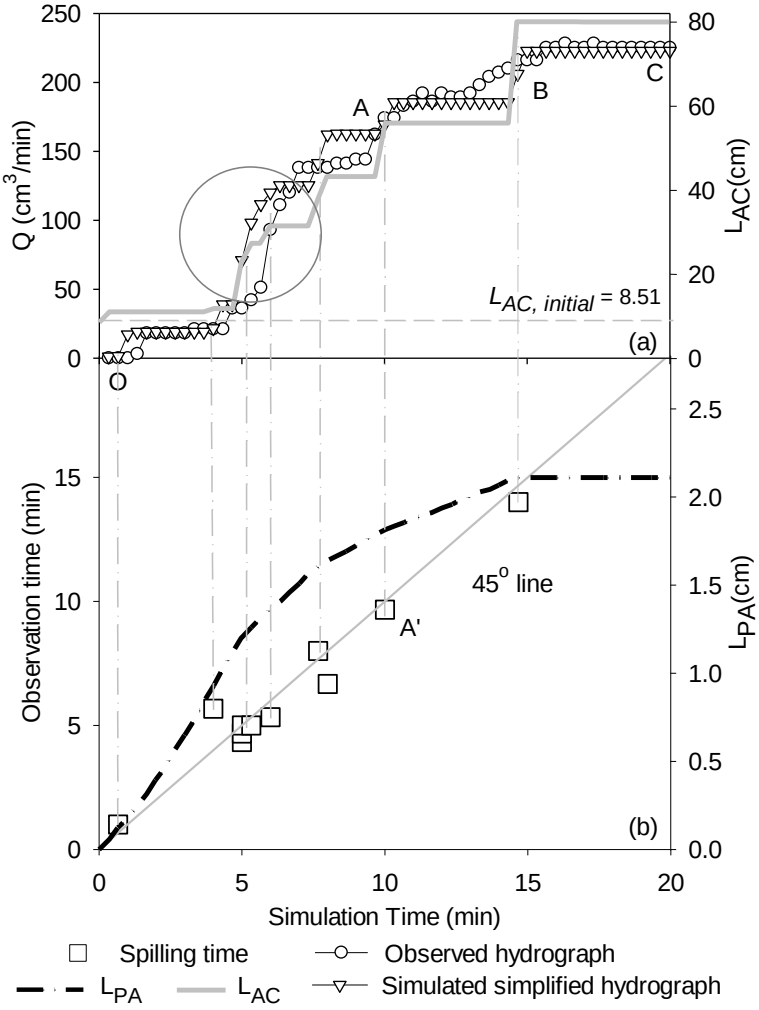

Fig. 3.4. Observed and simulated simplified hydrographs, critical times for P2P processes, and connectivity lengths of connected areas and ponded areas (L_{AC} and L_{PA}) for surface S1

indicated by the vertical lines in Figs. 3.4a and 3.4b (e.g., points A and A'). After all puddles are well connected and the evolution of ACs is completed, the entire surface contributes runoff water to the outlet and the simplified hydrograph reaches a plateau (line BC, Fig. 3.4a).

Simplified hydrograph and connectivity length of ACs (Fig. 3.4a) are two connectivity measurement indicators that have different hydrologic meanings and are calculated by different methods. However, these two indicators show considerable similarity in representing the system response and the behavior of runoff generation. They exhibit a similar step-wise increasing

pattern (Fig. 3.4a). Meanwhile, certain differences can be observed in the shapes of the connectivity length of ACs and the simplified hydrograph. The connectivity length of ACs at the beginning (t = 0, no ponded water) is greater than zero (8.51 cm, Fig. 3.4a), which represents the structural hydrologic connectivity property for the surface. Also, connectivity length of ACs shows more detailed stepwise increases/variations, as indicated in the circle in Fig. 3.4a. This is because connectivity length of ACs not only reflects the first type ACs as the simplified hydrograph does, but also is a function of the second type ACs. The difference between the changing patterns of the simplified hydrograph and connectivity length of ACs can be more significant for surfaces with complex topographic characteristics. Connectivity length of ACs increases from 8.51 cm (initial stage) to 79.96 cm (final stage) (Fig. 3.4a). Connectivity length of ACs quantifies the properties of both structural hydrologic connectivity (DEM-based hydrologic connectivity of the topographic surface) and functional hydrologic connectivity (P2P hydrologic connectivity of the dynamic overland flow system). Thus, connectivity length of ACs bridges the gap between structural and functional hydrologic connectivity for hydrologic connectivity analysis.

The connectivity length of PAs shows a continuous, significant increase before it reaches a plateau after 15 min (Fig. 3.4b). Each puddle makes flow contribution to the increase of connectivity length of PAs before it is fully filled. Resultantly, the shape of the curve of connectivity length of PAs changes when puddles are fully filled and start spilling in the runoff generation process. The magnitude of connectivity length of PAs indicates the average size of the water ponded areas across the entire surface at a time. The increasing pattern is determined by surface topography and characteristics of the source/sink terms of the drainage system.

In summary, the P2P filling-spilling-merging-splitting dynamics revealed the mechanism of overland flow generation and the unique hierarchical drainage pattern (Chu et al., 2013), as well as the related dynamic microtopography-controlled connecting process (i.e., P2P hydrologic connectivity). The comparison of the observed and simulated hydrologic connectivity results and the comparison of the existing index of simplified hydrograph (Antoine et al., 2009) and the new connectivity index proposed in this study (connectivity length of ACs and PAs) demonstrated that the new index was able to capture the spatio-temporal variations in hydrologic connections. Connectivity lengths of ACs and PAs not only can be used to quantify the static topography-associated hydrologic connectivity properties (i.e., structural hydrologic connectivity), but also the dynamic formation or evolution of the hydrologically connected areas (i.e., functional hydrologic connectivity).

3.4.2. Quantification of the spatio-temporal variations in hydrologic connectivity for various topographic surfaces

3.4.2.1. Structural hydrologic connectivity

Hydrologic connectivity associated with the static topographic properties (i.e., structural hydrologic connectivity) can be quantified by analyzing the spatial distribution of ACs and hydrologic connectivity indices, such as connectivity function and connectivity length of ACs. Figs. 3.5a – 3.5d illustrate the spatial distributions of ACs and their histograms for surfaces S2 and S5 (Figs. 3.2b and 3.2e). The original DEMs of these two surfaces exhibit topographic irregularity and non-uniformity, and the spatial distributions of their ACs also reflect such topographic characteristics (Figs. 3.5a and 3.5b). The average values of ACs for surfaces S2 and S5 are 14.1 cm^2 and 889.3 cm^2, respectively. The histograms of ACs for these two surfaces display a right-skewed distribution and small ACs account for high percentages of ACs (Fig.

3.5c and 3.5d). The skewness values of the areas of ACs for surfaces S2 and S5 are 1.54 and 2.67, respectively. The coefficient of variation values of their ACs are 0.79 and 1.70, respectively, indicating that surface S5 has higher non-uniformity in the AC distribution than surface S2. Thus, the ACs of the random roughness surface S2 are smaller and more uniformly distributed than those of surface S5. It also can be concluded that the spatial distribution of ACs for a topographic surface reflects the complexity/variability of its ACs.

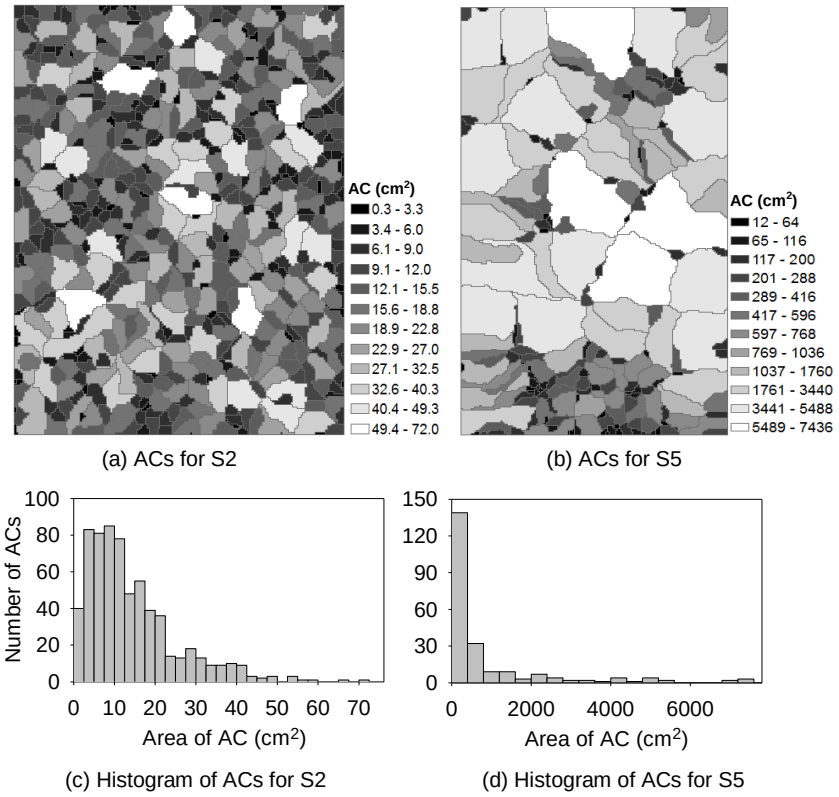

Fig. 3.5. Spatial distributions of connected areas (ACs) and their histograms (the number of ACs vs. the area of AC) for structural hydrologic connectivity analysis (t = 0, no ponded water) for surfaces S2 and S5

Fig. 3.6 shows the connectivity functions of ACs for surfaces S2 – S5 (i.e., structural hydrologic connectivity: $t = 0$). The connectivity function of ACs decreases with increasing separation distance h (Fig. 3.6). Surface S2 with a higher random roughness index has a greater connectivity function of ACs for the same separation h due to the larger ACs associated with

bigger soil aggregates (Fig. 3.6a). For the two field plot surfaces (S4 and S5), the rougher surface S5 has a higher connectivity function of ACs for the same separation (Fig. 3.6b). The connectivity lengths of ACs for surfaces S2 – S5 are 2.2, 1.5, 11.1, and 26.6 cm, respectively. In addition, the maximum connectivity length of ACs (i.e., *h* value for a zero connectivity function of ACs) varies, depending on the surface topographic characteristics. The preceding discussions demonstrate the capability of connectivity function, connectivity length, and maximum connectivity length of ACs in quantifying the structural hydrologic connectivity properties.

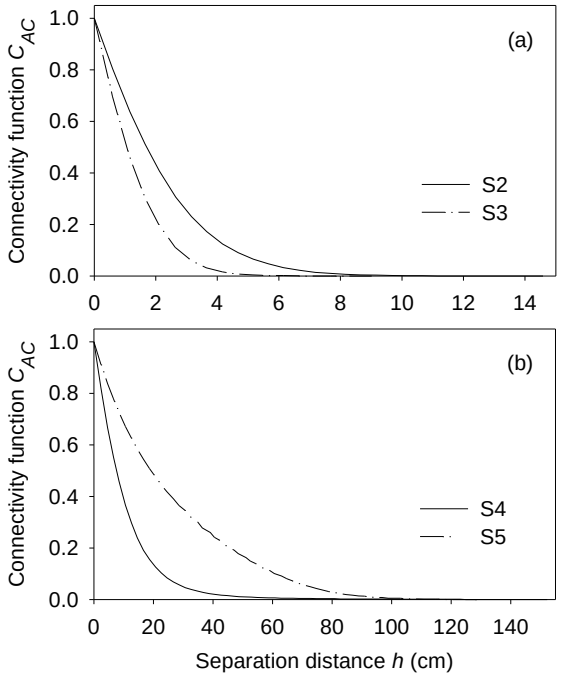

Fig. 3.6. Connectivity functions of connected areas (C_{AC}) for structural hydrologic connectivity (t = 0) of surfaces S2 - S5

3.4.2.2. Existing functional hydrologic connectivity indices: simplified hydrograph and relative surface connection function

The P2P dynamics during a rainfall event change ACs, which further alters the development of hydrologic connectivity (i.e., functional hydrologic connectivity). Fig. 3.7a displays the simulated simplified hydrographs (rainfall-normalized discharge vs. cumulative

rainfall) for surfaces S2 and S3. Different increasing patterns can be observed in these rainfall-normalized simplified hydrographs (Fig. 3.7a). A simplified hydrograph indicates the partitioning between outflow discharge and abstractions (e.g., depression storage). The area under the simplified hydrograph represents the quantity of outlet flow, while the area between the rainfall-normalized discharge curve and the line of rainfall-normalized discharge of 1 represents the water loss in depression storage (note that no infiltration is simulated) (Antoine et al., 2009). Two major characteristics can be observed in the simulated simplified hydrographs for surfaces S2 and S3 (Fig. 3.7a): (1) at the initial stage (cumulative rainfall < 400 cm^3), the simplified hydrographs of surfaces S2 and S3 are almost identical (Fig. 3.7a), and (2) beyond the initial stage (cumulative rainfall > 400 cm^3), the two simplified hydrographs exhibit significant differences in the increasing pattern and the timing to reach the steady state. For the same amount of rainfall input, the normalized discharge from surface S3 that features smaller roughness (Fig. 3.2c) tends to increase faster and reach the steady state much earlier than that from surface S2 (Fig. 3.2b). These differences in the simplified hydrographs for S2 and S3 can be attributed to their dissimilar surface depression storage and puddle organization, which are determined by the spatial distributions of puddles and their hydrologic relationships.

In order to examine the effects of puddle organization on simplified hydrographs of different topographic surfaces without considering their dissimilar maximum depression storage, the cumulative rainfall was normalized by maximum depression storage (i.e., maximum depression storage-normalized cumulative rainfall) (Antoine et al., 2009). Fig. 3.7b shows the normalized simplified hydrographs for surfaces S2 – S5. Fig. 3.8 shows the relative surface connection functions for these surfaces. The shape of the relative surface connection function curves is very similar to that of the normalized simplified hydrographs under steady uniform

rainfall (Figs. 3.7b and 3.8), and both represent the responses/behaviors of the areas that connect to the surface boundaries/outlets. As shown in Fig. 3.7b, as time proceeds, more runoff water drains to the boundaries/outlets of the surface. Fig. 3.8 shows significant increases in the relative surface connection functions at later stages, which can be attributed to the fact that more puddles were fully filled and they spilled and connected to the surface boundaries/outlets.

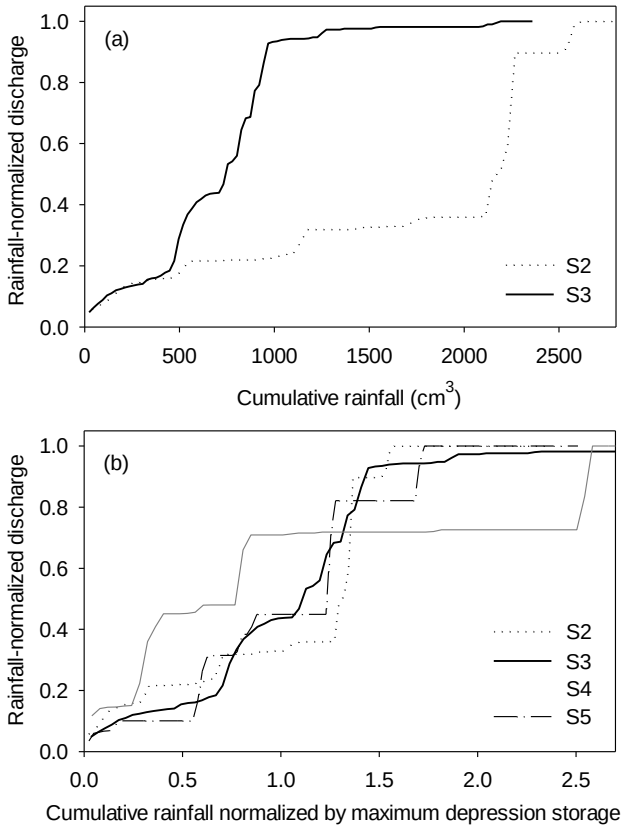

Fig. 3.7. Rainfall-normalized discharge vs. cumulative rainfall and cumulative rainfall normalized by maximum depression storage for surfaces S2 - S5

From Fig. 3.7b, two types of changing patterns of the simplified hydrographs and the relative surface connection functions can be identified. Surfaces S2, S3 and S5 have the first type of changing pattern while surface S4 belongs to the second type. The surfaces of the first type simplified hydrographs (S2, S3, and S5) have less runoff (smaller area under the hydrograph curve) and more depression storage loss (larger area above the hydrograph curve) for earlier time

period (Fig. 3.7b). The first type simplified hydrographs exhibit more runoff and less depression storage loss for the later stage of the overland flow generation processes (Fig. 3.7b). The relative surface connection function shows similar changing patterns. The values of coefficient of variation for puddle maximum depression storage, which reflects the degree of uniformity of puddle geometric properties, for surfaces S2, S3, and S5 are 3.06, 3.09, and 3.10, respectively, while the coefficient of variation of puddle maximum depression storage for surface S4 is as high as 6.30. This can be attributed to the stronger non-uniformity of the geometric properties of surface S4 (Fig. 3.2d), which allows surface S4 to easily develop hydrologic connectivity at the earlier time period. However, S4 shows lower prolonged connectivity at the later stage due to the existence of larger puddles (Figs. 3.7b and 3.8). It thus can be concluded that hydrologic connectivity may vary at different stages of overland flow generation, depending on the puddle organization (e.g., uniformity of puddle geometric properties).

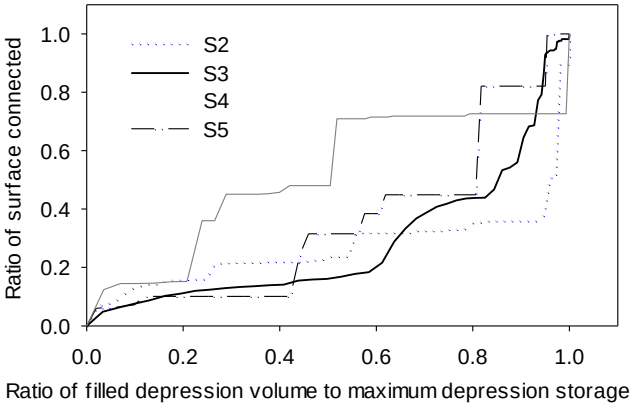

Fig. 3.8. Relative surface connection functions (the ratio of connected areas to the total surface area vs. the ratio of filled depression volume to maximum depression storage) for surfaces S2 - S5

3.4.2.3. New functional hydrologic connectivity indices: connectivity function and connectivity length

As an example, Figs. 3.9a and 3.9b respectively show the connectivity functions of ACs and PAs at six time points for surface S5 - a field plot surface featuring a number of well-organized puddles (e.g., different puddle sizes, levels, and relationships) (Fig. 3.2e). The corresponding cumulative rainfall values for the six time points are 0.00, 0.06, 0.13, 0.26, 0.65, and 0.88 cm (Fig. 3.9). For any selected time points or cumulative rainfall values, the curve of connectivity function of ACs shows a gradually decreasing trend with separation *h* (Fig. 3.9a). For example, the curves of connectivity function of ACs for cumulative rainfall of 0.00 cm (i.e., structural hydrologic connectivity, same as the curve in Fig. 3.6b for surface S5), 0.06, and 0.13 cm decrease from 1.0 to 0.0, which indicates a decreasing pattern of hydrologic connectivity. The maximum connectivity lengths of ACs for the corresponding times are 116.8, 198.9, and 220.9 cm, respectively. Hydrologic connectivity is improved with an increase in time. The separation distance *h* reaches the maximum connectivity length of 559.7 cm for cumulative rainfall of 0.88 cm for surface S5 (Fig. 3.9a). The connectivity function C_{AC} curve for cumulative rainfall of 0.88 cm also shows a slightly increase when *h* reaches or exceeds 320.0 cm due to the boundary effect. Fig. 3.9b shows the curves of connectivity function of PAs for the six selected time points. At the beginning (cumulative rainfall = 0.00 cm), the connectivity function of PAs equals 0.0 for any *h* values because there is no initial ponded water on surface S5. The connectivity function of PAs decreases with separation *h* for other time points and ponded water connectivity is improved over time (Fig. 3.9b). For any time or cumulative rainfall, the connectivity function of PAs for $h = 0$ represents the ratio of ponded area to the total surface

area. The *h* value corresponding to the zero connectivity function of PAs represents the maximum connectivity length of PAs (Fig. 3.9b).

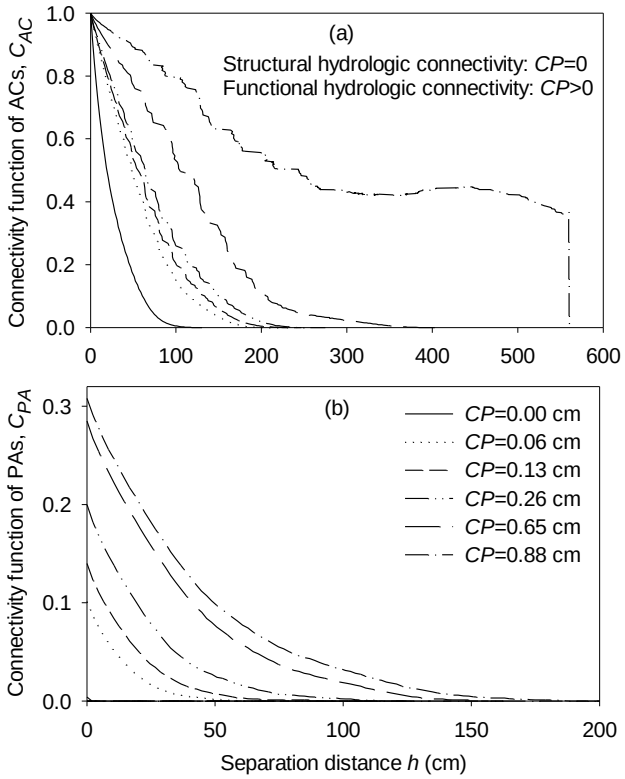

Fig. 3.9. Connectivity functions of connected areas and ponded areas (C_{AC} and C_{PA}) from simulations for surface S5 at six different time points or cumulative rainfall (*CP*) values (Notes: C_{PA} at $h = 0$ represents the ratio of ponded areas to the total surface area; and *h* for $C_{PA} = 0$ represents the maximum connectivity length of PAs)

Fig. 3.10 displays the changing patterns of the connectivity lengths of ACs and PAs for surfaces S2 – S5. The differences of the connectivity lengths of ACs and PAs between surfaces S2 and S3 are more significant at the later stage comparing with those at the beginning (Figs. 3.10a and 3.10b). This can be attributed to the fact that surface S2 (Fig. 3.2b) has more larger puddles than surface S3, and these larger puddles dominate the P2P spilling process and control the evolution of ACs at the later stage. For cumulative rainfall smaller than 2,000 cm^3, surface S3 with smaller roughness (Fig. 3.2c) shows greater connectivity length values (Fig. 3.10a), indicating improved hydrologic connectivity of ACs. The connectivity length of ACs for the

final stage depends on the topographic characteristics, sizes, and boundary conditions of the surface. Note that the maximum ponded areas of surfaces S2 and S3 are similar (2,217 and 2,115 cm^2, respectively). However, their final values of connectivity length of PAs show a significant difference (0.58 and 1.24 cm, respectively) (Fig. 3.10b). That is, although the two surfaces have similar total ponded areas, their average lengths of the ponded areas under the fully-filled condition are different due to their distinct sizes of depressions/puddles (Fig. 3.2b and 3.2c).

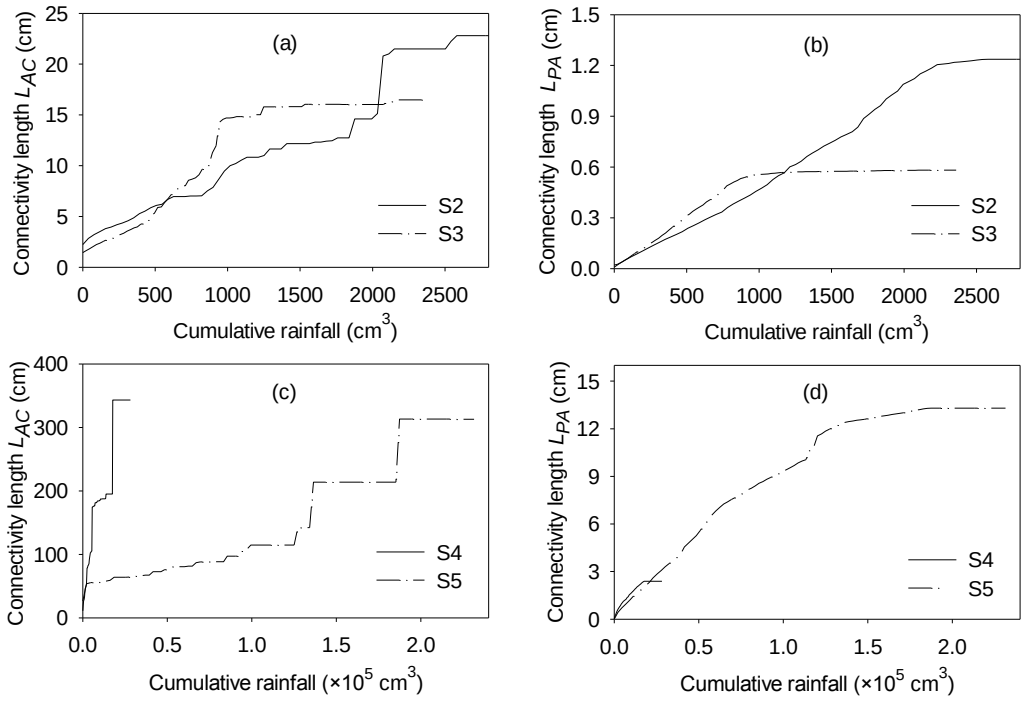

Fig. 3.10. Connectivity lengths of connected areas and ponded areas (L_{AC} and L_{PA}) from simulations for surfaces S2 - S5

For surfaces S4 and S5, more significant differences can be observed in the changing patterns of connectivity lengths of ACs and PAs than those from surfaces S2 and S3 (Figs. 3.10c and 3.10d). Such differences in connectivity lengths of ACs and PAs for surfaces S4 and S5 can be attributed to their distinct topographic characteristics (Figs. 3.2d and 3.2e). The curves of connectivity lengths of ACs and PAs of surface S4 show a much faster increase than those of surface S5, indicating quicker development of hydrologic connectivity for the smoother field plot

surface S4 under the same rainfall input (Figs. 3.10c and 3.10d). For surface S4, connectivity length of ACs reaches the maximum connectivity length (343.09 cm) when cumulative rainfall is equal to 17,810 cm^3 (Fig. 3.10c), which implies that all puddles on S4 are fully filled and the evolution of ACs is completed.

We demonstrated the quantification of structural hydrologic connectivity and its linkage to functional hydrologic connectivity indices, and quantified the hydrologic connectivity properties for surfaces with various microtopographic characteristics by using the hydrologic connectivity indices proposed in this study (connectivity function and connectivity length of ACs and PAs) and two indices proposed by Antoine et al. (2009) (simplified hydrograph and relative surface connection function). It can be concluded that the time-varying connectivity functions and connectivity lengths of ACs and PAs quantitatively describe and link structural and functional hydrologic connectivity properties. Comparing with the existing connectivity indicators, the new indices proposed herein effectively reveal the spatio-temporal variations in hydrologic connectivity in the topography-controlled overland flow generation process. The proposed "P2P hydrologic connectivity" concept helps better understand the topography-dominated hydrologic connectivity and the discontinuous P2P overland flow dynamics.

3.4.3. Effects of rainfall on hydrologic connectivity

The effects of rainfall on hydrologic connectivity were evaluated in this study by examining the system response (simplified hydrograph) to various rainfall events (Fig. 3.3) and the corresponding connectivity lengths of ACs and PAs for surface S2. For a steady uniform rainfall event, a higher rainfall intensity tends to expedite the P2P filling-spilling process and hence the evolution of ACs (i.e., development of hydrologic connectivity), resulting in an earlier steady state (full development of ACs). For the steady uniform rainfall events (R1, R2, and R3,

Fig. 3.3a), all the simplified hydrographs (rainfall-normalized discharge vs. time) and the curves of connectivity length of ACs show a similar step-wise increasing pattern with time resulting from the same P2P dynamic process and the development of hydrologic connectivity. But, the timing of each stepwise change is different (Figs. 3.11a1 and 3.11b1).

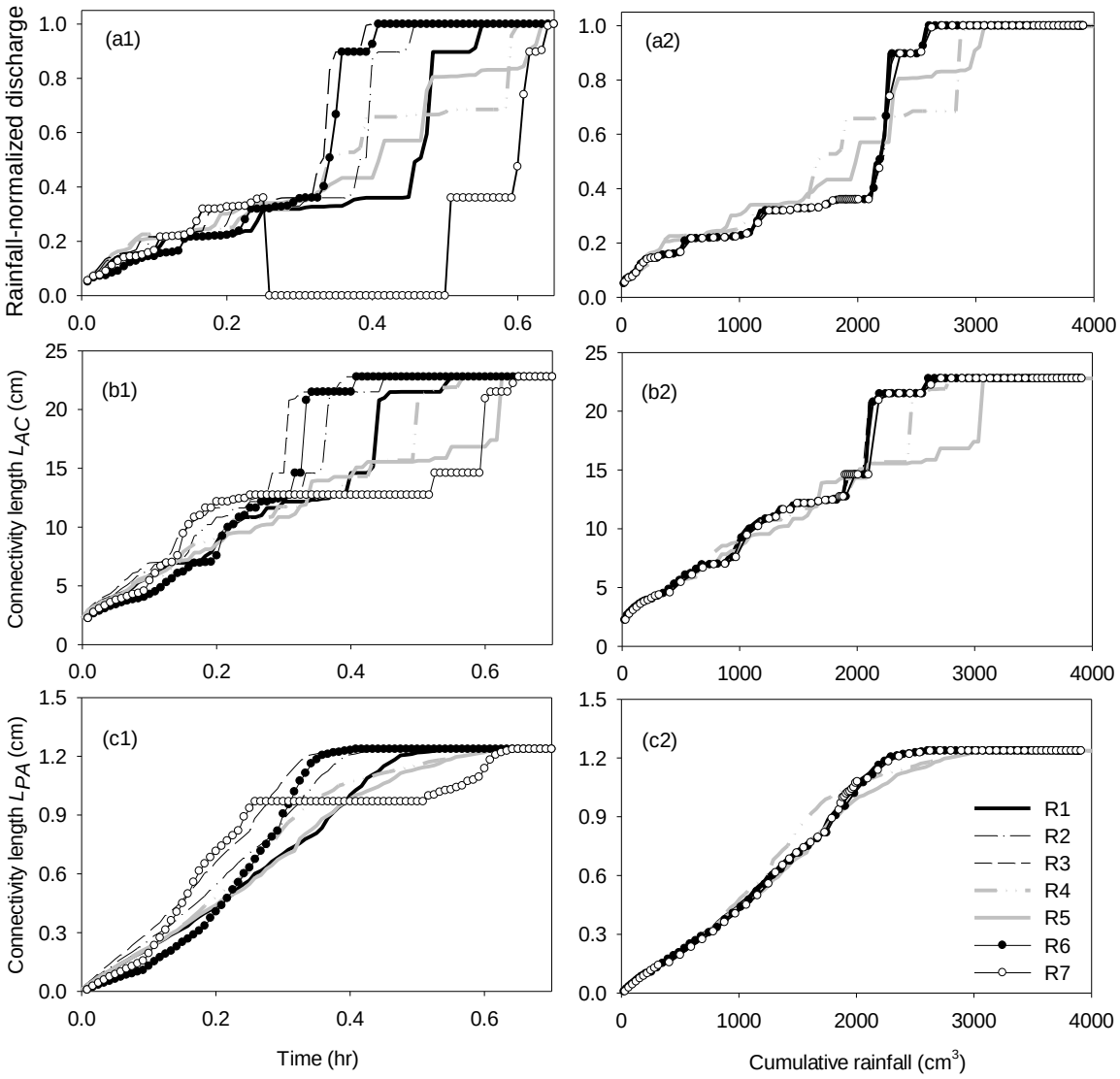

Fig. 3.11. Temporal variations in rainfall-normalized discharge, and connectivity lengths of connected areas and ponded areas (L_{AC} and L_{PA}) for surface S2 under seven different rainfall conditions [three steady uniform rainfall events: R1 (0.58 cm/hr), R2 (0.70 cm/hr), and R3 (0.82 cm/hr); two steady non-uniform rainfall events: R4 and R5 with average rainfall intensity of 0.58 cm/hr; and two unsteady uniform rainfall events: R6 and R7 with cumulative rainfall of 0.48 cm]

For the two steady, non-uniform rainfall events R4 and R5 (Figs. 3.3b and 3.3c), the changing patterns of the simplified hydrographs and the curves of connectivity length of ACs with time are different from those from R1, even though R1, R4, and R5 have the same average rainfall intensity (Figs. 3.11a1 and 3.11b1). As shown in the curves of rainfall-normalized discharge and connectivity length of ACs in Figs. 3.11a1 and 3.11b1, the system reaches the steady state earlier for event R1 than events R4 and R5. This can be attributed primarily to the delay in the P2P processes and the development of ACs in low rainfall intensity zones.

Figs. 3.11a1 and 3.11b1 also show the simplified hydrographs (rainfall-normalized discharge) and the curves of connectivity length of ACs for the two unsteady uniform rainfall events R6 and R7. Note that the rain events R6 and R7 (Fig. 3.3a) have the same cumulative rainfall (0.48 cm) as rain event R1. The distinct temporal variations in the three rainfall-normalized discharge curves demonstrate the significant effects of rainfall characteristics on simplified hydrographs (Fig. 3.11a1). From Figs. 3.11b1 and 3.3a, it can be observed that higher rainfall intensity accelerates the development of ACs (hydrologic connectivity) and hence increases connectivity length of ACs. Rainfall-normalized discharge may decline to zero when rainfall intensity equals to zero for the unsteady R7 event, while connectivity length of ACs remains constant during the zero rainfall period (note that no infiltration was simulated) (Fig. 3.11b1). These processes may become complicated if other loss terms (e.g., infiltration) exist. Depending on the spatial and temporal variability in the P2P processes, the connectivity length of ACs may increase or decrease with time due to the connection/merging or disconnection/splitting of ACs as the ponded water levels in some puddles rise to or drop below their thresholds. Thus, connectivity function and connectivity length can serve as useful

indicators to reveal the complexity and variability of the surface topography-dominated overland flow system.

Different from connectivity length of ACs, connectivity length of PAs exhibits a smoother increasing pattern for all rainfall events (Fig. 3.11c1). Higher intensity rainfall events (e.g., R3) accelerate the development of PAs and a non-uniform rainfall distribution (e.g., R4 and R5) may delay the timing to reach the maximum connectivity length of PAs (Fig. 3.11c1). In addition, significant effects of the temporal distributions of rainfall on the connectivity length of PAs can be observed from the results for the unsteady rainfall events R6 and R7 (Fig. 3.11c1).

Furthermore, we analyzed the relationships between cumulative rainfall and simplified hydrographs and connectivity lengths of ACs and PAs and found a very similar pattern for the uniformly distributed rainfall events (R1-R3 and R6-R7) (Figs. 3.11a2, 3.11b2, and 3.11c2), indicating that the temporal variations in rainfall may only affect the dynamic P2P filling-spilling-merging processes and the evolution of ACs and PAs. However, significant influences of the spatial variations in rainfall for the non-uniform events R4 and R5 (Figs. 3.3b and 3.3c) on the changing patterns of simplified hydrographs and connectivity lengths of ACs and PAs can be observed (Figs. 3.11a2, 3.11b2, and 3.11c2).

In summary, development of hydrologic connectivity not only depends on the topographic characteristics of surfaces, but also is significantly affected by the spatio-temporal rainfall distributions. Temporal variations in rainfall intensity do not alter the P2P processes and the evolution of ACs, but may change the occurrence timing of these processes. Spatial changes in rainfall intensity influence the overall development of hydrologic connectivity.

3.4.4. Preliminary study on the effects of surface slope on hydrologic connectivity

The simplified hydrographs (rainfall-normalized discharge vs. cumulative rainfall or cumulative rainfall normalized by maximum depression storage), the curves of connectivity length of ACs vs. cumulative rainfall, and the curves of connectivity length of PAs vs. cumulative rainfall for the four sloping surfaces (slope = 5.16%, 10.17%, 15.01%, and 19.81%) are respectively shown in Figs. 3.12a – 3.12d. At the initial period (cumulative rainfall < 600 cm^3), the simulated simplified hydrographs for the four sloping surfaces are close to each other (Fig. 3.12a). The larger the slope is, the earlier the stepwise increase occurs, which also leads to an earlier steady state. For a gentle slope (e.g., 5.16%), stronger influences of surface slope on the timing of stepwise increases and the steady state can be observed in Fig. 3.12a. The curves of rainfall-normalized discharge and connectivity length of ACs show dissimilar increasing patterns for the four sloping surfaces (Figs. 3.12a and 3.12c), which can be attributed to the changes in their maximum depression storage and puddle organizations induced by different slopes.

Fig. 3.12e displays the decreasing relationship between maximum depression storage and slope for surface S2. Maximum depression storage decreases from 1,660 cm^3 for the slope of 5.16% to 1,180, 1,016, and 854 cm^3 for the slopes of 10.17%, 15.01%, and 19.81%, respectively. An increase in surface slope may not only reduce the maximum depression storage of the surface due to the changes in puddle structures, but also alter the puddle organization. The rainfall-normalized discharge is affected by both maximum depression storage and puddle organization. Fig. 3.12b shows the maximum depression storage-normalized simplified hydrographs (i.e., the effect of maximum depression storage has been removed), which reveal the effects of changing puddle organizations on the simplified hydrographs. Comparison of Figs. 3.12a with 3.12b indicates that the change in surface maximum depression storage has more significant effects on

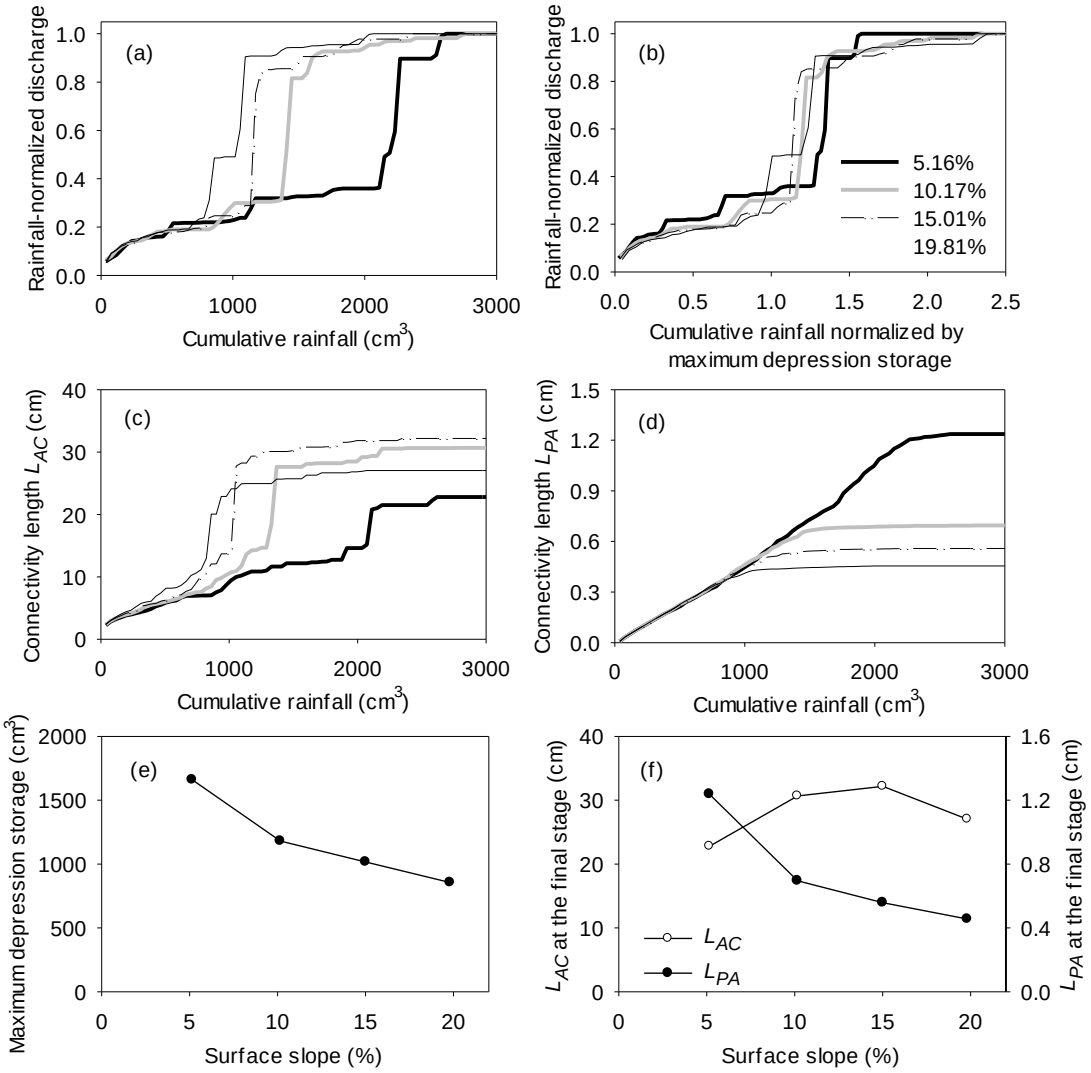

Fig. 3.12. Rainfall-normalized discharge and connectivity lengths of connected areas or ponded areas (L_{AC} and L_{PA}) vs. cumulative rainfall for surface S2 with four different slopes

the simplified hydrographs than the change in puddle organization. In addition, a higher slope leads to an earlier stepwise increase in connectivity length of ACs (Fig. 3.12c). However, connectivity length of ACs at the final steady stage is not necessarily greater for a surface with a higher slope (Figs. 3.12c and 3.12f). This can be attributed to the fact that flow drainage area may change significantly for certain critical slope(s). The connectivity lengths of PAs for the four sloping surfaces increase equally in the beginning (Fig. 3.12d), but the final connectivity

lengths of PAs at the steady stage decrease with an increase in surface slope (Fig. 3.12f), which also can be attributed to the decrease in their maximum depression storage (Fig. 3.12e).

3.5. Conclusions

A concept of "puddle-to-puddle hydrologic connectivity" was proposed to describe the overland flow generation dynamics. Hydrologic connectivity was investigated by analyzing the puddle filling-spilling processes, outlet discharge, and the evolution of hydrologically connected areas ACs and water ponded areas PAs through combined experimental and modeling studies. Two modified hydrologic connectivity indices, time-varying connectivity function and connectivity length, were proposed to quantify scale-dependent and time-varying hydrologic connectivity of ACs and PAs. In addition, the effects of surface topography, rainfall, and surface slope on hydrologic connectivity were analyzed. This research provided an insight into microtopography-controlled hydrologic connectivity and complexity of overland flow generation. The following conclusions have been reached:

The new connectivity function and connectivity length of ACs and PAs were capable of quantifying both structural and functional hydrologic connectivity for surfaces with various topographic characteristics. These two indices quantified the spatio-temporal variations in hydrologic connectivity and revealed the dynamic threshold behaviors of overland flow generation.

The P2P overland flow processes governed the evolution of hydrologic connectivity, controlled overland flow generation, and altered flow drainage patterns. A surface with smaller roughness was easier to be fully filled and tended to reach a steady stage earlier. For topographic surfaces, hydrologic connectivity may vary at different stages of the overland flow generation processes, depending on the puddle organization (i.e., uniformity of puddle structures).

Rainfall distribution had significant effects on development of hydrologic connectivity and the behaviors of the dynamic P2P overland flow processes. Temporal variations in rainfall intensity did not alter the P2P processes and the evolution of ACs, but changed their occurrence timing. The spatial variability in rainfall intensity influenced the overall evolution of hydrologic connectivity and the behaviors of overland flow generation.

Simplified hydrograph and connectivity length were significantly affected by surface slope due to the changes in puddle organization and maximum depression storage. Particularly, the results from this research emphasized the important role of surface depression storage, and implied the possible existence of critical slope(s) for a topographic surface, at which a sharp change in hydrologic connectivity and flow drainage area occurred. It should be noted that in addition to rainfall and surface slope, many other factors (e.g., infiltration) also may have significant influences on the P2P dynamics and P2P hydrologic connectivity. Detailed in-depth studies on the infiltration effects on hydrologic connectivity for real systems would be of great interest and important research value.

3.6. References

Antoine, M., 2010. Overland flow connectivity: Theory and application at the interrill scale. PhD Thesis. Universite catholique de Louvain, Belgium (http://hdl.handle.net/2078.1/33307-PDF_01).

Antoine, M., Javaux, M., and Bielders, C., 2009. What indicators can capture runoff-relevant connectivity properties of the micro-topography at the plot scale? Adv. Water Resour., 32(8), 1297-1310.

Antoine, M., Javaux, M., and Bielders, C., 2011. Integrating subgrid connectivity properties of the micro-topography in distributed runoff models, at the interrill scale. J. Hydrol., 403(3-4), 213-223.

Appels, W. M., Bogaart, P. W., and van der Zee, S. E. A. T. M., 2011. Influence of spatial variations of microtopography and infiltration on surface runoff and field scale hydrological connectivity. Adv. Water Resour., 34(2), 303-313.

Bracken, L. J., and Croke, J., 2007. The concept of hydrological connectivity and its contribution to understanding runoff-dominated geomorphic systems. Hydrol. Process., 21, 1749-1763.

Brierley, G., Fryirs, K., and Jain, V., 2006. Landscape connectivity: the geographic basis of geomorphic applications. Area, 38(2), 165-174.

Chu, X., Yang, J., Chi, Y., and Zhang, J., 2013. Dynamic puddle delineation and modeling of puddle-to-puddle filling-spilling-merging-splitting overland flow processes. Water Resour. Res., 49(6), 3825-3829.

Chu, X., Zhang, J., Chi, Y., and Yang, J., 2010. An improved method for watershed delineation and computation of surface depression storage. P1113-1122, In: Watershed Management 2010: Innovations in Watershed Management under Land Use and Climate Change, Proceedings of the 2010 Watershed Management Conference, edited by K. W. Potter and D. K. Frevert. American Society of Civil Engineers, Reston, VA.

Darboux, F., Davy, P., Gascuel-Odoux, C., and Huang, C., 2002. Evolution of soil surface roughness and flowpath connectivity in overland flow experiments. Catena, 46(2-3), 125-139.

Darboux, F., Gascuel-Odoux, C., and Davy, P., 2002. Effects of surface water storage by soil roughness on overland-flow generation. Earth Surf. Proc. Land., 17(3), 223-233.

Darboux, F., and Huang, C., 2003. An instantaneous-profile laser scanner to measure soil surface microtopography. Soil Sci. Soc. America J., 67 (1), 92-99.

Ibbitt, R. P., and O'Donnell, T., 1971. Fitting methods for conceptual catchment methods. Journal of the Hydraulics Division, 97(9), 1331-1342.

Lexartza-Artza, I., and Wainwright, J., 2009. Hydrological connectivity: linking concepts with practical implications. Catena, 79(2), 146-152.

Nash, J. E., and Sutcliffe, J. V., 1970. River flow forecasting through conceptual models. Part I-A discussion of principles. J. Hydrol., 10(3), 282-290.

O'Callaghan, J. F., and Mark, D. M., 1984. The extraction of drainage networks from digital elevation data. Comput. Vision Graph., 28, 323-344.

Pringle, C., 2003. What is hydrologic connectivity and why is it ecologically important? Hydrol. Process., 17(13), 2685-2689.

Tetzlaff, D., Soulsby, C., Bacon, P. J., Youngson, A. F., Gibbins, C., and Malcolm, I. A., 2007. Connectivity between landscapes and riverscapes – a unifying theme in integrating hydrology and ecology in catchment science? Hydrol. Process., 21(10), 1385-1389.

Western, A. W., Blöschl, G., and Grayson, R. B., 2001. Toward capturing hydrologically significant connectivity in spatial patterns. Water Resour. Res., 37 (1), 83-97.

Yang, J., Chu, X., Chi, Y., and Sande, L., 2010. Effects of rough surface slopes on surface depression storage, p4427-4436. In: Challenges of Change, Proceedings of the 2010 World Environmental and Water Resources Congress, edited by R. N. Palmer. American Society of Civil Engineers.

CHAPTER 4. EFFECTS OF DEM RESOLUTION ON SURFACE DEPRESSION PROPERTIES AND HYDROLOGIC CONNECTIVITY

4.1. Abstract

Surface DEM resolution receives an increasing attention due to its importance in topographic analysis (e.g., quantification of surface depressions) and hydrologic modeling. Varied, even contrary conclusions have been obtained concerning the effects of DEM grid size on surface depression properties. Land surfaces are featured with a number of microtopography-controlled, localized areas, and their connections may significantly alter hydrologic and geomorphologic processes. Few efforts have been made to examine the effects of DEM resolution on surface depression properties and hydrologic connectivity. This study aimed to evaluate such resolution effects by two dimensionless parameters: DEM representation scale λ_L (ratio of DEM grid size to correlation length, representing horizontal resolution) and surface roughness scale λ_R (ratio of random roughness to correlation length, representing vertical topographic variability). A puddle delineation program was utilized to quantify depression properties for a variety of topographic surfaces characterized by different DEM resolutions, including small scale surfaces with random roughness, field plots, and watershed surfaces. In particular, a puddle-to-puddle (P2P) conceptual model was used for hydrologic connectivity analysis. It was found that puddle properties depended on both dimensionless λ_L and λ_R. λ_L significantly influenced the calculations of structural and functional hydrologic connectivity. Using DEMs with a coarser resolution or higher λ_L tended to overestimate hydrologic connectivity and simplified hydrograph for a surface with numerous small-scale depressions. DEM resolution or dimensionless λ_L had significant influences on the development of functional hydrologic connectivity especially at the early stage of the rainfall-runoff process.

4.2. Introduction

The advancement in measuring surface elevation has made it easier to acquire high resolution DEMs, which in turn have improved hydrologic analysis and use of distributed hydrologic models. However, the horizontal resolution or grid size of DEMs often affects the determination of surface depression property parameters, delineation of surface topographic features, and modeling results. The effects of DEM resolution on hydrotopographic parameters have been examined by many researchers (e.g., Kuo et al., 1999; Molnár and Julien, 2000; Dutta and Herath, 2001; Thompson et al., 2001; Moglen and Hartman, 2001). According to their findings, a coarser resolution tends to produce a more continuous and less defined landscape that is featured with flattened slopes, reduced curvatures, shortened drainage lengths, and enlarged contributing areas (CA).

Surface depressions are important in regulating surface runoff and infiltration, groundwater recharge, and subsurface contaminant movement (Ullah and Dickinson, 1979; Hayashi et al., 2003). Studies have been conducted to evaluate the effects of DEM resolution on estimating surface depression properties. Huang and Bradford (1990) examined the effects of DEM resolution on maximum depression storage (MDS) in their experimental study and concluded that MDS decreased with an increase in grid size. Kamphorst et al. (2000) examined a variety of tilled soil surfaces of varying roughness and found that MDS did not structurally decrease with increasing grid size. Carvajal et al. (2006) found that the estimated MDS became smaller and smaller with an increase in grid size since the soil surface roughness was artificially smoothed for a larger grid size. Abedini et al. (2006) explored the relationships between DEM resolution and the topographic properties of depressions for fifteen runoff plots and found that maximum ponding area (MPA) increased with an increase in grid size while MDS increased with

grid size to a certain point and then started to decrease. In addition, they found a power-law relationship between MPA and CA for surfaces with different grid sizes. Ullah and Dickinson (1979) determined the power law relationships between mean puddle depth (HPM) and MPA, HPM and MDS, and MPA and MDS and found that the Weibull model was the best to fit the frequency distributions of MDS, MPA, and HPM without log transformation. Their results indicated that distributions of MDS, MPA, and HPM followed similar patterns for all surface plots. Most of the aforementioned studies centered on the DEM resolution effects for agricultural surfaces. Varied, even contrary conclusions have been obtained concerning the effects of grid size on depression properties (e.g., MDS). Thus, research is needed to systematically evaluate the resolution effects on depression properties, as well as their relationships and distributions for surfaces of distinct topographic characteristics.

Hydrologic connectivity has been studied in different disciplines in recent years (e.g., Brierley et al., 2006; Bracken and Croke, 2007; Antoine et al., 2009). Hydrologic connectivity is used to represent the continuous passage to transfer water and the related mass over a land surface (Pringle, 2003; Tetzlaff et al., 2007). Land surfaces are generally irregular with different types of topographic features (e.g., depressions) and the depressions result in independent and localized mass balance (Hayashi et al., 2003). Hydrologic connectivity of the locally connected areas determines the spatial and temporal conveyance of water and mass. Various hydrologic connectivity indicators have been proposed to describe surface topographic conditions and hydrologic processes. Antoine et al. (2009) compared different hydrologic connectivity indicators involving both structural hydrologic connectivity (SHC) and functional hydrologic connectivity (FHC). SHC is the hydrologic connectivity properties of a static surface DEM without considering water flow, while FHC represents the hydrologic response of a topographic

surface to the system inputs (Antoine et al., 2009). FHC depends on both surface microtopographic characteristics and system inputs/outputs, such as rainfall and infiltration processes. Different methods have been developed to calculate hydrologic connectivity. The conditional-walker method was used to simulate the processes of gradually filling depressions and forming a flow network to outlets (Darboux et al., 2002a; Antoine et al., 2009). Appels et al. (2011) investigated the effects of surface microtopography and infiltration on FHC by using an algorithm, which characterized depressions and their filling, merging, and connecting processes under an assumption of instantaneous water transfer.

Changes in hydrologic connectivity may affect a series of hydrologic processes (e.g., overland flow generation, infiltration, and soil erosion). Improved knowledge of hydrologic connectivity is needed in order to better understand the hydrologic and geomorphologic processes. The hydrologic connectivity study is particularly vital to explicit quantification of the effects of surface depressions on overland flow generation, which has been proven to be a challenge for hydrologists (Moore and Larson, 1979; Onstad, 1984; Sneddon and Chapman, 1989; Bruneau and Gascuel-Odoux, 1990; Darboux et al., 2002b). Although hydrologic connectivity and its importance have been well understood, to the best of our knowledge, few studies have been conducted to evaluate the effects of DEM resolution on hydrologic connectivity.

The objective of this study was to investigate the effects of DEM resolution or representation scale λ_L (ratio of DEM grid size to correlation length) on surface depression properties and hydrologic connectivity (both SHC and FHC) for surfaces of various microtopographic characteristics. In addition, the relationships and distributions of depression

property parameters are quantified and analyzed for the surfaces with different DEM resolutions or λ_L values.

4.3. Materials and Methods

4.3.1. Acquisition of surface DEMs

Eight surfaces (S1 – S8) with different topographic characteristics (Fig. 4.1) were selected to evaluate the DEM resolution effects on surface depression properties and hydrologic connectivity. Surfaces S1 – S3 (Figs. 4.1a-4.1c) were small laboratory surfaces with an area of 2.10 m by 0.81 m, characterized with randomly distributed soil aggregates (Chu et al., 2012; Chi et al., 2012), while Surfaces S4 and S5 (Figs. 4.1d and 4.1e) were smooth and rough field plots, respectively, with an area of 5.6 m by 3.2 m (Bogart, 2014). Surfaces S6 - S8 were watershed surfaces with an area of 8,040 m by 6,030 m, located in Minnesota. These DEMs were downloaded from the USGS website (Figs. 4.1f -4.1h, UTM coordinate system).

An instantaneous-profile laser scanner (Darboux and Huang, 2003; Chu et al., 2010) was used to acquire high-resolution DEMs for Surfaces S1 - S5. The horizontal and vertical resolutions of the scanned DEMs were 0.98 mm and 0.50 mm, respectively. Due to the limited coverage area of the laser scanner, a large surface (e.g., field plots S4 and S5) was scanned piece by piece and the DEM of the entire surface was obtained by combining all pieces using a scanned data combination program developed in the current project (Chu et al., 2014). The scanned data for Surfaces S1 – S3 were processed to generate 0.5-cm DEMs, which were further aggregated by using the Kriging method to create DEMs of coarser resolutions (1.0, 1.5, 2.0, 3.0, 4.0, and 5.0 cm). Similarly, DEMs of different resolutions (1.0, 2.0, 4.0, 6.0, 8.0, and 10.0 cm) were generated for Surfaces S4 and S5. The 30-m DEM data for Surfaces S6 – S8 were

downloaded from the USGS website. Based on the original 30-m resolution, 45, 60, 75, 90, and 120 m DEMs were generated.

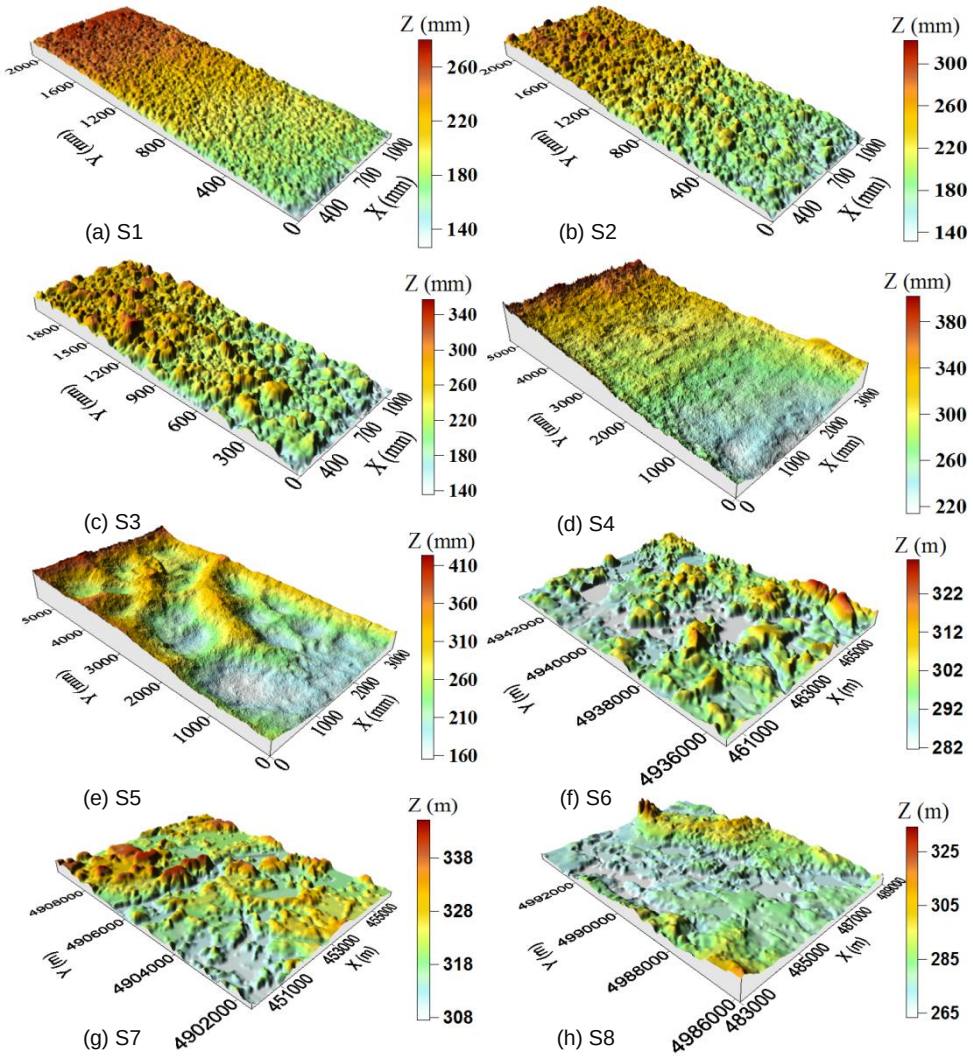

Fig. 4.1. DEMs of Surfaces S1 - S8

4.3.2. DEM representation scale and surface roughness scale

Real surfaces have varying topographic characteristics or roughness. DEMs of various resolutions or grid sizes (*DX*) represent surface topography differently. To effectively quantify surface topography and evaluate the effects of the scale-dependent DEM representations, four parameters, including correlation length *CL* (Blöschl, 1999), random roughness *RR* (i.e., standard deviation of surface elevations, Allmaras et al., 1966), dimensionless DEM representation scale

λ_L (ratio of *DX* to *CL*), and dimensionless surface roughness scale λ_R (ratio of *RR* to *CL*), were calculated in this study. *CL* reflects the horizontal scale of surface topography, while *RR* reveals the vertical variability in surface elevations. λ_L represents the DEM resolution relative to the spatial scale of surface topography; and λ_R quantifies the vertical topographic variability or roughness relative to the horizontal scale.

CL measures the degree of correlation and the spatial dimension (scale) of the variability in topographic elevations. It can be determined based on semivariogram $\gamma(\mathbf{h})$ (Chi et al., 2012):

$$\gamma(\mathbf{h}) = \frac{1}{2N(\mathbf{h})} \sum_{i=1}^{N(h)} [Z(\mathbf{s}_i + \mathbf{h}) - Z(\mathbf{s}_i)]^2 \tag{4.1}$$

where $\mathbf{s}_i$ = location *i*; $\mathbf{h}$ = lag distance; $Z(\mathbf{s}_i)$ = elevation at location $\mathbf{s}_i$; $Z(\mathbf{s}_i + \mathbf{h})$ = elevation at location $(\mathbf{s}_i + \mathbf{h})$; and $N(\mathbf{h})$ = number of pairs spaced at $\mathbf{h}$. To determine *CL*, the experimental variogram can be fitted by the following exponential function (Blöschl, 1999):

$$\gamma(h) = \sigma^2[1 - \exp(-h/CL)] \tag{4.2}$$

where σ^2 = variance of surface elevations. *CL* and *RR* were calculated by using the finest resolutions (0.5 cm for Surfaces S1 – S3; 1.0 cm for Surfaces S4 – S5; and 30 m for Surfaces S6 – S8). Table 4.1 shows the computed topographic parameters *CL*, *RR*, λ_R, and λ_L for Surfaces S1-S8.

Table 4.1. Surface topographic parameters

Surface	Correlation length *CL*	Random roughness *RR*	Slope (%)	Surface roughness scale λ_R (*RR*/*CL*)	DEM representation scale λ_L (*DX*/*CL*)
S1	2.24 cm	0.42 cm	5.14	0.187	0.22-2.23
S2	3.53 cm	0.81 cm	5.14	0.230	0.14-1.42
S3	5.00 cm	1.33 cm	5.14	0.267	0.10-1.00
S4	50.00 cm	0.47 cm	3.49	0.009	0.02-0.20
S5	90.91 cm	1.87 cm	2.63	0.021	0.01-0.11
S6	833.33 m	4.87 m	0.02	0.006	0.04-0.14
S7	769.23 m	4.12 m	0.02	0.005	0.04-0.16
S8	434.78 m	5.79 m	0.06	0.013	0.07-0.28

Note: *DX* = DEM grid size (resolution).

4.3.3. Surface delineation: introduction to the Window-based PD software

In this study, the puddle delineation (PD) software (Chu et al., 2010, 2013) was used to characterize depressions/puddles and calculate depression property parameters. The unique features of the PD software included its capabilities of delineating puddles at different threshold-controlled levels, determining their hierarchical relationships, and dealing with special topographic conditions such as flats, overflow thresholds shared by multiple puddles, and puddles of multiple thresholds. The software provided a user-friendly interface to effectively characterize the spatial complexity of topographic surfaces, visualize the spatial distributions of puddles at different levels, and improve the understanding of the related hydrologic processes.

The puddle delineation process involved four major steps (Chu et al., 2010, 2013): (1) identification of puddle centers, including flats; (2) identification of other cells in each puddle; (3) identification of overflow thresholds of puddles; and (4) determination of the puddle relationships. The PD software calculated flow directions, flow accumulations, MDS, MPA, CA, HPM, the average of maximum puddle depths (HPMA), the average of mean puddle depths (HPA), the number of puddle levels (NPL), and the number of puddles (NP). MPA was the

maximum water-covered area when a puddle or a surface was fully filled. CA of a puddle represented the total area that potentially contributed surface runoff to the puddle. HPMA was calculated for a surface as the average of maximum puddle depths, which were the elevation differences between puddle thresholds and centers. HPM was expressed as the ratio of MDS to MPA for the highest level puddles (i.e., all puddles were fully filled, reaching the overflow thresholds), while HPA of a surface was the average of HPM values of all puddles.

4.3.4. Statistical analysis of the surface depression properties

Surfaces S1 - S8 with different DEM resolutions were delineated by using the PD software and the surface depression property parameters (MDS, MPA, CA, HPMA, HPM, HPA, NPL, and NP) were calculated. The SAS software (version 4.3) was used for statistical analysis, including ANOVA test, regression analysis, and distribution fitting. Efforts were made to examine the effects of DEM resolution or λ_L on the spatial distributions of puddles, surface depression properties, and the relationships and distributions of the puddle property parameters.

DEM resolution or λ_L affects the delineation of surfaces, puddles, and their spatial distributions. To quantitatively evaluate such effects, Surface S8 with grid sizes of 30, 60, 90, and 120 m (i.e., λ_L = 0.07, 0.14, 0.21, and 0.28) was selected and delineated by using the PD software. Based on the delineation results, spatial distributions of puddles for the four resolutions were mapped and compared.

To assess the effects of DEM resolution or λ_L on surface depression properties, Surfaces S1 – S8 with different λ_L values were selected; a set of topographic parameters including MDS, MPA, HPMA, HPA, NPL, and NP were plotted against λ_L on a natural logarithm scale; and the best-fit curves were determined. Furthermore, the trends of the fitted curves were compared for different topographic surfaces.

Most puddle property parameters (e.g., MDS, MPA, and HPM) are often correlated to each other. Efforts were also made to investigate the effects of DEM resolution or λ_L on the CA-MPA, MDS-MPA, and MDS-HPM relationships, with focus on the topographic properties of individual puddles. Surfaces S3 - S6 with various λ_L values were selected and their puddle property parameters were plotted against each other on a natural logarithm scale. Their best-fit curves were determined and compared.

In addition, Surfaces S3 – S6 that represented three different types of surfaces (random roughness surface, field plot surface, and watershed surface) and various λ_L values were selected for examining the distributions of puddle property parameters MDS, MPA, CA, and HPM. Since the original data were extremely right-skewed, natural logarithm transformation was performed for the puddle property parameters. Three statistical models (Weibull, Gaussian, and Gamma) were used to fit the histograms of the puddle property parameters for Surfaces S3 – S6 with different λ_L values. Goodness-of-fit tests of these models were then performed for MDS, MPA, HPM, and CA of Surfaces S3 – S6.

4.3.5. P2P conceptual model and hydrologic connectivity analysis

The P2P conceptual model (Chu et al., 2013) was used for hydrologic connectivity analysis. The model simulated water movement by characterizing the dynamic puddle filling, spilling, merging, and separating processes over complex topographic surfaces. Particularly, the model was able to effectively handle overland flow routing under special topographic conditions such as flats and multi-threshold puddles. Since this study focused on hydrologic connectivity analysis under the influence of surface microtopography, it was assumed in the model that water transferred instantaneously between cells and puddles. To simplify the problem under discussion, no infiltration was simulated.

Depressions control the overall hydrologic connectivity of a topographic surface and break the surface into a number of well-connected areas that have relatively independent hydrologic characteristics. In this study, we emphasized the P2P features of hydrologic connectivity by detailing the connected areas, their formation/evolution during the rainfall-runoff processes, and the responses of the hydrologic system under the influence of surface microtopography.

4.3.5.1. Structural hydrologic connectivity analysis

The SHC indicators calculated by traditional approaches, such as semivariogram, relative bivariate entropy, *n*-point rectilinear connectivity, connectivity function integral scale, Euler number, and percolation thresholds may not be able to describe the spatial connectivity patterns and relate to the hydrologic behaviors of a topographic surface (Antoine et al., 2009). In this study, SHC of a topographic surface was analyzed by characterizing and quantifying the connected areas of the surface. The PD software facilitated surface delineation and further characterization of the spatial variability in structural hydrologic connectivity. In the P2P conceptual model, a searching process was implemented to track overland flow based on the D8 method (O'Callaghan and Mark, 1984) and identify all connected areas. SHC was quantified and visualized by the histograms of connected areas. As an example, the SHC of Surface S8 was mapped and four different DEM resolutions or λ_L values (0.07, 0.14, 0.21, and 0.28) were considered in the SHC analysis.

4.3.5.2. Functional hydrologic connectivity analysis

A puddle receives runoff water from its contributing cells and spills to its downstream cell(s) or puddle(s) when the water level reaches its threshold(s). This spilling process leads to expansion of connected areas by merging or connecting with the downstream areas. Gradually,

more areas are connected to the outlet of the surface, which results in increases in discharge at the outlet (hydrograph). In this study, the aforementioned hydrologic processes were characterized by two FHC indicators: (1) formation/evolution of connected areas, including the temporal changes in the number and the average of connected areas, and (2) simplified hydrograph (Darboux et al., 2002b; Antoine et al., 2009; Appels et al., 2011).

Formation/evolution of connected areas (1st indicator) was quantified by the temporal changes in the number and the average of connected areas, and the spatial variations and distributions of connected areas over time. By quantifying the formation/evolution of the connected areas during the rainfall-runoff process (FHC), SHC was linked to the related hydrologic processes (e.g., overland flow generation). Following Darboux et al. (2002b), Antoine et al. (2009), and Appels et al. (2011), simplified hydrograph (2nd indicator) was used to quantify the functional relationships between rainfall-normalized discharge ($r_{Q\text{-}P}$) and cumulative rainfall (CP) or MDS-normalized CP ($r_{CP\text{-}MDS}$). The dimensionless simplified hydrograph ($r_{Q\text{-}P}$ vs. $r_{CP\text{-}MDS}$) is independent of rainfall intensity and surface area (Appels et al., 2011). Simplified hydrograph provided critical information on overland flow generation and surface runoff affected by surface microtopography and rainfall conditions.

P2P water routing simulations were performed by using the P2P conceptual model for Surfaces S3 (random roughness surface, Fig. 4.1c), S5 (field plot surface, Fig. 4.1e), and S6 and S8 (watershed surfaces, Figs. 4.1f and 4.1h) with different DEM resolutions or λ_L values. The calculated FHC indicators for these surfaces and different λ_R values were analyzed and compared. Steady and uniform rainfall (2.0 cm/hr) was applied for the water routing simulations and hydrologic connectivity analyses. The rainfall intensity of 2.0 cm/hr was selected primarily based on the need for demonstrating the P2P overland flow dynamics and connections of contributing

areas. The simulations for the selected surfaces continued until all depressions were fully filled and hydrologic connectivity was well developed. Thus, the simulation time period varied for these surfaces, depending on their areas and MDS values.

4.4. Results and Discussion

4.4.1. Spatial distributions of puddles for surfaces of various grid sizes

A surface may have certain dominant puddle sizes, depending on the microtopographic conditions. DEM resolution or λ_L influences the number, size, and distribution of puddles, and their hierarchical relationships, which further affect hydrologic processes, such as overland flow generation, surface runoff, infiltration, and soil water flow. Thus, selection of λ_L or DEM resolution is critical to achieve a better representation of actual surfaces and realistic hydrologic modeling.

In this study, Surface S8 (Fig. 4.1h) was selected to discuss the changes in the spatial distributions of puddles and the related hydrologic properties for different DEM resolutions or dimensionless λ_L values. Fig. 4.2 shows the delineation results from the PD software for four λ_L values: 0.07, 0.14, 0.21, and 0.28. Significant changes in puddle distributions can be observed for Surface S8 due to the changes in λ_L (Figs. 4.2a-4.2d). The surface with a smaller λ_L value (i.e., high resolution) showed numerous small well-defined puddles (i.e., smoother boundaries and small scale variations). According to the delineation results, NP decreased from 1392 to 612, 358, and 217 and NPL decreased from 29 to 26, 17, and 14 as λ_L increased from 0.07 to 0.14, 0.21, and 0.28. With an increase in λ_L, shallow depressions were smoothed out.

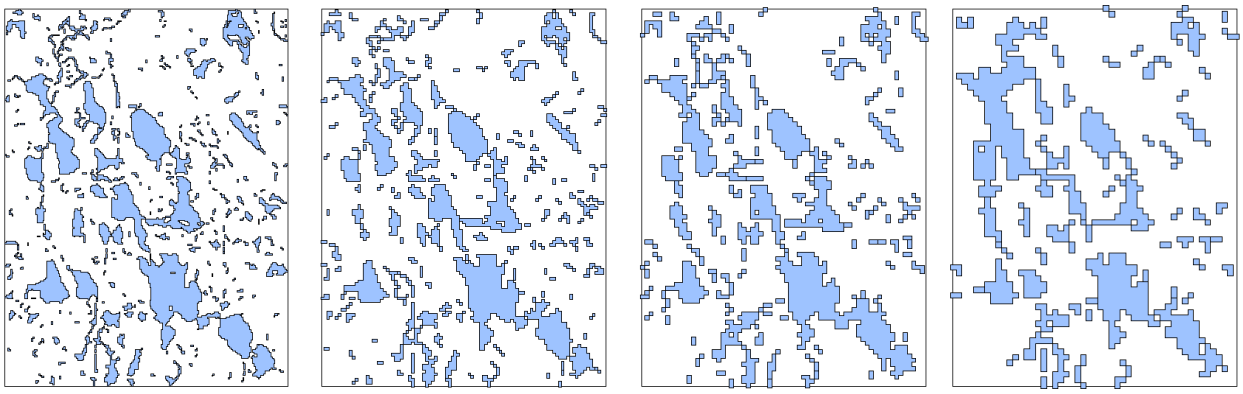

(a) λ_L = 0.07 (b) λ_L = 0.14 (c) λ_L = 0.21 (d) λ_L = 0.28

Fig. 4.2. Spatial distributions of depressions of Surfaces S8 (λ_R = 0.013) for four different DEM resolutions or dimensionless λ_L values

4.4.2. Effects of DEM representation scale on surface depression properties

The MDS and MPA of a topographic surface determine the capability of water retention and the overall distribution of ponded water. HPMA and HPA quantify the maximum and average vertical dimensions of puddles on a surface. NP and NPL characterize the complexity of the topographic surface. A surface with larger NPL and NP possesses more complex puddle relationships, threshold-controlled hydrologic connectivity, and P2P dynamic processes during a rainfall event. These topographic properties/processes subsequently affect a series of hydrologic processes, such as overland flow generation and infiltration. Thus, understanding the effects of DEM representation scale λ_L on depression property parameters is essential to improve the related hydrologic analysis and modeling.

Fig. 4.3 shows the relations of DEM resolution or λ_L and a set of surface depression property parameters including MDS, MPA, HPMA, HPA, NPL, and NP for Surfaces S1 – S8. MDS and MPA followed similar trends (Figs. 4.3a and 4.3b). Both increasing and decreasing power law relationships were observed for λ_L and MDS or MPA. For the eight surfaces, the average R^2 values of MDS and MPA were 0.82 and 0.84, respectively. With increasing λ_L, MDS

and MPA decreased for the smaller surfaces S1 – S5, and appeared to increase for the watershed surfaces S6 – S8 (Figs. 4.3a and 4.3b). For example, small puddles of Surface S3 were smoothed out and the MPA values for larger-sized puddles decreased with an increase in λ_L. The MPA for puddles larger than 16 cm^2 decreased from 3673.5 cm^2 to 2567.57 cm^2 as λ_L increased from 0.10 to 0.80. In contrast, for the watershed surface S6, the MPA of puddles larger than 1.43×10^4 m^2 increased from 0.83×10^7 m^2 to 1.27×10^7 m^2 as λ_L increased from 0.04 to 0.14. Although small puddles also were smoothed out for the watershed surfaces S6 – S8, they still displayed an increasing trend in MPA and MDS (Figs. 4.3a and 4.3b). In addition, a smoother surface might have a steeper decreasing trend of MDS and MPA than a rougher surface. This is, DEM resolution or λ_L tended to have greater influences on the computations of MPA and MDS for the smoother surface. In summary, MDS and MPA followed a similar increasing/decreasing trend with an increase in λ_L, depending on surface microtopographic characteristics. The changing pattern of λ_L and MDS or MPA seemed to be relevant to the surface topographic features or roughness (λ_R). Using a coarser resolution DEM (higher λ_L), MDS and MPA could be underestimated for a random roughness surface due to the smoothing effect.

Figs. 4.3c and 4.3d display obvious increasing/decreasing power law relationships between λ_L and HPMA or HPA. HPMA and HPA followed similar trends for different surfaces. Increasing patterns of HPMA and HPA can be observed for the two field plot surfaces S4-S5 (Figs. 4.1d and 4.1e) and the three watershed surfaces S6-S8 (Figs. 4.1f – 4.1h). For the three small random roughness surfaces S1-S3 (Figs. 4.1a – 4.1c), however, both increasing and decreasing trends can be observed for HPMA and HPA (Figs. 4.3c and 4.3d). This also can be attributed to the smoothing effect from the data aggregation process when creating coarser

resolution DEMs (i.e., larger λ_L values). Thus, interpolation/aggregation of elevation data affects the DEM-based computations of HPMA and HPA.

According to the delineation results, both NPL and NP had a decreasing power law relationship with λ_L (Figs. 4.3e and 4.3f). The average R^2 values of NPL and NP for the eight surfaces were 0.88 and 0.99, respectively. The gradients of the fitted lines depended on the distributions of puddles and surface microtopography. Hence, NPL and NP of a surface were affected by DEM resolution or λ_L, in addition to the microtopographic characteristics of the surface.

In conclusion, DEM resolution or dimensionless representation scale λ_L could significantly affect the geometric properties of surface depressions (e.g., size, depth, and shape), the number of puddles, and the complexity of puddle relationships. The changes in such topographic characteristics further altered hydrologic processes, such as surface depression storage, surface ponding, water retention, hydrologic connectivity, overland flow generation, and drainage patterns.

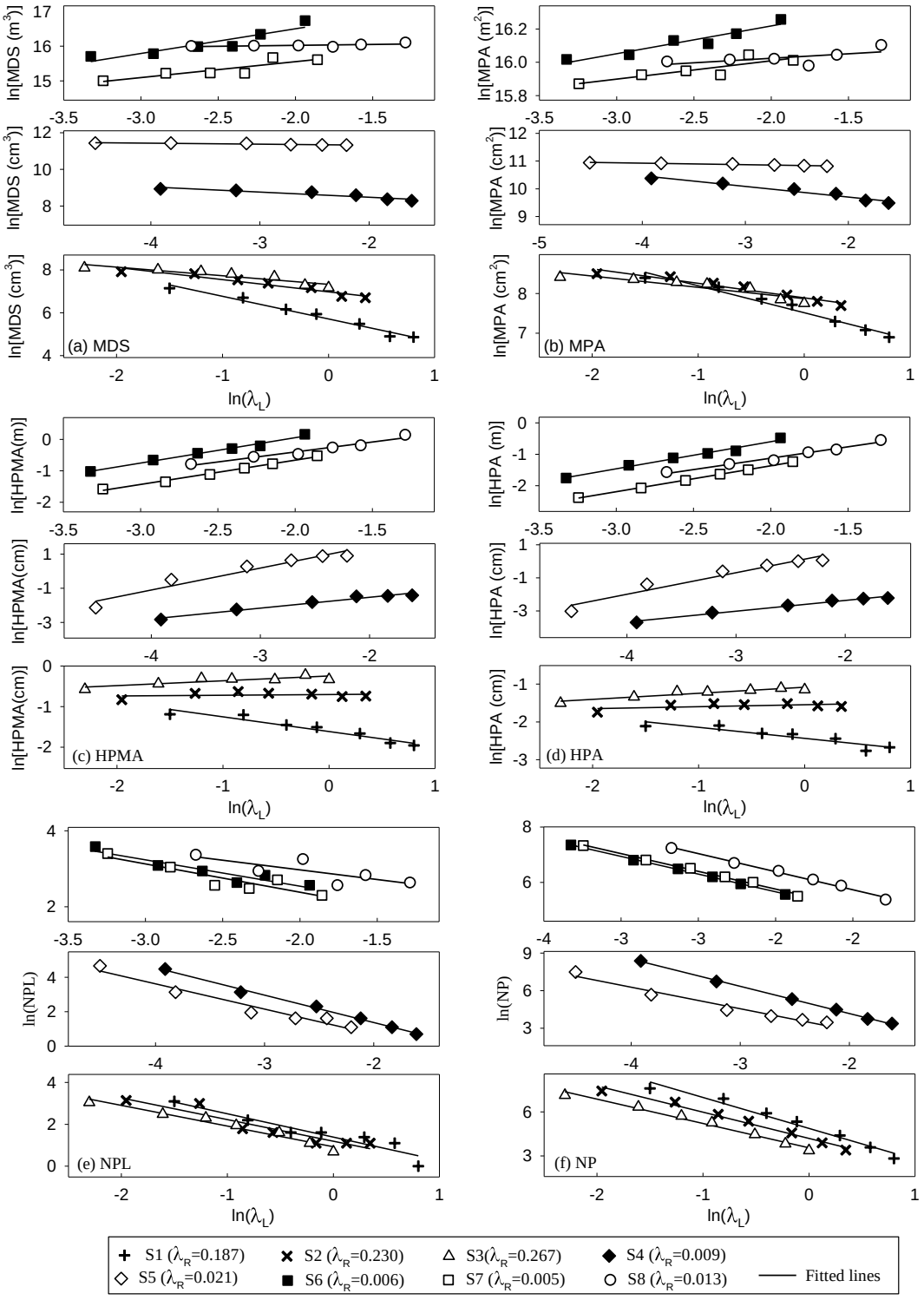

Fig. 4.3. Relationships of dimensionless DEM representation scale λ_L and puddle property parameters, including maximum depression storage MDS, maximum ponding area MPA, average of the maximum puddle depths HPM, average of the mean puddle depths HPA, number of puddle levels NPL, and number of puddles NP, for Surfaces S1 - S8

4.4.3. Relationships of surface depression property parameters

Surface depression property parameters (e.g., CA, MPA, MDS, and HPM) are positively correlated with each other and have power law relationships (Ullah and Dickinson, 1979; Abedini et al., 2006). However, it is still unclear whether surface topographic characteristics (or roughness scale λ_R) and DEM resolution (or DEM representation scale λ_L) affect such relationships. In this study, we examined the CA-MPA, MDS-MPA, and MDS-HPM relationships for various DEM resolutions or λ_L values and four representative topographic surfaces S3 – S6 (S3: small-scale random roughness surface, S4-S5: smooth and rough field plot surfaces, and S6: watershed surface).

As an example, Fig. 4.4 shows those relationships for Surface S3 plotted on a natural logarithm scale. A linear equation (i.e., power law relationship) could be fitted for all DEM resolutions (i.e., different λ_L values) for the CA-MPA, MDS-MPA, or MDS-HPM data set (Figs. 4.4a, 4.4b, and 4.4c, respectively). This implied that DEM representation scale λ_L did not significantly affect the relationships of these depression parameters for a specific topographic surface. However, the fitted lines varied for different surfaces that had dissimilar topographic characteristics (i.e., different λ_R values). Table 4.2 shows the regression coefficients and R^2 values of the fitted CA-MPA, MDS-MPA, and MDS-HPM lines for Surfaces S3 – S6. The average R^2 for the CA-MPA regression ($R^2 = 0.75$) was smaller than those for the MDS-MPA and MDS-HPM lines (0.86 and 0.85, respectively) for all surfaces (S3 – S6). This can be attributed to the fact that MDS, MPA, and HPM directly measured the geometric properties of puddles, while CA was less relevant to the puddle geometric properties and more dependent on surface topographic characteristics (e.g., local slopes). MDS, MPA, and HPM respectively represented third-, second-, and first-order spatial variables. The average exponent of the CA-

MPA power law relationships (i.e., slopes of the fitted lines) for Surfaces S3 – S6 was 0.75 (<1.0, Table 4.2), while the average exponents of the MDS-MPA and MDS-HPM power law relationships were 1.59 and 1.83, respectively (>1.0, Table 4.2).

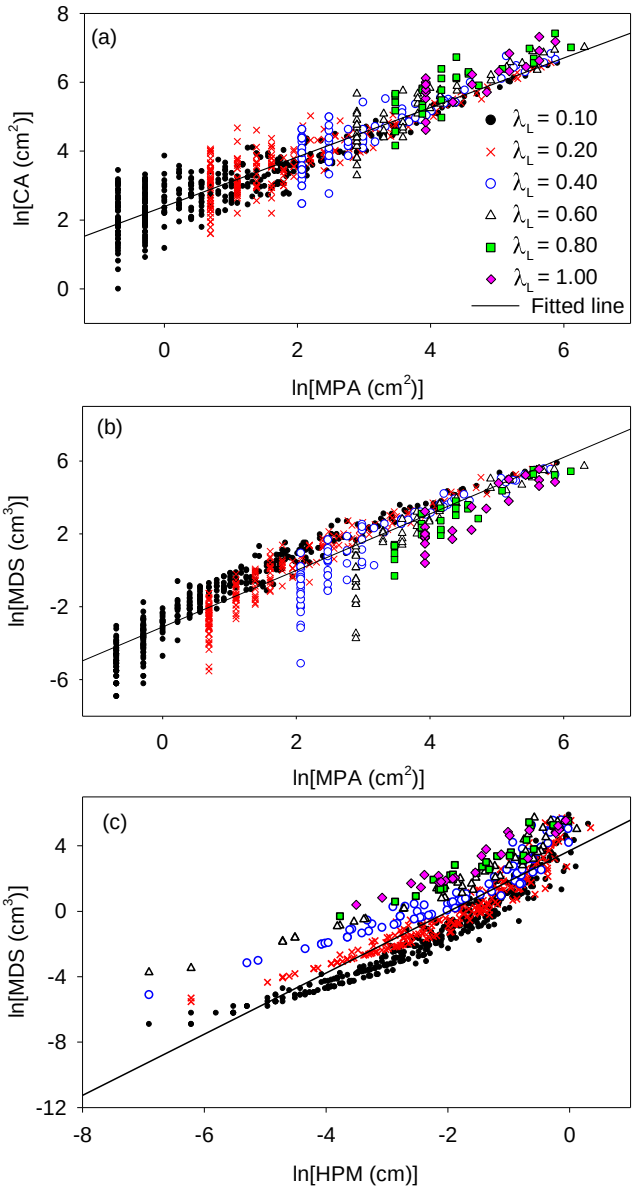

Fig. 4.4. Relationships of maximum ponding area MPA and contributing area CA, maximum ponding area MPA and maximum depression storage MDS, and mean puddle depth HPM and maximum depression storage MDS for Surfaces S3 (λ_R = 0.267) with various DEM resolutions or dimensionless λ_L values

Table 4.2. Regression coefficients of the linear equation Ln(y) = aLn(x) + Ln(b) for the CA-MPA, MDS-MPA, and MDS-HPM Power-Law relationships $y = bx^a$ for surfaces S3 - S6

Relationship	Surfaces	Intercept Ln(b)	Gradient a	Coefficient of determination R^2
CA - MPA	S3	2.391	0.719	0.863
	S4	2.834	0.743	0.725
	S5	2.574	0.798	0.731
	S6	4.680	0.720	0.671
MDS - MPA	S3	-3.103	1.551	0.882
	S4	-4.621	1.399	0.856
	S5	-5.388	1.687	0.939
	S6	-9.044	1.723	0.759
MDS – HPM	S3	3.703	1.871	0.810
	S4	5.604	1.832	0.826
	S5	6.360	2.080	0.915
	S6	10.588	1.518	0.832

Note: CA = contributing area; MPA = maximum ponding area; MDS = maximum depression storage; and HPM = mean puddle depth.

4.4.4. Frequency distribution of surface depression properties

An attempt was first made to examine the distributions of MDS, MPA, CA, and HPM without the natural logarithm transformation for the four representative surfaces S3 – S6. It was found that these depression property parameters had extremely right-skewed distributions with a great amount of data points falling in the lowest class. The parameters then rapidly decreased, and finally decreased to the highest class. To better visualize and analyze the effects of DEM resolution (or λ_L) on the distributions of these parameters, natural logarithm transformation was performed. The plotted histograms of the parameters for Surfaces S3 – S6 with different DEM λ_L values were fitted by three models (Weibull, Gaussian, and Gamma). The goodness of fit tests, including the Kolmogorov-Smirnov D, Anderson-Darling, and Cramér-von Mises tests, were conducted and evaluated. Since the theoretical significance level value α was highly influenced by the sample size (in this study, the sample sizes were large with an average of 396), a

significance level α of 0.01 was selected to examine the p-value for assessing the goodness-of-fit tests. The p-values from the three tests for the puddle property parameters of the four surfaces indicated that MPA did not follow any of the three models and that the Weibull model was the best one among the three models that fitted the distributions of MDS, HPM, and CA for all the selected surfaces. Fig. 4.5 shows the fitted Weibull probability density function (pdf) curves of MDS, HPM, and CA for Surfaces S3 – S6 with different DEM resolutions or λ_L values.

Significant differences can be observed in the distributions of MDS, HPM, and CA for various DEM resolutions or λ_L values (Fig. 4.5). For most puddle property parameters and surfaces, the peaks of the pdf curves shifted to the right (i.e., higher parameter values) as DEM resolution or λ_L increased (Fig. 4.5). With an increase in DEM resolution or λ_L, small puddles tended to be eliminated or combined due to the smoothing effect. These changes in puddles and their structures subsequently altered the MDS, HPM, and CA of individual puddles and their distributions. Consequently, with increasing DEM resolution, the range and skewness of the puddle property parameters decreased, and their mean and median values increased. For example, the range of MDS for Surface S3 decreased from 360.71 to 262.22 cm^3 as λ_L increased from 0.1 to 0.4; and the skewness decreased from 6.27 to 2.72. Thus, the distributions of MDS, HPM, and CA of a surface were determined by the surface microtopographic characteristics and highly influenced by DEM resolution or λ_L.

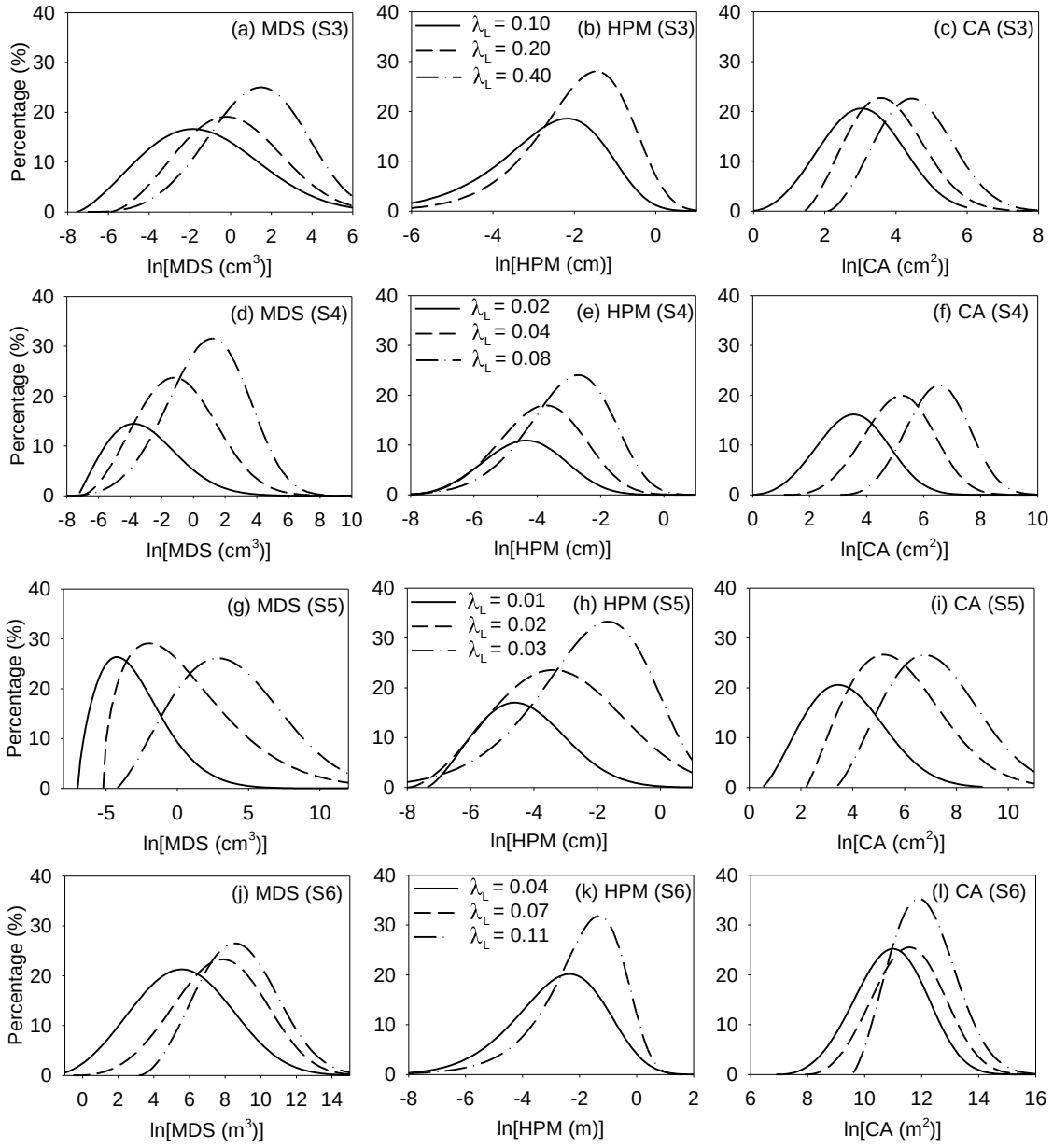

Fig. 4.5. Fitted Weibull pdf curves of maximum depression storage MDS, mean puddle depth HPM, and contributing area CA for Surfaces S3 (λ_R = 0.267), S4 (λ_R = 0.009), S5 (λ_R = 0.021), and S6 (λ_R = 0.006) with various DEM resolutions or dimensionless λ_L values

4.4.5. Hydrologic connectivity analysis

4.4.5.1. Structural hydrologic connectivity for a surface with different resolutions

Each connected area is a localized and well-connected hydrologic unit, which includes a number of contributing cells, an overflow threshold(s), and a puddle that potentially collects and

stores runoff water. The number of connected areas and their spatial variability depend on surface microtopography and DEM resolution. The connectivity property of a topographic surface affects a series of hydrologic and environmental processes such as overland flow trigging, infiltration, surface runoff, as well as solute and sediment transport.

Figs. 4.6 and 4.7 show the spatial distributions and histograms of connected areas for Surface S8 (λ_R = 0.013) with λ_L values of 0.07, 0.14, 0.21, and 0.28. The influence of λ_L or DEM resolution on the spatial distributions of connected areas can be observed in Fig. 4.6. The histograms of connected areas of Surface S8 for different DEM λ_L values (Fig. 4.7) indicated that the number of connected areas remarkably decreased and the size of individual connected areas significantly increased with an increase in λ_L. For the DEM with a λ_L value of 0.07 (highest resolution), there were 926 connected areas with an average area of 5.23×10^4 m^2 (Fig. 4.6a). As λ_L increased from 0.07 to 0.14, 0.21, and 0.28, the number of connected areas deceased to 439, 269, and 164, respectively, and the average of connected areas increased to 1.11×10^5, 1.83×10^5, and 3.03×10^5 m^2, respectively. That is, a coarser resolution DEM (a greater λ_L) tended to "artificially" increase the structural hydrologic connectivity of a topographic surface.

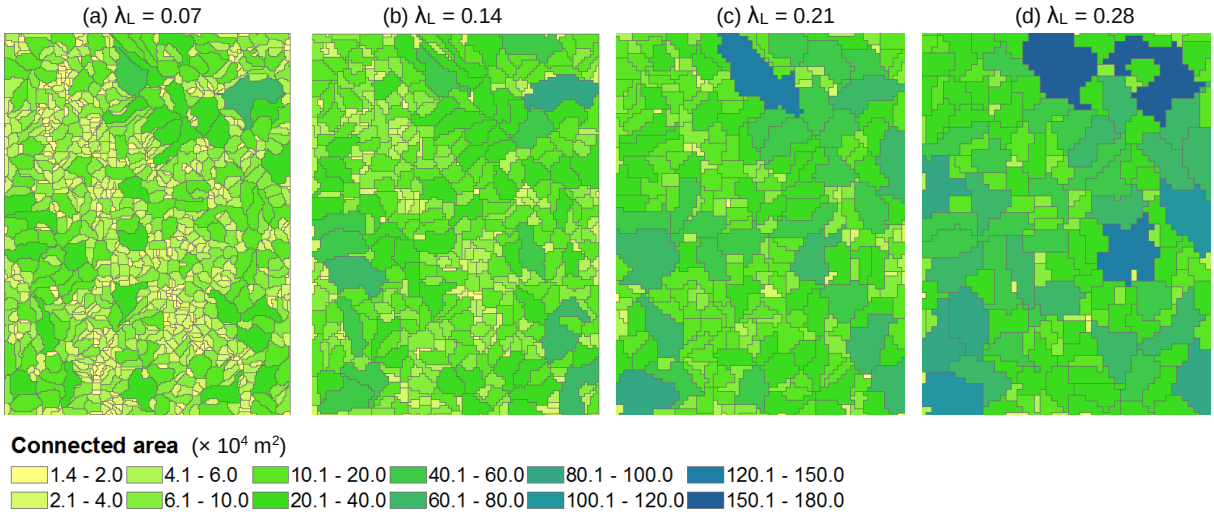

Fig. 4.6. Spatial distributions of structural hydrologic connectivity of Surface S8 for four different DEM resolutions or dimensionless λ_L values

A connected area has the potential to connect with other connected areas during the rainfall-runoff process. Such potential connections are determined by surface depression properties, such as the hierarchical relationships of puddles and the spatial and temporal distributions of rainfall. DEM resolution or λ_L affects these potential connectivity relationships. Hence, it is important to characterize the properties of connected areas and their formation/evolution so as to better understand and quantify the dynamic hydrologic processes under the influence of surface microtopography.

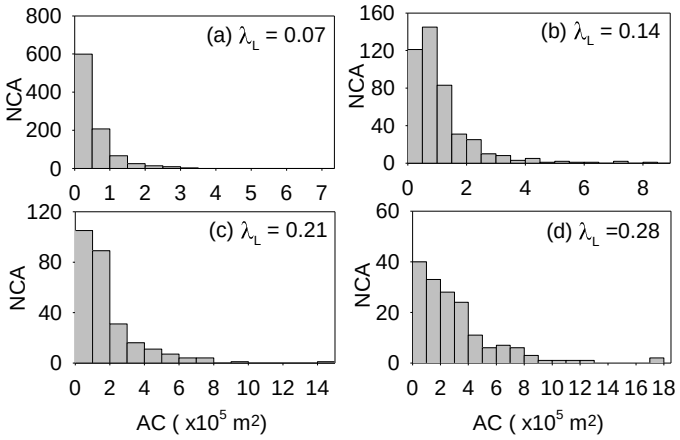

Fig. 4.7. Number of connected areas NCA vs. area of connected areas (AC) for Surface S8 with four different DEM resolutions or dimensionless λ_L values

4.4.5.2. Functional hydrologic connectivity for a surface with different resolutions

Fig. 4.8 shows the formation/evolution of connected areas at t = 1 hr and t = 20 hr for Surface S8 with the four different DEM resolutions or λ_L values. The distributions of connected areas changed as λ_L increased from 0.07 to 0.14, 0.21, and 0.28 for the two time points (Fig. 4.8). At t = 1 hr, the number of connected areas was 184 for λ_L = 0.07. It decreased to 162, 141, and 95 for λ_L = 0.14, 0.21, and 0.28, respectively. The average sizes of connected areas at t = 1 hr were 2.56×10^5, 3.02×10^5, 3.49×10^5, and 5.23×10^5 m^2 for λ_L values of 0.07, 0.14, 0.21, and 0.28, respectively. At t = 20 hr, higher λ_L values resulted in larger connected areas and the system

eventually approached to the final stage, at which most areas were well connected to the system boundary or outlet (Figs. 4.8g – 4.8h). At either time, 1 hr or 20 hr, the majority of connected areas of Surface S8 with different DEM resolutions or λ_L values showed similar shapes and distribution patterns, implying a similar development process of hydrologic connectivity (Figs. 4.8a – 4.8d or Figs. 4.8e – 4.8h). However, numerous local differences in the shape and distribution of connected areas existed (Fig. 4.8) due to the changes in surface elevations and puddle organizations (i.e., puddles and their relationships) resulting from the differences in DEM resolutions or λ_L values. Thus, under the same rainfall condition, a topographic surface with different DEM resolutions or λ_L values could have localized dissimilarities in hydrologic connectivity, flow drainage patterns, and other hydrologic properties.

Fig. 4.9 shows the temporal changes in the number and percentage of connected areas of Surface S8 for the four different λ_L values or DEM resolutions. The number of connected areas decreased and the percentage of connected areas increased with time for all λ_L values (Figs. 4.9a and 4.9b). The number of connected areas decreased dramatically before t = 2.5 hr for S8 with various DEM resolutions or λ_L values, and then leveled off (Fig. 4.9a). The average decreasing rate of the number of connected areas decreased from 150 hr^{-1} (before 2.5 hr) to 14 hr^{-1} (after 2.5 hr). This can be attributed to the fact that most small puddles were fully filled within a short time period and the corresponding areas merged with larger connected areas at the beginning of the rainfall-runoff process. Similarly, the percentage of connected areas increased significantly prior to t = 2.5 hr. Beyond t = 2.5 hr, an increase in the percentage of connected areas continued for larger λ_L values (e.g., 0.21 and 0.28) (Fig. 4.9b) since a coarser DEM surface had fewer, larger depressions and the puddle-filling-connecting processes took more time (Fig. 4.9b). Thus, DEM resolution or λ_L had significant effects on the formation/evolution of connected areas, especially

at the early stage of the rainfall-runoff process. A coarser resolution DEM or higher λ_L tended to delay the completion of the puddle filling-spilling-merging processes. The formation/evolution of connected areas did reflect the dynamic changes in hydrologic connectivity properties of a microtopographic surface for a specific system input (e.g., rainfall).

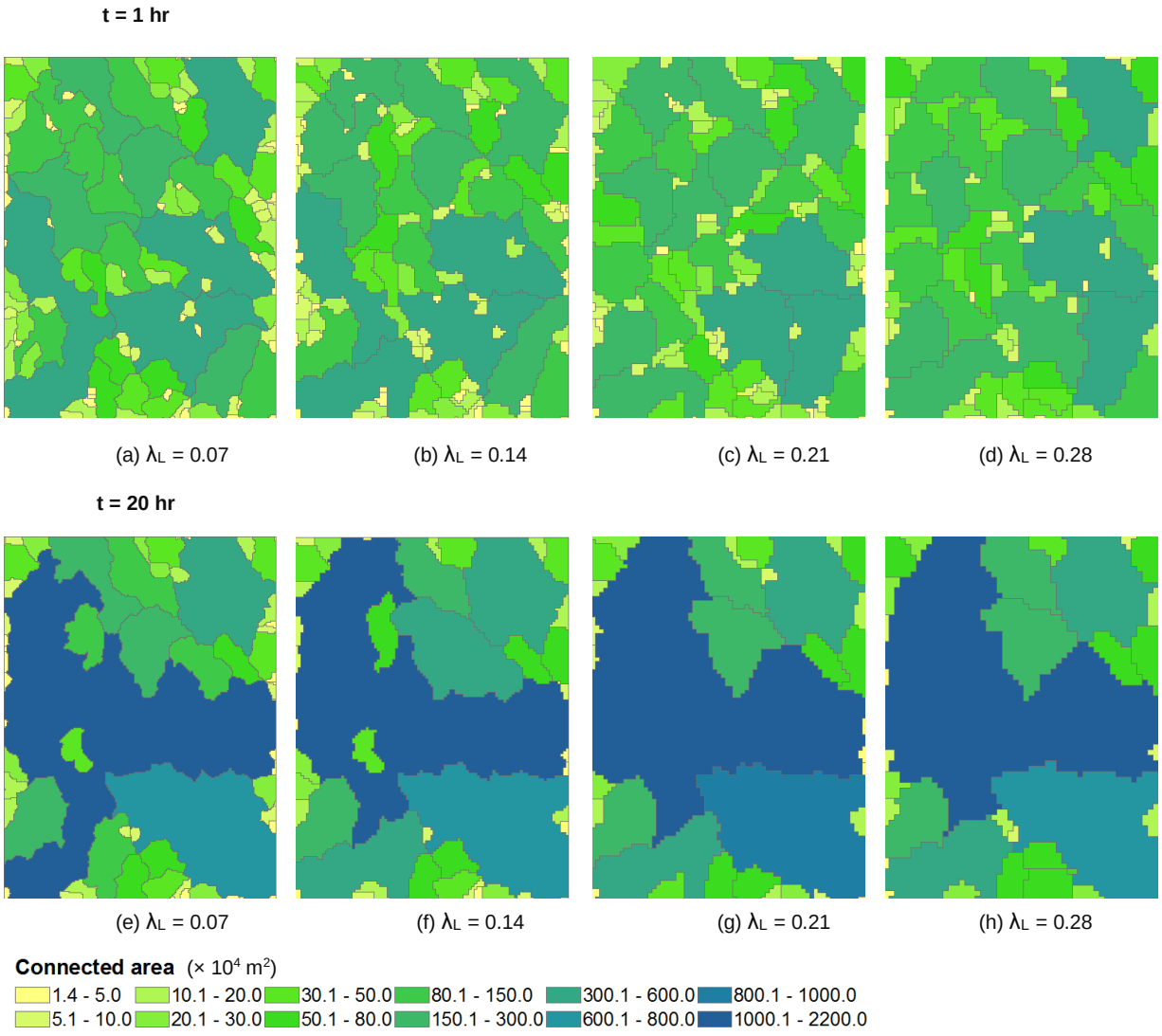

Fig. 4.8. Functional hydrologic connectivity of Surface S8 for four different DEM resolutions or dimensionless λ_L values at t = 1 hr and t = 20 hr

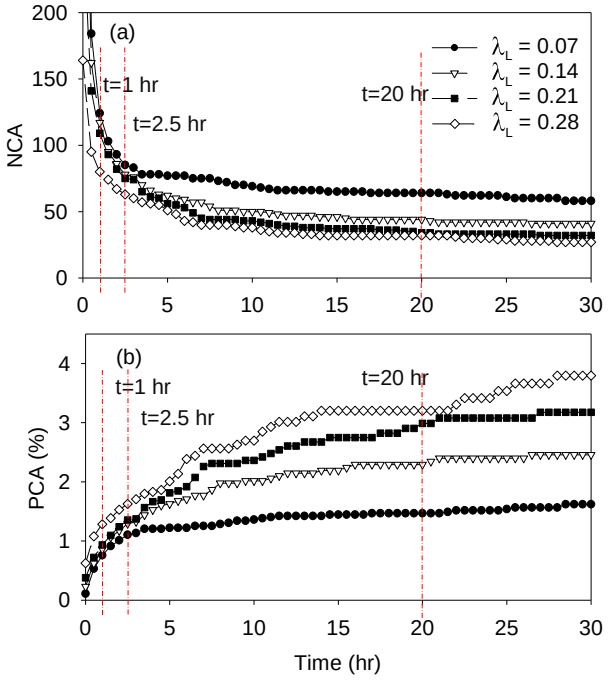

Fig. 4.9. Hydrologic connectivity developing curves (number of connected areas NCA and percentage of average connected areas PCA vs. time for Surface S8 (λ_R = 0.013) for four different DEM resolutions or dimensionless λ_L values

In addition to spatially mapping the evolution of connected areas for surfaces with various DEM resolutions and visualizing the changes in hydrologic connectivity, simplified hydrograph is another essential indicator of FHC, which quantifies the response of a hydrologic system to rainfall input. Fig. 4.10 shows the simplified hydrographs simulated for Surfaces S3, S5, S6, and S8 with various DEM resolutions or λ_L values. The simplified hydrographs exhibited different changing patterns for different surfaces and λ_L values, implying that the simplified hydrographs were highly influenced by surface microtopographic characteristics (different surfaces) and DEM resolutions (different λ_L values). Stepwise increases in the simplified hydrographs can be observed for the four surfaces (Fig. 4.10), which can be attributed to the developing process of hydrologic connectivity (i.e., puddle filling-merging-spilling-connecting process, and the subsequent expansion of connected areas) and the associated threshold-driven overland flow processes.

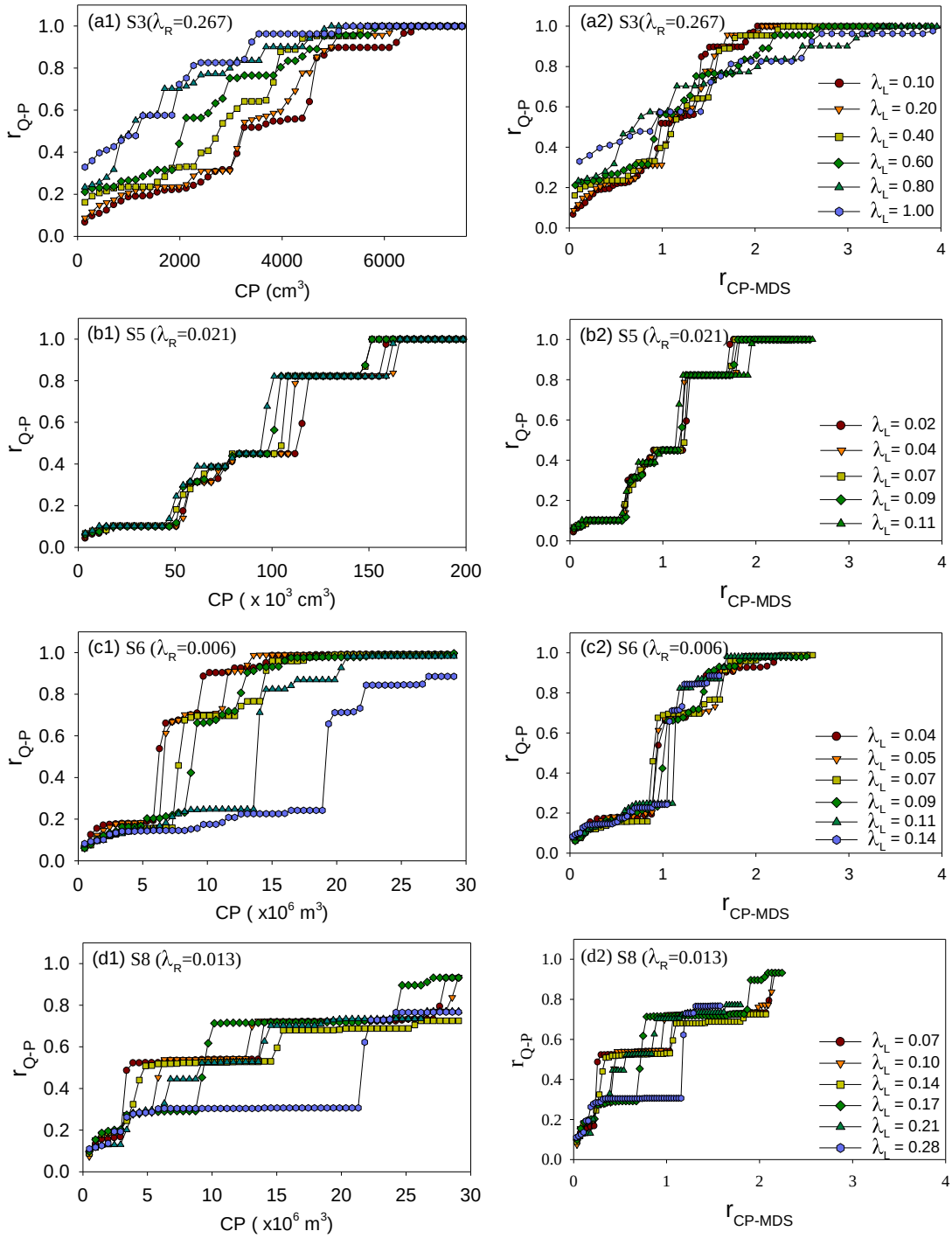

Fig. 4.10. Ratio of discharge to rainfall input $r_{Q\text{-}P}$ vs. cumulative rainfall CP or normalized cumulative rainfall $r_{CP\text{-}MDS}$ for Surfaces S3, S5, S6, and S8 with various λ_L values

Figs. 4.10a1, 4.10b1, 4.10c1, and 4.10d1 displayed the effects of DEM resolution or λ_L on simplified hydrographs: (1) the simplified hydrographs increased rapidly and eventually

reached the steady state earlier for the random roughness surface S3 (λ_R = 0.267) with a larger λ_L value or coarser DEM resolution (Fig. 4.10a1); (2) an increase in λ_L had less effects on simplified hydrographs for the field rough surface S5 (λ_R = 0.021) (Fig. 4.10b1); and (3) for the watershed surfaces S6 (λ_R = 0.006) and S8 (λ_R = 0.013), the simplified hydrographs increased rapidly and reached the steady state earlier for a smaller λ_L value (Figs. 4.10c1 and 4.10d1). These effects can be mainly attributed to two factors: changes in surface MDS and changes in puddle organization. MDS may increase or decrease with increasing λ_L (Fig. 4.3). Under the same rainfall condition, the surfaces with higher λ_L values had less water stored in surface depressions and hence produced more surface runoff (e.g., S1, S2, and S3), and vice versa (e.g., S6, S7, and S8). The alteration in puddle organization included the changes in puddle relationships and elimination of puddles due to the smoothing effect from the aggregation processing of DEM data (from fine to coarse resolutions).

Different topographic surfaces exhibited dissimilar properties of hydrologic connectivity for the same rainfall condition (Figs. 4.10a1, 4.10b1, 4.10c1, and 4.10d1). To further compare the functional connectivity properties for surfaces of different areas and MDS, we normalized cumulative rainfall CP by MDS (i.e., we considered the same magnitude level of MDS for different DEM resolutions) and expressed simplified hydrograph as a function of dimensionless $r_{CP\text{-}MDS}$ (ratio of CP to MDS) and $r_{Q\text{-}P}$ (ratio of discharge to rainfall) (Figs. 4.10a2, 4.10b2, 4.10c2, and 4.10d2). In this way, the simplified hydrographs also highlighted the influences from the changes in puddle organization. Comparison of the two simplified hydrographs for each surface (e.g., Figs. 4.10a1 and 4.10a2 for S3) revealed how the two factors (i.e., changes in MDS and changes in puddle organization) affected hydrologic connectivity. Changes in surface MDS seemed to play a more important role in hydrologic connectivity for Surfaces S3 and S6 (Figs.

4.10a1 and 4.10a2 and Figs. 4.10c1 and 4.10c2, respectively) than the second factor (changes in puddle organization). Both factors did not show significant effects for Surface S5 (Figs. 4.10b1 and 4.10b2).

Compared with Surfaces S3, S6, and S8, Surface S5 had less percent change in MDS with an increase in DEM resolution or λ_L, and the coefficient of variation (CV) of MDS for Surface S5 from different DEM resolutions or λ_L values was 0.05, which was much smaller than those for Surfaces S3, S6, and S8 (CV = 0.32, 0.43, and 0.16, respectively). In addition, Surface S5 was dominated by few big puddles. During a rainfall event, local hydrologic connectivity within these big puddles occurred. However, such local connected areas did not make any contribution to the outlet flow (i.e., simplified hydrograph) until the localized puddle system reached its overflow threshold. Such major threshold behaviors for S5 (stepwise increases) can be observed in Figs. 4.10b1 and 4.10b2. Thus, changes in MDS from different resolutions or λ_L values of a surface could significantly affect its simplified hydrograph.

In summary, surfaces with various DEM resolutions or λ_L values had different hydrologic connectivity properties or dissimilar simplified hydrographs, which could be attributed to two factors: changes in MDS and changes in puddle organization. The former seemed to play a more important role in simplified hydrographs for varying DEM resolutions or dimensionless representation scale λ_L values. Using DEMs of a coarser resolution or a higher λ_L might result in overestimation of the simplified hydrograph for surfaces characterized by numerous small depressions (e.g., Surfaces S1 – S3 with small scale, randomly distributed depressions).

4.5. Conclusions

A puddle delineation program was used in this study to delineate puddles and calculate surface depression property parameters. A group of surfaces of varying topographic

characteristics were selected for evaluating the effects of DEM resolution or dimensionless representation scale λ_L on depression properties and the relationships and distributions of different depression property parameters. Furthermore, a P2P conceptual model was utilized to examine the effects of λ_L on structural and functional hydrologic connectivity. Based on the current studies, following conclusions have been reached:

DEM resolution or λ_L significantly influenced the spatial distributions of puddles, their hierarchical relationships, and the drainage patterns. The maximum depression storage MDS, maximum ponding area MPA, and the average of maximum/mean puddle depths HPMA/HPA varied with λ_L, depending on surface microtopographic characteristics. The number of puddles NP and the number of puddle levels NPL decreased with increasing λ_L.

The CA-MPA, MDS-MPA, and MDS-HPM relationships followed a power law function for surfaces with various DEM resolutions or λ_L values. λ_L did not show significant influences on the relationships of these depression property parameters, which were primarily determined by surface microtopographic characteristics, i.e., vertical roughness scale λ_R.

DEM resolution or λ_L significantly influenced structural hydrologic connectivity. With increasing λ_L, the number of connected areas decreased while the total connected area increased.

Simplified hydrographs were characterized with a series of stepwise increases, due to the threshold behavior of overland flow determined by the complexity in surface microtopography. It appeared that DEM resolution or λ_L had greater effects on simplified hydrographs for surfaces featuring numerous small-scale depressions.

DEM resolution or λ_L had remarkable effects on the development of functional hydrologic connectivity, especially at the early stage of the rainfall-runoff process.

In the current study, two unique dimensionless parameters λ_L and λ_R, which respectively represented horizontal DEM scale and vertical topographic variability or surface roughness, were proposed and utilized for examining the DEM resolution effects on depression properties and hydrologic connectivity based on a limited number of surfaces. Although the selected surfaces did cover different spatial scales (small laboratory surfaces, field plots, and watersheds) and various topographic features, more in-depth studies and extensive statistical analyses for a wide range of real-world land surfaces (including infiltrating soil surfaces) should be conducted in the future, which would improve the understanding of the scale-dependent hydrotopographic processes and enhance the practical applicability of the developed methodologies.

4.6. References

Abedini, M. J., Dickinson, W. T., and Rudra, R. P., 2006. On depressional storages: The effects of DEM spatial resolution. J. Hydrol., 318(1-4), 138-150.

Allmaras, R. R., Burwell, R. E., Larson, W. E., and Hotl, R. F., 1966. Total porosity and random roughness of the interrow zone as influenced by tillage. U.S. Dep. Agric. Conserv. Res. Rep. 7, U.S. Governmem Printing Office, Washington, DC, 22 pp.

Antoine, M., Javaux, M., and Bielders, C., 2009. What indicators can capture runoff-relevant connectivity properties of the micro-topography at the plot scale? Adv. Water Resour., 32(8), 1297-1310.

Appels, W. M., Bogaart, P. W., and van der Zee, S. E. A. T. M., 2011. Influence of spatial variations of microtopography and infiltration on surface runoff and field scale hydrological connectivity. Adv. Water Resour., 34(2), 303-313.

Blöschl, G., 1999. Scaling issues in snow hydrology. Hydrol. Process., 13(14), 2149-2175.

Bracken, L. J., and Croke, J., 2007. The concept of hydrological connectivity and its contribution to understanding runoff-dominated geomorphic systems. Hydrol. Process., 21(13), 1749-1763.

Brierley, G., Fryirs, K., and Jain, V., 2006. Landscape connectivity: the geographic basis of geomorphic applications. Area, 38(2), 165-174.

Bruneau, P., and Gascuel-Odoux, C., 1990. A morphological assessment of soil microtopography using a digital elevation model on one square metre plots. Catena, 17(4-5), 315-325.

Carvajal, F., Aguilar, M. A., Agüera, F., Aguilar, F. J., and Giráldez, J. V., 2006. Maximum depression storage and surface drainage network in uneven agricultural landforms. Biosyst. Eng., 95 (2), 281-293.

Chi, Y., Yang, J., Bogart, D., and Chu, X. 2012. Fractal analysis of surface microtopography and its application in understanding hydrologic processes. Transactions of the ASABE. 55(5), 1781-1792.

Chu, X., Yang, J., and Chi, Y. 2012. Quantification of soil random roughness and surface depression storage: Methods, applicability, and limitations. Transactions of the ASABE. 55(5), 1699-1710.

Chu, X., Yang, J., Chi, Y., and Zhang, J. 2013. Dynamic puddle delineation and modeling of puddle-to-puddle filling-spilling-merging-splitting overland flow processes. Water Resour. Res., 49(6), 3825-3829.

Chu, X., Zhang, J., Chi, Y., and Yang, J. 2010. An improved method for watershed delineation and computation of surface depression storage. In Watershed Management 2010: Innovations in Watershed Management Under Land Use and Climate Change, Proc. of the 2010

Watershed Management Conf., 1113-1122. K. W. Potter and D. K. Frevert, eds. Reston, Va.: ASCE.

Chu, X., Zhang, J., Yang, J., Habtezion, N., Chi, Y., and Yang, Y. 2014. P2P Tools, User's Manuals, Version 1.50, North Dakota State University, 64 pages.

Darboux, F., Davy, P., and Gascuel-Odoux, C., 2002a. Effect of depression storage capacity on overland flow generation for rough horizontal surfaces: water transfer distance and scaling. Earth Surf. Proc. Land., 27(2), 177-191.

Darboux, F., Gascuel-Odoux, C., and Davy, P., 2002b. Effects of surface water storage by soil roughness on overland-flow generation. Earth Surf. Proc. Land., 27(3), 223-233.

Darboux, F., and Huang, C., 2003. An instantaneous profile laser scanner to measure soil surface microtopography. Soil Sci. Soc. America J. 67(1), 92-99.

Dutta, D., and Herath, S., 2001. Effect of DEM accuracy in flood inundation simulation using distributed hydrological models. Seisan Kenkyu, 53(11), 602-605.

Hayashi, M., van der Kamp, G., and Schmidt, R., 2003. Focused infiltration of snowmelt water in partially frozen soil under small depressions. J. Hydrol., 270(3-4), 214-229.

Huang, C., and Bradford, J. M., 1990. Depressional storage for Markov-Gaussian surfaces. Water Resour. Res., 26 (9), 2235-2242.

Kamphorst, E. C., Jetten, V., Guerif, J., Pitkanen, J., Iversen, B. V., Douglas, J. T., and Paz, A., 2000. Predicting depressional storage from soil surface roughness. Soil Sci. Soc. Am. J., 64(5), 1749-1758.

Kuo, W., Steenhuis, T. S., McCulloch, C. E., Mohler, C. L., Weinstein, D. A., DeGloria, S. D., and Swaney, D. P., 1999. Effect of grid size on runoff and soil moisture for a variable-source-area hydrology model. Water Resour. Res., 35(11), 3419-3428.

Moglen, G. E., and Hartman, G. L., 2001. Resolution effects on hydrologic modeling parameters and peak discharge. J. Hydrol. Eng., 6(6), 490-497.

Molnár, D. K., and Julien, P. Y., 2000. Grid-size effects on surface runoff modeling. J. Hydrol. Eng., 5(1), 8-16.

Moore, I. D., and Larson, C. L., 1979. Estimating micro-relief surface storage from point data. T. ASAE, 22(5), 1073-1077.

O'Callaghan, J. F., and Mark, D. M., 1984. The extraction of drainage networks from digital elevation data. Comput. Vision Graph., 28, 323-344.

Onstad, C. A., 1984. Depressional storage on tilled soil surfaces. T. ASAE, 27(3), 729-732.

Pringle, C., 2003. What is hydrologic connectivity and why is it ecologically important? Hydrol. Process., 17(13), 2685–2689.

Sneddon, J., and Chapman, T. G., 1989. Measurement and analysis of depression storage on a hillslope. Hydrol. Process., 3(1), 1-13.

Tetzlaff, D., Soulsby, C., Bacon, P. J., Youngson, A. F., Gibbins, C., and Malcolm, I. A., 2007. Connectivity between landscapes and riverscapes-a unifying theme in integrating hydrology and ecology in catchment science? Hydrol. Process., 21(10), 1385-1389.

Thompson, J. A., Bell, J. C., and Butler, C. A., 2001. Digital elevation model resolution: effects on terrain attribute and quantitative soil-landscape modeling. Geoderma, 100(1-2), 67-89.

Ullah, W., and Dickinson, W. T., 1979. Quantitative description of depression storage using a digital surface model II. Characteristics of surface depressions. J. Hydrol., 42(1-2), 77-90.

CHAPTER 5. OVERALL CONCLUSIONS

Surface microtopography is one of the critical factors that affect hydrologic processes. Under the influence of surface depressions, overland flow is featured with spatio-temporal discontinuity and variability. It has been a challenge to physically simulate topography-dominated overland flow and infiltration processes. In this study, a topography-dominated puddle-to-puddle (P2P) overland flow model was developed, which explicitly incorporated surface depressions and accounted for their hydrologic roles. The P2P model was a physically-based overland flow model coupled with an infiltration and unsaturated flow model for simulating the real microtopography-controlled P2P filling-spilling-merging-splitting overland flow dynamics, infiltration, and unsaturated flow in heterogeneous soils under any spatio-temporally varying rainfall conditions. The developed P2P model can be used to improve the understanding of the mechanism of discontinuity and variability of overland flow generation process, e.g., how do the depressions on topographic surfaces affect the rainfall partitioning and influence the runoff generation? This model also can be applied to investigate the complexity and dynamic of the threshold behaviors of hydrologic systems and analyze depression storage/runoff/infiltration relationships for overland flow generation and infiltration processes.

In this study, a concept of "puddle-to-puddle hydrologic connectivity" was proposed to describe the variability, dynamics, and complexity of overland flow generation process. Two hydrologic connectivity indices, connectivity function and connectivity length, were proposed to quantify scale-dependent and time-varying hydrologically connected areas and ponded areas. The results showed that the two indices were capable of quantifying both structural and functional hydrologic connectivity for surfaces with various topographic characteristics and serving as a linkage to bridge the gaps between structural and functional hydrologic connectivity.

The two proposed indices quantified the spatio-temporal variations in hydrologic connectivity and revealed the dynamic threshold behaviors of overland flow generation for microtopography-dominated hydrologic systems. Efforts have also been devoted to evaluate the effects of DEM resolution, surface topography, rainfall distribution, and surface slope on hydrologic connectivity. It was found that for topographic surfaces, hydrologic connectivity varied at different stages of the overland flow generation processes, depending on the puddle organization. Rainfall distribution had significant effects on the development of hydrologic connectivity and the behaviors of the dynamic P2P overland flow processes.

Furthermore, efforts have been devoted to investigate two unique dimensionless parameters λ_L and λ_R (i.e., horizontal DEM scale and vertical topographic variability or surface roughness) on the effects of depression properties and hydrologic connectivity. It was found that λ_L had remarkable effects on the structural hydrologic connectivity and the development of functional hydrologic connectivity, especially at the early stage of the rainfall-runoff process. DEM resolution or λ_L significantly influenced the spatial distributions of puddles, their hierarchical relationships, and the flow drainage patterns.